ON THE PROBLEMS RELATED TO HYDROPHOBIZATION AND ASSEMBLY OF INORGANIC NANOPARTICLE

THESIS SUBMITTED TO

THE UNIVERSITY OF PUNE

FOR THE DEGREE OF

DOCTOR OF PHILOSOPHY

IN

CHEMISTRY

BY

Mr. ASHAVANI KUMAR

PHYSICAL CHEMISTRY DIVISION
NATIONAL CHEMICAL LABORATORY
PUNE – 411 008
INDIA

OCTOBER 2003

Dedicated
to my
Family
And Teachers

CERTIFICATE

This is to certify that the work discussed in the thesis entitled **"ON THE PROBLEMS RELATED TO HYDROPHOBIZATION AND ASSEMBLY OF INORGANIC NANOPARTICLE"** by **Mr. Ashavani Kumar** for the degree of philosophy in chemistry was carried out under my supervision in the Physical Chemistry Division of National Chemical Laboratory, Pune. Such material as has been obtained by other sources has been duly acknowledged in this thesis. To best of my knowledge, the present work or any part thereof, has not been submitted to any other university for the award of any other degree or diploma

Date:

Place: Pune

Dr. Murali Sastry

(Research guide)

CANDIDATE`S DECLARATION

I , Mr. Ashavani Kumar hereby declare that the work incorporated in this thesis entitled " **On the problems related to hydrophobization and assembly of inorganic nanoparticles**"for the degree of philosophy in chemistry was carried out by me under the guidance of Dr. Murali Sastry (Physical Chemistry Division of National Chemical Laboratory, Pune). Such materials as has been obtained by other sources has been duly acknowledged in this thesis . I declare that present work or any part thereof, has not been submitted to any other university for the award of any other degree or diploma.

Date: Ashavani Kumar

Place:

Acknowledgements

I take this opportunity to express my reverence to my research supervisor **Dr. Murali Sastry** who introduced me to a fascinating realm of chemistry. His inspiring guidance and constant motivation have helped me to understand better and remain optimistic. I am grateful to him for giving me liberty in the work undertaken and for continuous encouragement during the course of the present study. Although this eulogy is insufficient, I preserve an everlasting gratitude for him.

It gives me great pleasure to thank Dr. K. N. Ganesh, head, organic synthesis division, and Dr. Rajiv Kumar, catalysis division, National Chemical Laboratory and Dr, C. V. Dharmadikari, Department of Physics, University of Pune for their motivation, subtle guidance, constant help, technical support, valuable suggestions and making all the facilities available for characterization.

I wish to thank Dr. S. K. Date, and Dr. S. Pal former and present Heads, Physical Chemistry Division, for their constant support and encouragement. I also wish to place on record my sincere thanks to Dr. B. L. V. Prasad for all his support.

My heartfelt thanks to my friend and colleague, Mrunalini Pattarkine, Priyabrata Mukherjee, Suvarna datar for their untiring and continued support during my thesis work. Her timely help and friendship shall always be remembered. Thank-you.

I always had a hearty inspiration from my labmates: Anand Gole, Vidya, Saikat, Sumant, Debabrat, Chinmay Damle, Kannan, Shankar, Anita, Madhu, Neeta, Jaspreet, Hrushikesh, Senthil, Sujata, Ambrish, umesh, Amit, Akilesh, Kedar, Sarouv, Vipul, Atul, Ritwik, Manhi, Tanushree . This work remained incomplete without their help, cooperation and discussions. A special mention of thanks to my friends . Thank-you Subashini, Prashant, Akilesh Tanwar, Manas Sharma, Manish, Hemanta, Tarun for their help and charming company.

Working under a single roof, it was a pleasant company of Ms. S. Adyanthaya who has always helped me in one-way or the other. I would also like to thank Mrs. Renu Pasricha,

Dr. Sainkar, Dr. Mandale, Dr. Bhadbade and Dr. Pavaskar for all the help and support they gave me.

I'm grateful to Dr P. Ratnaswamy and Dr. S. Sivaram, former and present directors of NCL, Pune for giving me the opportunity to work in this institute and making all the facilities available for my research work.

My thanks are duly acknowledged to CSIR, New Delhi for their valuable support in the form of a Research Fellowship.

List of Contents

CHAPTER I

Introduction

This chapter describes the historical background, properties, application of nanoparticles and various methods known for the organization of nanoparticles. It also highlight about the phase transfer of nanoparticles from organic phase to aqueous phase and vice versa and their advantages in nanotechnology.

1.1. Historical background

Colloid chemistry is one of the oldest branches of chemistry. Numerous examples could be sited wherein mankind has unknowingly used colloidal particles for some of their applications. For example stained glass is known from 11th century A.D, wherein different kinds of metal and metal oxide particles were used to obtain different colors, such as cadmium for yellow, copper oxide for blue, dichromate or iron oxide for green etc. This branch of chemistry had received considerable attention after the pioneering work of Faraday on the synthesis of gold hydrosols (gold nanoparticles dispersed in water).[1] From their simple applications in stained glasses etc. many centuries ago, colloidal particles have become an integral part of technology where the progress in a diametric direction of diminishing scale has proved increasingly vital to the society. Nobel laureate Prof. Feynman once said:

What I want to talk about is the problem of manipulating and controlling the things on a small scale….

As soon as I mention this, people tell me about miniaturization, and how far it has progressed today. They tell me about electric motors that are the size of the nail on your small finger. And there is a device on the market, they tell me, by which you can write the Lord's Prayer on the head of a pin. But that's nothing: that's most primitive, halting step in the direction I intent to discuss. It's a staggeringly small world that is below. In the year 2000, when they look back at this age, they will wonder why it was not until the year 1960 that anybody began seriously to move in this direction……..

He used these words in his famous talk at Caltech: "There is a plenty of room at the bottom". He was the one among the first persons who predicted many advances and potential application in this area of research in 1959.[2] Among his playful suggestions, which 30 years later were fast being realized: etching lines a few atoms wide with a beam of electrons, building circuits on the scale of angstroms to make new kinds of computers, manipulating atoms to control the very properties of matter, and like many of the nanotechnologists of today, Feynman credited his inspiration to the molecular-scale machines and information systems of living things.

In the mid 1980s, Eric Drexler introduced the term "nanotechnology" to describe atomically precise molecular manufacturing systems and their products. Advanced nanotechnology could probably make many dreams (and nightmares) first articulated in

the literature of science fiction a possibility. In simple words we can define "Nanotechnology" as the building of devices and materials at the level of atoms and molecules and the exploitation of the novel properties at this scale. It gets its name from "nanometer," the unit of measurement representing one-billionth of a meter, or about ten times the size of an individual atom. "Nanotechnology" generally refers to work done at the scale between 0.1 and 100 nanometers. The novel properties of nanoscale matter are due to the different behavior of things at this scale compared with either isolated molecules or bulk structures of the same material.

1.2 Properties and application of nanosize materials

The physics of nanosize materials can be understood in terms of quantum effects which occur at dimensions comparable to the de Broglie wavelength of an electron, and the mean free path of excitons,[3a,d] which are in the nanosize dimensions.

- Three-dimensional confinement of electron hole pairs results in a "quantum dot".
- Two-dimensional confinement of charge carriers results in "quantum wire".
- One-dimensional confinement of charge carriers results in "quantum well".

This phenomena is very important because it leads to mechanical, chemical, electrical, optical, magnetic, optoelectronic and magneto-optical properties[3] of nanomaterials that are significantly different from those observed for bulk materials. These properties of nanoparticles are very useful in applications such as optoelectronic,[4] catalysis,[5] reprography,[6] single electron transistor and light emitting diode,[7] nonlinear optical devices[8] and photo electro-chemical applications.[9] Magnetic nanoparticles are being used in memory storage devices,[10] magnetic resonance image enhancement[11] and could probably be employed in interesting applications such as magnetic refrigeration.[12] Semiconductor nanoparticles are very attractive because of their size dependent optical properties for use in quantum dot lasers.[13] Other than these, nanomaterials have potential applications in nano-computers, synthesis of advanced materials, energy storage devices, electronic and optical display, chemical and bio- sensors as well as biomedical devices.[14] All these applications require preparation of nanoscale materials of desired property and their assembly in required geometry. Therefore, the most fundamental theme of

nanotechnology is the controlled synthesis of those building blocks and their subsequent assembly into nanostructures for useful devices.

1.3. Methods of synthesis of nanoparticles

The first ten years of research in nanomaterials was devoted to understand the size dependent properties of the particles and in the development of better preparation and characterization methods for materials in nanodimensions. A variety of methods were used for the formation of nanoparticles such as molecular beam epitaxy,[15] chemical vapor deposition,[16] reduction by ionizing radiation,[17] thermal decomposition in organic solvents,[18] chemical reduction or photoreduction in reverse micelles[19] and chemical reduction with[20] or without[21] stabilizing polymers, biological methods[22] which are shown in schematic. It is now well understood that the colloidal stability, particle size, and their shapes depend strongly on the specific method of preparation.

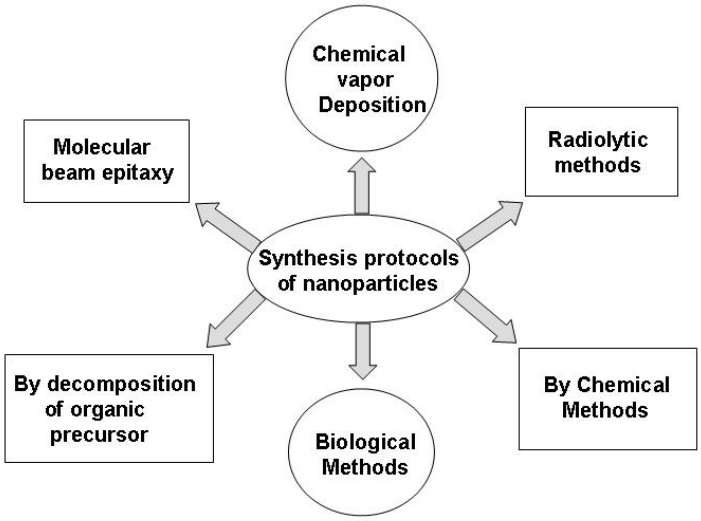

Among all the methods, wet chemical methods for nanoparticle synthesis are very useful and have many advantages over the other ones such as

- Easy synthesis
- Good control over the size
- Easy to modulate the shape
- Easy modification with desired chemical functionalities
- High monodispersity
- Capable for large scale synthesis

The nanoparticles are in general unstable due to their high surface free energy and hence need to be stabilized against aggregation by surface modification. The surface modification can be done by capping the nanoparticles with a number of molecules depending on their chemical nature. For example, for simple metallic nanoparticles the capping agents routinely used include alkanethiols,[23a] ω-functionalized alkanethiols,[24] aromatic thiols[25] and other thiol derivatives,[26] fatty acid, fatty amine[27a], amino acid[27b], etc.

Now the next most important step in nanotechnology is to use these surface modified nanoparticles for various applications. For certain applications such as catalysis, gene therapy and targeted drug delivery etc., nanoparticles can be used directly with required surface modification. However, for many electronic and magnetic applications like single electron transistors (SET), optoelectronics, light emitting diodes, magnetic storage devices etc, there is a need for the assembly of nanoparticles in circuits with interconnects in nanoscale dimensions. This thesis has arisen out of our efforts in this direction wherein we have tried to develop novel processes to assemble nanoparticles based on different templates. Before we detail our strategy we provide below a brief account of the literature in this area.

1.4. Organized assemblies of nanoparticles

The approaches being pursued for the generation of organized nanoscale assemblies can be broadly categorized under two sections; the "top down" and "bottom-up" methods. In the "top down" approach the patterned structures are grown by suitable lithographic methods. This is based on a projection-printing system in which, the image of a pattern is reduced and projected onto a thin film of photoresist coated on the desired substrate through a high numerical aperture lens system. The photoresist is then etched off by chemical methods leaving behind the pattern of the desired material in nanoscale dimensions. In the late 1960s and early 1970s, Gorden Moore, founder of Fairchild Semiconductor and Intel Corporations, projected that the number of transistors in an integrated circuit would be doubled every 18 months or so. This prediction was latter known as Moore`s Law. Over the past two decades many trends in the semiconductor industry have followed this law. The continuous development of photolithography has

allowed the reduction of the size of a feature by a factor of approximately one half every three years. It is plausible that a feature as small as 100 nm can be manufactured optically in the future by employing advanced mask/resist technologies and deep UV (DUV) radiation.[28] Below this size, however, it is generally accepted that current strategies for photolithography may be blocked by optical diffraction and by opacity of the materials used for making lenses or support of photo masks. While the continued shrinking of the size towards 100 nm poses new technical challenges for photolithography, this may not be the best technique, for all micro fabrication needs in the first place. For example, this process is

- Very expensive
- Ineffective in generating three-dimensional structures
- Unable to introduce specific chemical functionality

These limitations suggest the need for an alternate micro fabrication technique. It is thus, desirable to have new approaches based on completely different principles to overcome the problem of further miniaturization and fabrication of patterned structures for different applications.

The alternate approach is the 'Bottom-up' method in which the nanostructures are built up from individual atoms or molecules. There are two main approaches for building useful devices in this direction. The first approach is based on controlled positioning of nanoscale objects by direct application of forces, electric fields etc., which involves nanomanipulation by using Scanning Probe Microscopy technique[29-36].

In their pioneering work, Eigler and Schweizer organized xenon atoms on Ni(110) surface by a *scanning tunneling microscopic* (STM) tip which was used to pick up the xenon atom and placed at a specific site of Ni(110) surface. Thus, they were able to write the IBM logo at atomic-resolution patterns on the surface.[29] The beauty of this technique is that it has a capability of removing single atom from the surface[30] and to create atomic switchs.[31] Mirkin and co-workers follow a different approach in which an AFM tip was used to write alkanethiol patterns with 30 nanometer line width resolution on a gold thin film in a manner analogous to that of a dip pen[35] as shown in Figure 1.

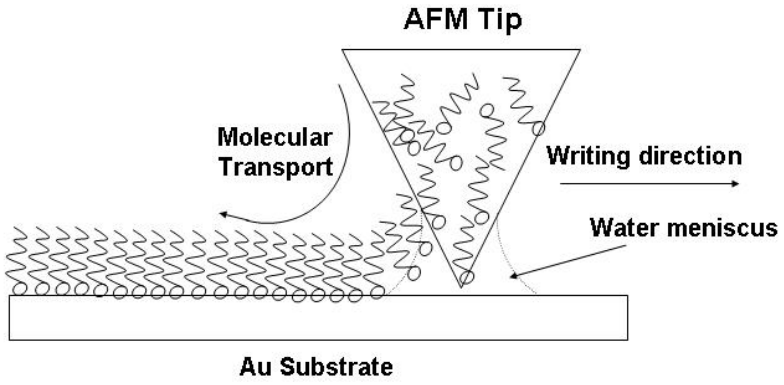

Figure 1: Schematic representation of formation of patterned SAM of octadecane thiol on gold substrate by Atomic Force Microscopic tip.

The atom-by-atom growth of nanostructure is definitely exciting, however it is very difficult to grow massively parallel structures at industrial scale by this technique. This is the main challenge in nanotechnology and opens up a need for alternative approaches.

The second approach in the area of nanoscale manipulation is based on the self-assembly of molecular and nanoscale building blocks to create large nano/micro structures. This self-assembly is very common phenomena in nature.

Nature is an ultimate nanotechnologist

Nature builds many structures at nanoscale that can perform complex tasks. For example, bacteria and virus have existed in nature since the beginning of life and perform similar tasks as expected from nanorobots. Cells contain many sorts of nanomachines including 12 nm diameter-rotating motors called ATPase,[37] and sensitive chemical sensors based on 4 nm sized ion channels. Materials in nanoscale are found in spider webs, silk and abalone shells that are tougher or stronger than the best synthetic materials. The preparation and assembly of all of these materials is done without any use of toxic solvents, billion dollar factories and endless pollution.

Presently the main focus of research in the construction of organized nanostructured materials is inspired by mother nature's organization ability which relies on the self-assembly of molecules or nanoscale objects.[38] Self-assembly is a reversible and self repairing process and has the capability of generating large number of correctly associated aggregates rapidly and conveniently. These characteristics make self-assembly a conceptually attractive strategy for mass fabrication of small devices. The term self-

assembly implies the spontaneous assembly of atoms, molecules or nanoscale objects into ordered functioning entities without human intervention.[38] A number of examples of self-assembly are well known in natural and unnatural system such as lipid

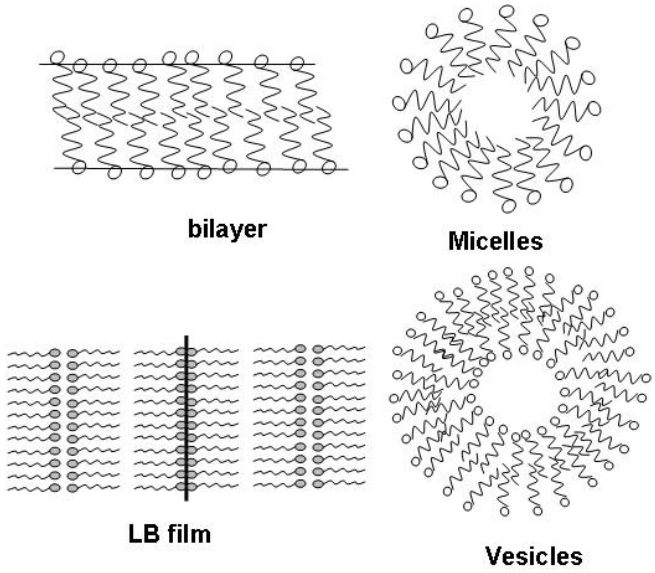

Figure2: Few examples of self-assembly found in natural and un-natural systems.

bilayers,[39a] vesicles and micelles,[39b] emulsions,[39b] phase separated polymers,[39c] self-assembled monolayers,[39d] DNA double helix,[38] Langmuir Blodgett films,[39e] the helical TMV,[53f] of which some are shown Figure 2. In all these examples the self-assembly is driven by weak interactions such as hydrogen bonds, electrostatic interactions, hydrophobic interactions, aromatic π-stacking and van der Waals interactions. The self-assembly has also been used for the organization of mesoscale objects such as polymer particles of micron size. The polymer particles of millimeter dimension and various shapes were self-assembled at the interface of perfluorodecalin and water using hydrophobic and capillary forces.[40] This kind of assembly is easy in case of micron size particles because the van der Waals interactions are sufficiently strong to create secondary minimum in the potential energy-distance curve between the particles.[41] For very small particles this type of ordering may not be possible because the secondary minimum is too shallow at room temperature to allow ordering. Small particles are therefore less stable and coalescence could lead to collapsing into the primary minimum,

i.e. to irreversible coagulation. Therefore, various techniques have been developed for the modification of nanoparticles to prevent this phenomenon and to arrange the nanoparticles into different organized structures. We briefly discuss the general procedures adopted for organization of nanoparticles in next section.

1.5. Various methods for the organization of nanoparticles

1.5.1. Organization by electrophoretic technique

In 1990, Schmid *et. al*. prepared gold nanoparticles using triphenylphosphine derivatives as adsorbates, which can be concentrated to form powders and are fully redispersible in water[42]. These colloids readily form densely packed monolayers on microscope grids; however, no significant ordering was reported to occur. The packing of the nanoparticles to form ordered structures is limited by the fact, that when the gold nanoparticle solution is allowed to dry on microscope grids, the evaporation of solvent leads to the creation of circular voids from which, the nanoparticles an excluded. Subsequently, Mulvaney and co-workers[43] used electrophoresis to deposit gold nanoparticles into well-ordered 2-dimensional monolayers with the interparticle spacing corresponding to the thickness of the adsorbed capping agents. They also showed the formation of ordered monolayers of alkanethiol capped gold nanoparticles in which the inter particle separation can be tailored by the stabilizer chain length.

1.5.2. Organization at air-water interface

Fendler *et. al.* and subsequently other groups have recognized the utility of the air-water interface in the synthesis and organization of hydrophobic, surfactant-stabilized nanoparticles and have shown that multilayer films of nanoparticles can be deposited by the versatile Langmuir-Blodgett (LB) technique.[44] Growth of multilayer nanoparticle films by the LB technique was also shown to be possible through interaction of suitably derivatized nanoparticles present in the subphase with the polar groups of the Langmuir monolayer. Initially the air-water interface was used to prepare the nanocryatalline particulate films of gold,[44f] silver,[44e] PbS,[44c,45a,b] CdS,[44a,b,c 45c,d] ZnS,[44a,b,c,45c] CdSe,[45e] PbSe[45e] nanoparticles. Their strategy involved the reduction of metal ions attached to the

oppositely charged monolayer by exposing them to gaseous reducing agents. The formation of nanoparticles occurs at the monolayer/aqueous solution interface which serves as a nucleation site and the growth of the nanoparticles proceeds into solution away from the relatively passive interface. Cadmium sulfide, zinc sulfide, lead sulfide, cadmium selenide and lead selenide, silver, gold and other metallic nanoparticulate films have been grown, in-situ, under the monolayer using this technique. In an other work a negatively charged Langmuir monolayer was taken, which provide binding sites for silver ions. These ions were reduced at cathodic surface where silver particles are formed. These silver particles extend towards the cathode and provide a mechanism for continuous reduction of silver counter ions at the monolayer surface. With time, silver particles grew concentrically, forming larger and larger circles at the monolayer-water interface.[46]

Some other reports are also available in which the hydrophobized nanoparticles are organized at air-water interface. Fendler and co-workers reported the formation of oleic acid stabilized clusters in aqueous medium and subsequent phase transfer to organic phase. Particulate films were then formed from these organic solutions at the air-water interface by dispersing such nanoparticles on an aqueous subphase in a Langmuir trough. Monolayers and multilayers of surfactant coated cadmium sulfide,[47a] TiO_2,[47b] Fe_2O_3,[47c] lead zirconium titanate,[47d] palladium,[47e] silver,[47f,g] platinum,[48a] and gold[48b] nanoparticles have been prepared using this technique. A prerequisite for this strategy is the hydrophobic nature of nanoparticles. Sastry and co-workers developed a simple protocol for the hydrophobization of nanoparticles synthesized in aqueous phase.[48] For example, negatively charged lauric acid modified CdS[48a] nanoparticles and 4-carboxythiophenol (4-CTP) capped gold nanoparticles[48b] were hydrophobized by electrostatic complexation with octadecyl amine molecule (ODA). Platinum nanoparticles were hydrophobized by capping them by poly vinylpyrrolidone (PVP).[48c] In a related work, the gold nanoparticles were modified by direct coordination with ODA molecules.[48d] Thereafter, they showed that the monolayer films of hydrophobized nanoparticles can be organized at the air–water interface which can be successfully transferred to solid substrates to obtain reasonably close-packed particulate structures.

In a different approach metal ions complexed with Langmuir monolayer were transferred layer-by-layer fashion onto different substrates to obtain Y-type films and nanoparticles were prepared from this metal ligand film by carrying out reactions in-situ. Semiconductor nanoparticles such as CdS,[49a] CdSe, CdTe,[49b] CdSxSe-1x, [49b] CdSxTe1-x,[49b] CoS,[50c] PbS[50a,e,f] particles were synthesized by this way. A gold nanoparticle film was also formed by exposing the octadecylamine/chloroaurate ions[50g] film to UV light.

Alternately, Sastry and co-workers showed the organization of modified gold,[51a,b] silver,[52] and CdS[53] nanoparticles at air-water interface by electrostatic complexation of nanoparticles with Langmuir monolayer. This is a very general method and can be used to grow multilayer films consisting of different layers of nanoparticles in any desired sequence by using different troughs containing the desired nanoparticle solutions succesively.[54a,b] The strategy involves the electrostatic complexation of functionalized gold, silver, CdS nanoparticles at the air-water interface with the oppositely charged fatty amine/acid Langmuir monolayers. The nanoparticles incorporation process is driven by the strength of the electrostatic interaction. The main advantage of this technique lies in the fact that the nanoparticles density in the film can be readily controlled. The degree of nanoparticle incorporation into the Langmuir monolayer has been systematically controlled by varying the charge on the monolayer and of the nanoparticles subphase with pH and good quality films were transferred onto solid substrate. The other advantage of this approach is the ability to form multilayer nanoparticle films by sequential immersion of solid supports into the Langmuir monolayer-nanoparticle complexes by the versatile Langmuir-Blodgett (LB) technique. Recently the same group developed a different strategy which involves the spontaneous reduction of chloroaurate ions present in the subphase of Langmuir monolayers of hexadecyl aniline (HDA) which leads to the formation of highly oriented, flat gold sheets and ribbon like nanocrystals bound to the monolayer.[54c] A major advantage of this approach is that the multilayer superlattice films of close-packed nanoparticle assemblies may be deposited by the LB method in one step.

1.5.3. Organization of nanoparticles in thermally evaporated lipid Films

Dr. Sastry`s group has shown that thermally evaporated films of fatty acids can be spontaneously organized via selective ionic interaction of cations by immersion of the

film in a suitable electrolyte. This leads to an organized lamellar film structure similar to *c*-axis-oriented *Y*-type LB films and was cleverly used for the synthesis/organization of nanoparticles.

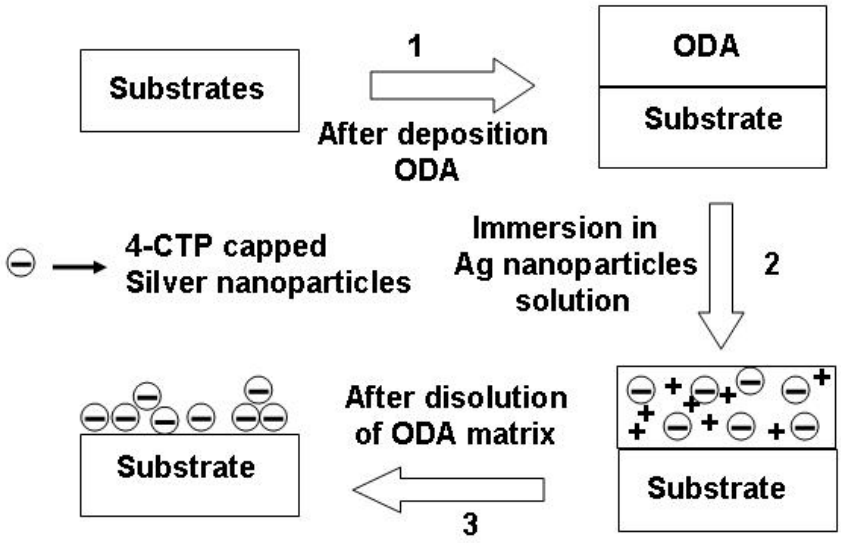

Figure 3: Organization of 4-CTP capped silver nanoparticles in the thermally evaporated ODA film. Step 1: formation of ODA film, step 2: incorporation of 4-CTP modified nanoparticles, step 3: dissolution of ODA matrix.

It was also demonstrated that negatively charged carboxylic acid derivatized silver,[55a,b] gold[55c,d] and CdS[55e] nanoparticles can be incorporated into thermally evaporated fatty amine films as shown in Figure 3. The process of incorporation of the nanoparticles in fatty amine films is due to *selective electrostatic binding* of the nanoparticles to the amine matrix and this process strongly depends on the nanoparticles concentration, solution pH, and film thickness. They have also demonstrated the formation of thin, patterned, *hetero-nanoparticle* assemblies of gold, silver, and Q-state CdS[55f] by appropriate masking and immersion protocols. Thus a spatially separated assembly of hetero nanoparticles may be easily obtained.

1.5.4. Ordering of nanoparticles mediated by self assembled monolayers

Self-assembled monolayers (SAMs) are the most widely studied and best developed examples of non biological, self-assembling system. SAMs are formed spontaneously by chemisorption and self-organization of functionalized long chain

organic molecules on the surface of appropriate substrate. SAMs are usually prepared by immersing an appropriate substrate in the solution containing a ligand that is reactive towards the surface. The advantage of SAMs is their easy preparation, low density of defects, good stability, and amenability to controlling interfacial property by replacing monofunctional ligands with bifunctional compounds. 2D SAMs were used for the first time for organization of CdS nanoparticles.[56] Alivisatos and co-workers showed that CdS nanoparticles could be chemisorbed on 2D SAMs of a dithiol molecule. In a similar approach Drouard *et. al.* have shown that organized structures of CdS nanoparticles can be grown by chemical methods.[57] Alivisatos and co-workers also demonstrated the self-assembly of CdS nanoparticles synthesized in water and functionalized with carboxylic acid group on aluminium thin film. The self-assembly in this case occurs through binding of the free carboxylate ions on the CdS surface with the aluminium atoms on the 2D surface.

Sastry *et. al.* showed that either covalent or electrostatic attachment of silver nanoparticles is possible on the SAMs of a novel aromatic bifunctional molecule, 4-carboxythiophenol (4-CTP), on Au and Al surface.[58a] Since two different functional groups are present at either end of the aromatic ring the organization of this molecule on different metal surfaces such as Al and Au is particularly interesting. Depending on the metal surface, the organization of this molecule results in different surface functionalities of the SAMs. The SAMs formed on Al surfaces present a surface rich in thiol functionality, while SAMs on gold surface are formed in such a way that the carboxylic group is exposed. Therefore, both electrostatic (4-CTP SAMs on gold) and covalent interaction (4-CTP SAMs on Al) can be used to organize the nanoparticles. In other work they used electrostatic interaction to assemble the carboxylic acid functionalized silver nanoparticles (with 4-CTP) on 4-amino thiophenol (4-ATP) SAMs formed on gold surface.[58b] The beauty of this work is that the density of nanoparticles can be tailored by changing the pH of the solution, thus changing the electrostatic interaction between amine moiety of 4-ATP and the carboxylic group on the silver nanoparticle. The reversible and controllable formation of organized structures of this work is extremely attractive and distinguishes it from other schemes, where the control on the nanoparticles assembly is poor.

In all these approaches, the molecules are used like linkers to assemble the nanoparticles. The covalent cross-linking methodology can also be used for the organization of nanoparticle multilayers. Rao and co-workers[59] showed layer-by-layer assembly of colloidal Pt and CdS nanoparticles on gold substrate by forming a covalent linkage between the nanoparticle in different layers via the bifunctional molecule. Furthermore, Brust and co-workers showed the multilayer assembly of gold nanoparticles using thiol as cross linker on functionalized glass surface[60]. These thin film materials obtained by successive self-assembly of Au nanoparticles linked with organic dithiol molecules exhibit nonmetallic optical and electronic properties. The electronic conductivity of the thin films resembles that of nanostructured materials. These results give strong evidence that the individual nanoparticles do not fuse to form bulk gold. They also suggest that it should be possible to control the physical properties of the materials by variation of particle size and spacing, and by the introduction of chemical functionalities as part of the linker units. Natan *et. al.* also adopted a similar strategy to form multilayer of colloidal gold nanoparticles and showed a change in conductivity of the film with the growth of multilayers.[61]

The main drawback of assembling nanoparticles using covalent linkages is that it is irreversible and we do not have any control on the cross linking of the nanoparticles. The other strategy is based on electrostatic interaction in which the driving force for the multilayer film buildup is primarily due to the electrostatic attraction and complex formation between the oppositely charged species.

Electrostatic layer-by-layer self-assembly (LBL-SA) is based on spontaneous ionic adsorption of oppositely charged materials from their aqueous solution and can be a promising technique to fabricate multifunctional thin films containing nanoparticles.[62] The LBL-SA method is an extremely simple process because of its self-assembling nature and can control thickness at a molecular level without costly equipments. Among some advantageous features of LBL, the tolerance to the substrate's shape and material and the dual, organic-inorganic nature of the coatings should be mentioned. Unlike methods with in-situ formation of nanoparticles[63] the LBL technique employs pre made nanoparticles, which provides much higher degree of control over their properties. Since the LBL-SA technique is based on dipping in aqueous solutions, there would be basically

no limitation on the size and shape of substrates with a water-based, environmental friendly process.

Iler showed for the first time the formation of alternate layers of negatively charged silica and positively charged colloidal boehmite alumina particles on smooth surfaces such as glass.[64] The assembly was formed by alternatively immersing the substrate in the two colloidal solutions. However, true layer-by-layer growth was not fully established in this case.[64] Later, Decher and co-workers[65] explored the technique based on alternate adsorption of oppositely charged polyelectrolytes. They demonstrated the layer-by-layer electrostatic self-assembly of cationic and anionic polyelectrolytes as well as multilayer structures consisting of combinations of charged colloidal particles including biomacromolecules such as DNA.[65] Similar strategies were followed by several other groups for the organization of multilayer films of proteins/polyelectrolytes,[66] polyelectrolye/inorganic nanoparticle sandwich structures with nano-magnetite,[67] TiO_2/CdS,[68] SiO_2, TiO_2 and CeO_2,[69] Au[70] as well as quantum dots of CdSe.[71] Electrostatic LBL assembly of inorganic nanoparticles may also be accomplished on the surface of (sub) micron sized polymer spheres.[72] Caruso *et. al.* have shown that anionic SiO_2 nanoparticles of ca. 25 nm diameter may be assembled on the surface of 640 nm diameter negatively charged polystyrene (PS) latex particles using the cationic polyelectrolyte poly(diallyldimethylammonium chloride) PDADMAC as the electrostatic 'glue'. While this method is a simple and general one for preparing surface multilayer films, it suffers from the inevitability of layer interpenetration and some variability of interlayer distances. We have also developed a simple method where gold nanoparticles were directly assembled on polyurethane microspheres. These polyurethane spheres were amine rich and utilized to assemble the gold nanoparticles. These polymer-nano composite materials have great implications in immobilization of biologically important species such as enzymes and in heterogeneous catalytic reactions.[72c]

This technique was extended by Mallouk and co-workers[73] in which they showed the sequential layering of structurally well-defined, two-dimensional colloidal polyanions with a variety of oligomeric and polymeric cations. The anion used was the exfoliated α-$Zr(HPO_4)_2$ (α-ZrP) which was formed by partial exchange of acidic protons of α-$Zr(HPO_4)_2$(α-ZrP) with tetra-n-butylammonium (TBA^+) by reaction with tetra-n-

butylammonium hydroxide (TBA^+OH^-). Sufficient amounts of TBA^+ can be intercalated to cause complete exfoliation, and single, separate layers can be suspended indefinitely in water. When the suspension is placed in contact with a protonated amine-modified surface, the surface NH_3^+ groups displace TBA^+ on one side of the inorganic layers, electrostatically anchoring them to the surface. Virtually any cation can then bind to the surface by replacing the loosely held TBA^+ cations that remain on the other side of the α-ZrP layer. For this purpose polymeric or oligomeric cations, such as poly(ally1amine) hydrochloride (PAH), $Al_{13}O_4(OH)_{12}(H_2O)_{24}^{+7}$ (Al_{13}^{+7}), and cytochrome (cyt *c*) were used. This technique eliminates interlayer penetration and ensures a constant and predictable interlayer distance, while retaining the ease and generality of the polyelectrolyte adsorption process.

A number of groups have used the self-assembled monolayer (SAMs) to construct thin films of nanoparticles by using electrostatic interaction. Earlier work in our laboratory have highlighted that SAMs of 4-aminothiophenol (4-ATP) chemisorbed on thin films of gold may be used to electrostatically bind with silver nanoparticles charged negatively with carboxylic acid functionality by simple immersion of the SAMs in the aqueous nanoparticle solution.[74] In this study, they showed that the density of nanoparticles on SAM is strangely dependent on the pH of the solution. Auer *et. al.* have shown that bis-benzamidines could be used as positively charged bifunctional electrostatic linker molecules in the assembly of negatively charged gold nanoparticles on negatively charged mercaptoundecanoic acid (MUA) SAMs on gold surfaces.[75] The main advantage of this linker molecule is that the total charge density and stability of intermediate double charge linker molecule can be altered by changing the intermediate alkyl chain length of the bis-benzamidine from pentamidine (PAM), to octamidine(OAM) and to dodecamidine (DODAM) which results in potentially tuneable and switchable properties of the entire assembly.

In a different approach based on SAMs, Murray and co-workers have used carboxylate-Cu^{2+} chemistry to assemble nanoparticles in solution as well as to assemble *multilayers* of tiopronin-capped gold nanoparticles on SAMs of mercaptoundecanoic acid (MUA).[76] In the first step, SAMs of MUA on gold thin films was immersed in an ethanolic solution of Cu^{2+} ions to bind the ions to the free, terminal carboxylate ions in

the MUA SAM. This process leads to charge reversal on the SAM and further immersion of the Cu^{2+} ion-covered MUA SAM in a solution containing tiopronin-capped gold nanoparticles leads to the formation of a monolayer of gold nanoparticles on the surface of the SAM. Simple alternate immersion of that film in ethanolic solution of Cu^{+2} and tiopronin-capped gold nanoparticles leads to the formation of multilayers of the tiopronin-gold nanoparticles on the underlying MUA SAM.[76]

We have also developed the methods for the layer-by-layer assembly of metal nanoparticles. The formation of alternating layers of positive and negatively charged nanoparticles on glass substrates occurs due to electrostatic interaction between oppositely charged nanoparticles. The details of this study are discussed in chapter 3.

1.5.5. Bio-macromolecule based methods

As mentioned earlier, the organization of nanoparticles using thiol molecule as a cross linker is irreversible in nature. Therefore, material scientists started looking for alternative strategies for reversible assembly and they found that biomacromolecules can also be used as a cross linking agent to assemble nanoparticles.

Mann and co-workers demonstrated a biomolecule-derived route to the self-assembly of inorganic nanoparticles using the recognition properties of surface-attached antibodies.[77a] This strategy involves the attachment of IgE or IgG antibodies with specific affinity towards dinitrophenyl (DNP) and biotin, respectively, to individual Au nanoparticles. This was followed by addition of bivalent antigens with appropriate double-headed functionalities to these modified nanoparticles. Antigens with homo- (DNP±DNP) or hetero- (DNP -biotin) Janus structures connected by at least an eight-atom spacer were synthesized for this purpose. The formation of specific antibody antigen cross-links between the particles results in the formation of metallic or bimetallic aggregates comprising covalently-linked Au, or Au and Ag nanoparticles. They also showed that higher-order structures in the form of macroscopic filaments of the self-assembled nanoparticles are also produced under certain conditions. In other work Fitzmaurice used streptavidin/biotin interaction to assemble the nanoparticles.[77b] They followed two routes for assembly of nanoparticles in solution. The first route involves the modification of gold nanoparticles by chemisorption of a disulfide biotin analogue

(DSBA), followed by the subsequent addition of streptavidin, while the second route involves the binding of DSBA to the streptavidin prior to addition to gold nanoparticles. Similar strategy was followed by Li *et. al.* in the organization of the iron storageprotein ferritin. The protein ferritin consists of a hollow polypeptide shell of 8 and 12 nm inner and outer diameter respectively, and a 5 nm ferric oxide core.[78] Horse spleen ferritin was biotenylated by nucleophilic coupling of a succinamide derivative of biotin to expose the lysine residue on the protein surface. Subsequently, addition of the tetrameric protein streptavidine to the biotinylated ferritin solution in a controlled manner led to the cross linking of the ferritin molecule and streptavidin and the formation of an organized assembly of the iron oxide core nanoparticles.

Many other reports are also available in which the organization of nanoparticles was done using biological templates such as bacteria, virus, and antibody/antigens. The self-assembled bacterial S-layer was used for the synthesis and organization of quantum dots of CdS.[79a] S-layers are two-dimensional crystalline structure of single protein or glycoprotein monomers (relative molecular mass, M_D 40000 to 200000), and exhibit either oblique (*p*1, *p*2), square (*p*4) or hexagonal (*p*3, *p*4) lattice symmetry with spacing between the morphological units in the range 3-30 nm. Most S-layers are 5-15 nm in thickness, possess pores of identical size and morphology in the 2-6 nm range, and have inner and outer surfaces that are markedly different in topography and physicochemical properties. In this work Shenton *et. al*. first assembled S-layer on a Ni TEM grid by chemical treatment and thereafter, the mineralization of the S-layer was done by placing a drop of $CdCl_2$ solution on it. Finally the S-layer with Cd^{+2} ions were placed in vacuum desiccators containing a dish of acidified Na_2S solution. The transmission electron microscopy measurement of the grid clearly showed the formation of CdS nanoparticles of dimension of 2-3 nm on the S-layer films. The nanoparticles were preferentially deposited within pores between subunits in the S-layers.

Similar strategy was also followed for the synthesis of silica, CdS, PbS and iron oxide nanoparticles using tobacco mosaic virus (TMV) as a template.[79b] The TMV is roughly 300× 18 nm long cylinder structure with a 4 nm wide central channel consisting of 2130 identical protein sub-units arranged in a helical motif around an RNA single strand. The charged amino acid residue on the surface of protein may be used as

nucleation site for inorganic particle deposition and this was demonstrated by the growth of CdS and PbS quantum dots, iron oxide, and SiO_2 on the surface of TMV structures.

DNA is also an excellent template for assembly because of its physicochemical stability and linear structure. These molecules behave like a rigid rod spacer between two tethered functional molecular components on both ends because of the great mechanical rigidity of short double helices.[80] The main advantage of these molecules is their molecular recognition property which could be used to obtain different mesoscopic structure such as junctions (forks), polygons and polyhedra.[81] DNA as a molecular tool is enhanced by our ability to synthesize virtually any DNA sequence of desired length by automated methods, and to amplify any DNA sequence from microscopic to macroscopic quantities by means of polymerase chain reaction (PCR). DNA molecule has all the required properties for molecular construction in the range of about 5 nm up to few micrometer and certainly far better then other materials like polymers, proteins etc.

The first report on the usage of DNA as a stabilizer/template was by Coffer and co-workers in which, they utilize DNA to form mesoscopic aggregates of CdS nanoparticles.[82a] The nanoparticles in their study were formed by first mixing an aqueous solution of calf thymus DNA with Cd^{2+} ions in a sub-stoichiometric quantity.[82a] Then, one molar equiv of Na_2S was added to the solution, resulting in the formation of CdS. High-resolution transmission electron microscopy (HRTEM) confirmed the formation of polydisperse CdS nanoparticles with an average particle size of 5.6 nm. The particles exhibited optical properties characteristic of the formation of quantum-confined particles with an absorption edge of 480 nm, which is blue-shifted from bulk CdS (510 nm). Further studies demonstrated that DNA base sequence, and more specifically the content of the base adenine, had a significant effect on the size of the CdS nanoparticles formed and their resulting photophysical properties.[82b]

These results show the templating action of DNA molecule during formation of the nanoparticles. However, the main problem was the lack of control of predesigned mesoscale structure due to the conformational flexibility of DNA molecule. To overcome the problems of forming well-defined mesoscale structures in solution, Coffer and co-workers developed a new strategy in which they synthesized the nanoparticles onto DNA molecule, which is immobilized on solid substrate.[82c] The size and shape of resultant

nanoparticles assembly can be controlled by selection of the size, shape, and sequence of the polynucleotide template. In a typical experiment, Cd^{2+} ions were added to a solution containing the plasmid DNA to form a plasmid DNA/Cd^{2+} complex, which was subsequently bound to a polylysine- coated glass surface. Exposure to H_2S led to the formation of CdS nanostructures. The measured circumference of the ring (1.2 μm) closely matches the predicted value of the relaxed circular conformation of the plasmid DNA molecule (1.17 μm). They obtained 5 nm sized of CdS nanoparticles along the DNA backbone. Although this strategy is very good for obtaining a different kind of mesostructured just by controlling the sequence and length of DNA, the main drawback of this approach is that it is very difficult to control the particles' size due to weak interaction between nanoparticles and DNA backbone. Other drawback is the relative spacing and orientation of the resulting nanoparticles within the mesostructure and predicting the resulting properties of the materials becomes cumbersome.

Brawn and co-workers used DNA as nanotemplate for growing silver nanowire.[83] A DNA template connecting two gold electrodes was formed first. Next, the sodium ions bound to the phosphate backbone of the λ-DNA were exchanged with Ag ions, and the latter were chemically reduced by hydroquinone. The small silver aggregates formed along the DNA backbone were then used as catalysts for further reductive deposition of silver, eventually leading to the formation of a silver nano wire. This micrometer-sized element with a typical width of 100 nm had a granular morphology. Richter *et. al.* reported the use of λ-DNA for the templated growth of Pd clusters.[84] This was achieved by activation of the DNA with palladium acetate and subsequent reduction of the DNA-bound Pd ions with a sodium citrate/lactic acid/ dimethylamine borane solution. This led to the formation of DNA-associated one- and two-dimensional arrays of well separated 30 ± 5 Å Pd clusters. Subsequent work has focused on the preparation of highly conductive nano wires by using DNA templates.[84]

In a different approach, Mirkin *et. al.* used the molecular recognition properties of DNA to tailor the assembly of nanoscale structures into periodic two and three dimensional structures and this approach was also utilized to develop a colorimetric detection scheme for DNA.[85] In this work, they modified the citrate-stabilized gold nanoparticles with 3' and 5' alkanethiol-capped 12-mer oligonucleotide which are non

complementary to each other. These DNA modified nanoparticles were cross-linked with linker DNA molecule by using Watson-Crick base-pairing. The importance of this strategy is that it allows one to predict arrangement on the nanometer length scale over the meso- and macroscopic distance. Because of the molecular recognition properties associated with the DNA interconnect, this strategy allows one to control particle's periodicity, inter particle distance, and size of the aggregates.

There were several fascinating properties associated with this initial system. First, the particles could be reversibly assembled simply by cycling the temperature of the reaction vessel above and below the melting temperature of the DNA. Second, transmission electron microscopy at early stages in the assembly process revealed two types of nanostructures, small two-dimensional aggregates and larger three-dimensional structures. The third unusual property of this system was the optical change that accompanied particle assembly. The plasmon band that is characteristic of Au nano particles is very sensitive to inter particle distance[86] and also to aggregate size in these systems. It experiences a red shift from 520 to 600 nm as the linking DNA assembles the particles into extended structures. This result in a striking red to blue color change in the solution that can be reversed upon heating the system above the denaturation temperature of the duplex interconnects. From the initial observation of this phenomenon, it became obvious that this system could be useful for studying the factors that control the optical properties of aggregates of nanoclusters and might also be useful for colorimetrically detecting DNA.

Similar strategy was employed by the same group to prepare binary (two-component) network[85b] materials comprising two different-sized oligonucleotide-functionalized nanoparticles. Importantly, the proof-of-concept demonstrations reported herein suggest that this strategy could be extended easily to a wide variety of multicomponent systems where nanoparticle building blocks, which vary in chemical composition or size, are arranged in space on the basis of their interactions with complementary linking DNA. Because of its chemical origin, this strategy is not limited by physical particle size selection rules in forming extended structures; for example, they can prepare unusual structures where particle size ratios ordinarily would not be suitable

for forming binary AB-AB structures (e.g., via sedimentation). They used similar strategy to form layer-by-layer assembly of nanopaticles on solid support.[87]

Shortly after this initial discovery of Mirkin and co-workers, Alivisatos *et. al.* demonstrated that nanocrystal modified with single stranded DNA oligonucleotide of defined length and sequence can be assembled into dimer and trimer on addition of a complementary single stranded DNA template.[88a] On the basis of TEM images of a series of systems studied, the authors concluded that they could align two or three 1.4 nm diameter particles on a single-stranded DNA template such that the particles were aligned in a "head-to-head" or "head-to-tail" fashion. In other reports, they showed the arrangement of DNA modified nanoparticles of 5 and 10 nm into heterodimeric and heterotrimeric[88b] instead of arranging homodimeric and homotrimeric structure. Niemeyer *et al.* have demonstrated a variant of this templating strategy, which utilizes the molecular recognition properties of both DNA/RNA and streptavidin-biotin interactions to organize 1.4 nm Au particles.[89] In this strategy, biotinylated 1.4 nm Au particles are bound to streptavidin-modified oligonucleotides, which are subsequently organized in a "head-to-tail" fashion onto an RNA template. This technique was also used to fabricate two dimensional Au-DNA complexes using a DNA network.[90] DNA was used to create a large template (area over 25 μm^2) on which Au nanoparticles were assembled with an average separation of 260 nm. The structure of the complex was changed by controlling the cross linking of the DNA network. This work shows the potential for controlling the two dimensional arrangement of Au nanoparticles on a large scale. The limitation of this approach is that the hybridized duplex DNA is not sufficiently rigid to dictate a precise spatial arrangement of nanoparticles and it requires the modification of DNA with, for example, thiol functional groups.

The DNA molecule is negatively charged at physiological pH due to phosphate group present in the backbone of DNA molecule. Therefore, electrostatic interaction can also be used to assemble the nanoparticles on DNA chain. Torimoto *et. al.* showed the linear assembly of positively charge thiocholine- modified CdS nanoparticles on DNA chain.[91] As a result of the electrostatic interaction between positively charged nanoparticle surfaces and the phosphate groups of DNA, the particles were found to be assembled in the form of chains. The CdS nanoparticles were arranged in quasi-one-

dimensional dense packing, which revealed interparticle distances of about 3.5 nm, correlating with the height of one helical turn of the DNA double strand.

Our efforts on the organization of nanoparticles using DNA has been highlighted in the chapter 4 of this thesis in which the organization of nanoparticles was done by interconnecting nanoparticles by DNA or by electrostatic complexation of nanoparticles with DNA molecules. Herein, we used DNA as interconnector or as a template for organization of already prepared nanoparticles and for complexation of metal ions and their subsequent reduction leading to arranged nanoparticle assemblies.

1.5.6. Evaporation induced self-assembly of nanoparticles

One of the simplest ways to organize the nanoparticles is by the solvent evaporation technique. The main advantage of this technique is that the formation of a monolayer of nanoparticles organized in a hexagonal network occurs over a long distance range without any external force.

Brust and co-workers[92] developed a protocol in which they synthesized alkanethiol modified nanoparticles in an organic medium. These nanoparticles assemble in hexagonally close packed arrays on a range of surfaces by simple drop coating of the colloidal solution on the desired surface and on evaporation of the solvent.[93] Pileni and co-workes showed the organization of semiconductor Ag_2S nanoparticles on solvent evaporation.[94] They also showed that when a solid support is left in a colloidal solution, self assembly of multilayers organized in the face centered cubic structure is observed. Anders and co-workers reported the formation of a molecularly linked metal cluster from a self-assembled 2-dimensional superlattice.[93c] First they cast the two dimensional assembly of thiol capped gold clusters onto a flat substrate and thereafter they cross linked the nanoparticle by aryl dithiol or aryl di-isonitrile molecules. Thus, most of the protocols in this area pertain to thiol/amine modified nanoparticles where the nanoparticles are in the organic phase in the presence of capping agent.[93d,95] It is often observed that these nanoparticles organize into close-packed structure within an annular ring. Gelbart and co-workers[96] have explained the formation of such annular ring structures in terms of a thermodynamic model.[96c] Schiffrin and co-workers[97a] showed that nanoparticles stabilized by the phase transfer agent ($R_4N^+Br^-$) can be assembled in close

packed structure in which the interparticle separation depends on chain length of $R_4N^+Br^-$. They proposed that the growth of superstructures results from the presence of surface ions on the Au particles. This, in combination with inter-chain dispersion forces, leads to preferential occupancy of the 2 fold sites. They also showed that these alkanethiol-derivatized gold nanocrystals of different well defined sizes organize themselves spontaneously into complex, ordered two dimensional arrays that are structurally related to either colloidal crystal or alloys depending on the particle radii. They found three different kinds of organization on mixing three different sizes of the particles; i) ordered bimodal arrays, ii) size aggregation region containing hexagonal-close packed monodispersed particles and iii) a structure in which particles of different sizes occupy random position in a pseudohexagonal lattice.[97b]

It can be seen from above that the organization of nanoparticles by solvent evaporation technique requires a hydrophobic surface on the particles and this type of ordering is not possible in aqueous environment. In most of the works described above, the nanoparticles are synthesized in organic phase by procedure developed by Brust and co-workers,[92] which involves extraction of metal ion such as chloroaurate ions into toluene using a phase transfer molecule such as tetra-alkylammonium bromide. Thereafter, the reduction of metal ions is done using sodium borohydride in presence of capping agents such as alkanethiol, alkaneamine molecules etc. This protocol has very good control over particles size and monodispersity of nanoparticles; however it is a multi step process, has a poor control on shape of particles and limited for only metals. An alternative approach would be the hydrophobization of nanoparticles synthesized in aqueous phase, which are easier to synthesize than Brust protocol and can be easily extended to other nanomaterials such as semiconductors etc. The hydrophobization facilitates the phase transfer of nanoparticles from aqueous phase to organic phase. The main advantage of these protocols is the transfer of nanoparticles of desired size and shape in organosol and all water soluble reducing reagent and impurity can be easily washed away.

Rao an co-workers developed a simple procedure wherein metal nanoparticles of desired size and shape in a hydrosol can be transferred into nonpolar solvent containing alkanethiol molecule.[98] The alkanethiol molecules capped metal nanoparticles form

nanocrystalline arrays on solvent evaporation. In a related study they showed that alkane thiol modified Pd nanoparticles obtained by phase transfer process, form stable closed packed hexagonal crystalline arrays whose d/l (d:diameter of nanoparticles, l: length of capping agent) value lies in the range of 1.5- 3.8. Large crystals (d/l> 3) form collapsed structure while the nanocrystal with long capping agent (d/l<1.5) is associated structure and exhibit low ordering.[98c] Similar strategy was followed by Chen and co-workers where they showed the phase transfer of cubic platinum nanoparticles in organic solvent containing dodecanethiol (DDT) molecules.[99] These DDT protected nanocrystal also self assembled on transmission electron microscopic grid on solvent evaporation.

Other than organization of nanoparticles in closed packed structure, another importance of this nanoparticle phase transfer is the application of metal particles as catalysts for organic reactions in nonpolar solvents[100] and in the study of effect of physiochemical environment on colloids and on the state of adsorption of molecules on the surface of solid particles in contact with various environments.[101] Therefore various other methods are also available in literature for the phase transfer of nanoparticles. We have also developed the process in which hydrophobization was done by using fatty amine molecules. These amine modified nanoparticles also organized in hexagonal close packed assembly on solvent evaporation, which have been discussed in chapter 5?

Although various methods are known for the phase transfer of nanoparticles from aqueous phase to organic phase, we observed that the phase transfer of nanoparticles in reverse direction (organic phase to aqueous phase) is rare. These protocols could become very useful to obtain

- High concentration of nanoparticles in aqueous phase
- High monodispersity
- Desired size of nanoparticles

Thus, even though this was not directly related to the overall theme of this thesis, we have undertaken certain studies where the reverse phase transfer protocols were developed. In these studies we have utilized an interesting strategy where the formation of interdigitated bilayers on the surface of nanoparticles was exploited to render them hydrophilic. The details of this study have been discussed in chapter 6.

1.6. Work described in the thesis:

The thesis consists of seven chapters. In chapter 2, experimental characterization techniques such as UV-visible spectroscopy, Quartz crystal microgravimetry (QCM), Transmission electron microscopy (TEM), Scanning tunneling microscopy (STM), Fourier Transform infrared spectroscopy (FTIR), X-Ray Photoemission spectroscopy (XPS), etc. that are extensively used for characterization of the nanoparticles have been discussed. The physical principles on which the different techniques are based and their application to understand various aspects of formation of the colloidal nanocomposites have been outlined. The synthesis and surface modification of nanoparticles have also been highlighted in this chapter.

In Chapter 3, the layer-by-layer organization of surface modified nanoparticles (silver and gold) has been discussed. The layer-by-layer assembly was formed by simple immersion of the substrate alternatively in different surface modified nanoparticle solutions. The assembly is driven by attractive electrostatic interaction between charged silinol group on glass slide and the surface group on the particles. It is observed that nanoparticles surfaces modified with the amino acid valine show an amphoteric nature i.e. the charge on the nano particles depends on the pH of the solution. This feature was utilized to form superlattices of nanoparticles on glass which can be easily controlled by changing the pH of the solution.

Chapter 4 outlines the organization of amino acid lysine modified gold nanoparticles in a linear array by using DNA molecule as a template in solution. The process was simplified and a protocol was developed for organizing the nanoparticles just by drop coating. The later part of the chapter is based on the templated synthesis of nanoparticles using immobilized DNA. The DNA molecules were immobilized in thermally evaporated fatty amine films, followed by the incorporation of silver ions and their subsequent reduction. We have also carried out experiments where the DNA was used as an inter connector between the nanoparticles and the details are described in this chapter.

Chapter 5 details our results on the phase transfer of metal nanoparticles from aqueous to organic medium. The main challenge in the synthesis of nanoparticles is to transfer them to various physicochemical environments. In our case the phase transfer of

metal nanoparticles was achieved by modifying them with fatty amine molecule. The nature of bonding of amine molecule with metal nanoparticles was studied by XPS and NMR spectroscopy. In the later part of the chapter, the phase transfer of semiconductor nanoparticles is also discussed.

Chapter 6 describes the phase transfer of nanoparticles from organic phase to aqueous phase. The phase transfer was achieved by modifying the hydrophobized nanoparticles by water-soluble surfactant. These surfactants form a bilayer on the surface of nanoparticles, which make the particles sufficiently hydrophilic and water dispersible. These particles are also highly stable in wide range of pH and high salt concentration.

Chapter 7 summarizes the salient feature of the work detailed in the thesis and briefly discusses possible avenues for future work.

References

1. Faraday, M., Philos.Trans.R.Soc.London.1857, 147, 145.
2. The talk is available on the web at htpp://www.zyvex.com/nanotech/Feynman.html.
3. a) Colvin, V. L.; Goldstein, A. N.; Alivisatos, A. P. *J. Am. Chem. Soc.* **1992**, *114*, 5221. b) Henglein, A. *Ber. Bunsen-ges. Phys. Chem. Chem. Phys.* **1995**, *99*, 903. c) Weller, H. *Angew. Chem. Int. Ed. Engl.* **1993**, *32*, 41. d) Alivisatos, A. P. *Science* **1996**, *271*, 933.
4. a) Colvin, V. L.; Schlamp, M. C. and Alivisatos, A. P. *Nature* **1994**, *370*, 354. b) Wang, Y. and Herron, N. *J. Phys. Chem.* **1991**, *95*, 525.
5. a) Schmid, G. *Chem. Rev.* **1992**, *92*, 1709. b) Hoffman, A. J.; Mills, G.; Yee, H. and Hoffman, M. R. *J. Phys. Chem.* **1992**, *96*, 5546.
6. Hamilton J. F. and Baetzold, R. C. *Science* **1979**, *205*, 1213.
7. a) Klein, D. L.; Roth, R.; Lim, A. K.. L.; Alivisatos, A. P.; and Mceuen P. L. *Nature* **1997**, *389*, 699. b) Weller, H. *Angew. Chem. Int. Ed. Engl.* **1998**, *37*, 1658.
8. a) Wang, Y.; *Acc. Chem. Res.* **1991**, *24*, 133.b)Yoffe, A. D. *Adv. Phys.* **1993**, *42*, 173.
9. Mansur, H. S.; Grieser, F.; Marychurch, M. S.; Biggs, S.; Urquhart, R. S. and Furlong, D. N. *J. Chem. Soc. Faraday Trans.* **1995**, *91*, 665.
10. Symonds, J. L. *Phys. Today* **1995**, *48*, 26.

11. Butlte, J. W. M.; Douglas, T.; Mann, S.; Frankel, R. B.; Mosokovitz, B. M.; Brooks, R. A.; Baumgamer, C. D.;Vymazal, J. and Frank, J. A. *Invest. Radiol.* **1994**, *29*, 5214.
12. Shull, R. D.; McMichael, R. D. and Ritter, J. J. *Nanostruct. Mat.* **1993,** *2*, 205.
13. Ledentsov, N. N.; Grundmann, M.; Kirstaedter, N.; Schmidt, O.; Heitz, R.; Bohrer, J.; Bimberg, D.; Ustinov, V. M.; Shchukin, V. A.; Egorov, Yu. A.; Zhukov, A. E.; Zaitsev, S.; Kop`ev, P. S.; Alferov, Zh. I.; Ruvimov, S. S.; Kosogov, A. O.; Werner, P.; Gosele, U. and Heydenrich, *J. Solid State Electron* **1996**, *40*, 785.
14. Dagani, R. *Chem eng news* **2000** feb 28,
15. Bahnemann, D. W. *Isr. J. Chem*. **1993**, *33*, 115.
16. Satoh, N.; Kimura, K. *Bull. Chem. Soc. Jpn*. **1989**, *62*, 1758.
17. Henglein, A. *J. Phys. Chem*. **1993**, *97*, 5457.
18. Esumi, K.; Tano, T.; Torigoe, K.; Meguro, K. *Chem. Mater*. **1990**, *2*, 564.
19. Pileni, M. P.; Lisiecki, I.; Motte, L.; Petit, C.; Cizeron, J.; Moumen, N.; Lixon, P. *Prog. Colloid Polym. Sci*. **1993**, *93*, 1.
20. Toshima, N.; Yonezawa, T.; Kushihashi, K. *J. Chem. Soc., Faraday Trans*. **1993**, *89*, 2537.
21. Liz-Marzan, L. M.; Philipse, A. P. *J. Phys.Chem*. **1995**, *99*, 15120.
22. a) Southam, G., and Beveridge, T. J. Geochim .Cosmochim.Acta **1996**, *60*, 4369. b) Klaus-Joerger, T., Joerger, R., Olsson, E. and Granqvist, C.G., *Trends Biotech* .**2001**, 19, c) Mukherjee, P., Ahmad, A., Mandal, D., Senapati, S., Sainkar, S.R., Khan, M. I.; Ramani, R., Parischa, R., Ajayakumar, P.V., Alam, M., Sastry, M., Kumar, R. *Angew. Chem. Int. Ed.* **2001**, *40*, 3585. d) Mukherjee, P., Senapati, S., Mandal, D., Ahmad, A., Khan, M. I., Kumar, R., Sastry, M., *ChemBioChem*. **2002**, *3*, 461.
23. a) Brust, M.; Walker, M.; Bethell, D.; Schiffrin, D. J.; Whyman, R. *J. Chem. Soc. Chem. Commun.* **994**, 801; b) Porter, L.A.; Ji, D.; Westcott, S.L.; Graupe, M.; Czernuszewicz, R. S.; Halas, N. J.; Lee, T. R. *Langmuir* **1998**, *14*, 7378.
24. a) Weisbecker, C.S.; Merritt, M.V.; Whitesides, G.M. *Langmuir* **1996**, *12*, 3763; b) Templeton,A. C.; Hostetler, M. J.; Kraft, C.T.; Murray, R. W. *J. Am. Chem. Soc.* **1998**, *120*, 1906.
25. a) Brust, M.; Fink, J.; Bethell, D.; Schiffrin, D. J.; Kiely, C. *J. Chem. Soc. Chem. Commun.* **1995**, 1655; b) Johnson, S. R.; Evans, S. D.; Mahon, S. W.; Ulman, A.

Langmuir **1997**, *13*, 51; c) Mayya, K. S.; Patil, V.; Sastry, M. *Langmuir* **1997**, *13*, 3944.

26. a) Maye, M. M.; Chun, S. C.; Han, L.; Rabinovich, D.; Zhong, C-J. *J. Am. Chem. Soc.* **2002**, *124*, 4958; b) Tan, Y.; Li, Y.; Zhu, D. *Langmuir* **2002**, *18*, 3392; c) Liu, J., Mendoza, S., Roman, E., Lynn, M.J., Xu, R., Kaifer, A.E., *J .Am. Chem. Soc.*, 1999, **121**, 4304.
27. a) a) Leff, D. V.; Brandt, L.; Heath, J. R. *Langmuir* **1996**, *12*, 4723; b) Sastry, M.; Kumar, A.; Mukherjee, P. *Colloids Surf. A* **2001**, 181, 255;c) Kumar; A.; Pattarkine, M.; Bhadbhade, M.; Mandale, A. B.; Ganesh, K. N.; Datar, S. S.; Dharmadhikari, C. V.; Sastry, M. *Adv. Mater* **2001**. *13,* 341.
28. Younan Xia, Y.; Whitesides, G. M. *Angew. Chem. Int. Ed.* **1998**, *37*, 550.
29. Eigler, D. M.; Schweizer, E. K. *Nature* **1990**, *344*, 524.
30. Lyo, L. W.; Avouris, Ph. *Science* **1991**, *253*, 173.
31. Eigler, D. M.; Lutz, C. P.; and Rudge, W. E. *Nature* **1991**, *352*, 600.
32. Resh, R.; Baur, C.; Bucacov, A.; Koel, B. E.; Echternach, P. M.; Madhukar, A.; Montoya, N.; Requicha, A. A. G.; and Will, P. *J. Phys. Chem. B* **1999**, *103*, 3647.
33. Resch, R.; Baur, C.; Bugacov, A.; Koel, B. E.; Madhukar, A.; Requicha, A. A. G. and Will, P. *Langmuir* **1998**, *14*, 6613.
34. Kim, Y. and Lieber, C. M. *Science* **1992**, *257*, 375.
35. Piner, D. R.; Zhu, J.; Xu, F.; Hong, S. and Mirkin, C. A. *Science* **1999**, *283*, 661.
36. Zambroni, F. P. and Crooks, R. M. *J. Amer. Chem. Soc*. **1998**, *120*, 9700.
37. a) Berg, H. C. *Nature* **1998**, *394*, 324.b) Boekema, E. J.; van Breemen,J F. L.; Brisson, A.; Ubbink-Kok, T.; Konings, W. N.; Lolkema, J. S. *Nature* **1999**, *401*, 37.
38. a) Whitesides, G. M. *Sci. Amer. Sept* **1995**, 114.b)Philip, D. and Stoddart, J. F. *Angew. Chem. Int. Ed. Engl.* **1996**, *35*, 1155.
39. a) Radler, J. O.; Koltover, I.; Jamieson, A.; Salditt, T. and Safinya, C. R. *Langmuir* **1998**, *14*, 4272.b) Fendler, J. H. " Biomimetic Chemistry," Wiley, New York **1982.** c) Mansky, P.; Tsui, O. K.; Ressell, T. P.; Gallot, Y. *Macromolecules* **1999**, *32*, 4832.d) Sunder, V. A.; Liedberg, B.; Allara,D. L. *Langmuir* **1995**, *11*, 3882.e)Ulman, A.; " An introduction to ultrathinorganic films: From Langmuir Blodgett to self

assembly," Academic Press, New York, **1991**. f) Whitesides, G. M.; Mathias, J. P. and Seto, C. T. *Science* **1991**, *254*, 1312.

40. Sun, Y.; Walker, G. C. *J. Phys. Chem. B* **2002**, *106,* 2217.
41. Ottewill, R. H. *Langmuir* **1989**, *5*, 4.
42. Dusemund, B.; Hoffmann, A.; Salzmann, T.; Kreigbig, U.; Schmid, G.; *Z. Phys. D* **1991**, *20*, 305.
43. a) Giersig, M.; Mulvaney, P.; *J. Phys. Chem.* **1993**, *97*, 6334. b) Giersig, M.; Mulvaney, P. *Langmuir* **1993**, *9*, 3408.
44. a) Zhao, X. K.; Xu, S.; Fendler, J. H. *Langmuir* **1991**, *7*, 520. b) Zhao, X. K.; Fendler, J. H. *Chem. Mater* **1991**, *3,* 168. c) Zhao, X. K.; Fendler, J. H. *J. Phys. Chem.* **1991**, *95*, 3716. d) Zhao, X. K.; Fendler, J. H. *J. Phys. Chem.* **1990**, *94*, 3384. e) Yi, K. C.; Horvolgyi, Z.; and Fendler, J. H. *J. Phys. Chem.* **1994**, *98*, 3872. f) Yi, K. C. Mendieta, V. S.; Castanares, R. L.; Meldrum, F. C.; Wu, C. and Fendler, J. H. *J. Phys. Chem.* **1995**, *99*, 9869.
45. a) Zhao, X. K.; McCormick, L. D.; Fendler, J. H. *Adv. Mater.* **1992**, *4*, 93.b) Zhao, X. K.; Yang, J.; McCormick, L. D.; Fendler, J. H. *J. Phys. Chem.* **1992**, *96*, 9933. c). Yi, K. C.; Fendler, J. H. *Langmuir* **1990**, *6*, 1519 d) Zhao, X. K.; McCormick, L. D.; Fendler, J. H. *Chem. Mater.* **1991**, *3*, 922. e)Zhao, X. K.; McCormick, L. D.; Fendler, J. H. *Langmuir* **1991**, *7*, 1255.
46. Kotov, N. A.; Zaniquelli, M. E. D.; Meldrum, F. C.; Fendler, J. H.; *Langmuir* **1993**, *9*, 3710.
47. a) Kotov, N. A.; Meldrum, F. C.; Wu, C.; Fendler, J. H. *J. Phys. Chem.* **1994**, *98*, 2735. b) Kotov, N. A.; Meldrum, F. C.; Fendler, J. H. *J. Phys. Chem.* **1994**, *98*, 8827. c) Meldrum, F. C.; Kotov, N. A.; Fendler, J. H. *J. Phys. Chem.* **1994**, *98*, 4506.d) Kotov, N. A.; Zavala, G.; Fendler, J. H. *J. Phys. Chem.* **1995**, *99*, 13065. e) Meldrum, F. C.; Kotov, N. A.; Fendler, J. H. *Chem. Mater.* **1995**, *7*, 1112. f) Meldrum, F. C.; Kotov, N. A.; Fendler, J. H. *Langmuir* **1994**, *10*, 2035. g) Meldrum, F. C.; Kotov, N. A.; Fendler, J. H. *J. Chem. Soc. Faraday Trans.* **1995**, *90*, 673.
48. a) Damle, C.; Gole, A.; Sastry, M. *J. Mater. Chem.* **2000**, *10*, 1389 b) Sastry, M.; Gole, A.; Patil, V. *Thin Solid Films* **2001**, *384*,125. c)Sastry, M.; Patil, V.; Mayya, K.

S.; Sainkar, S. R.; Singh, P. *Thin Solid Films* **1998**, *324*, 239. d) Swami, A.; Kumar, A.; Selvakannan, PR.; Mandal, S.; Sastry, M. *J. Colloi. Inter. Sci.* **2003**, *260*, 367.

49. a) Smotkin, E. S.; Lee, C. A.; Bard, J.; Campion, A.; Fox, M. A.; Mallouk, T. E. Webber, S. E.; White, J. M. *Chem. Phys. Lett.* **1988**, *152*, 265.b) Grieser, F.; Furlong, D. N.; Scoberg, D.; Ichinose, I.; Kimizuka, N.; Kunitake, T.; *J. Chem. Soc. Faraday Trans.* **1992**, *88*, 2207. c) Furlong, D. N., Uquhart, R.; Grieser, F.; Tanaka, K.; Okahata, Y.; *J. Chem. Soc. Faraday Trans.* **1993**, *89*, 2031. d) Xu. S.; Zhao, X. K.; Fendler, J. H. *Adv. Mater.* **1990**, *2*, 183. e) Moriguichi, I., Hosoi, K.; Nagaoka, H. Tanaka, K.; Teraoka, Y.; Kagawa, S.; *J. Chem. Soc. Faraday Trans*. **1994**, *90(2)*, 349. f) Geddes, N. J.; Urquhart, R. S.; Furlong, D. N.; Lawrence, C. R.; Tanaka, K.; Okahata, Y. *J. Phys. Chem.* **1993**, *97*, 13767.
50. a)Peng, X. G.; Lu, R.; Zhao, Y. Y.; Qu, L. H.; Chen, H. Y.; Li, T. J. *J. Phys. Chem.* **1994**, *98*, 7052 b). Pike, J. K.; Byrd, H.; Morrone, A. A.; Talman, D. R. *Chem. Mater.* **1994**, *6*, 1757. c)Luo, X. Z.; Zhang, Z. Q.; Liang, Y. Q. *Langmuir* **1994**, *9*, 3213. d) Urquhart, R. S.; Furlong, D. N.; Mansur,, H.; Grieser, F.; Tanaka, K.; Okahata, Y. *Langmuir* **1994**, *10*, 899. e) Peng, X.; Guan, S.; Chai, X.; Jiang, Y.; Li, T. *J. Phys. Chem.* **1992**, *96*, 3170. f) Zhu, R.; Min, G.; Wei, Y.; Schmitt, H. J. *J. Phys. Chem.* **1992**, *96*, 8210. g) Ravaine, S.; Fanucci, G. E.; Seip, C. T.; Adair, J. H.; Talham, D. R. *Langmuir* **1998**, *14*, 708.
51. (a) Mayya, K. S.; Patil, V.; Sastry, M. *Langmuir* **1997**, *13*, 2575. (b) Mayya, K. S.; Patil, V.; Sastry, M. *J. Chem. Soc., Faraday Trans.***1997**, *93*, 3377.
52. (a) Sastry, M.; Mayya, K. S.; Patil, V.; Paranjape, D. V.; Hegde, S. G. *J. Phys. Chem. B* **1997**, *101*, 4954. (b) Mayya, K. S.; Sastry, M. *J. Phys. Chem. B* **1997**, *101*, 9790. c) Mayya, K. S.; Sastry, M. *Langmuir* **1998**, *14*, 74.
53. Mayya, K. S.; Patil, V.; Kumar, P. M.; Sastry, M. *Thin Solid Films* **1998**, *312*, 300.
54. a)Sastry, M.; Rao, M.; Ganesh, K. N. *Acc. Chem. Res.* **2002**, *35*, 847.b). Sastry, M.; Mayya, K. S. *J. Nanopart. Res.* **2000**, *2*, 183. c) Swami, A.; Kumar, A. ; Selvakannan, PR.; Mandal, S. ; Pasricha, R. ; Sastry, M. *Chem. Mater.* **2003,** *15,* 17.
55. a) Sastry, M.; Patil, V.; Mayya, K. S. *Langmuir* **1998,** *14,* 2707. b)Sastry, M.; Patil, V.; Sainkar, S. R. *J. Phys. Chem. B* **1998,** *102,* 1404. c) Sastry, M.; Patil, V.; Mayya, K. S. *Langmuir* **1997,** *13,* 4490. d) Patil, M.; Malvankar, R. B.; Sastry, M. *Langmuir*

1999, *15*, 8197. e) Patil, M.; Sastry, M. *J. Chem. Soc. Faraday Trans.* **1997**, *93*, 4247. f) Sastry, M.; Gole, A.; Sainkar, S. R. *Langmuir* **2000**, *16*, 3553.

56. Colvin, V. L.; Goldstein, A. N.; Alivisatos, A. P. *J. Am. Chem. Soc.* **1992**, *114*, 5221.
57. Drouard, S.; Hickey, S. G.; Riley, D. J. *J. Chem. Soc. Chem. Commu.* **1999**, *67*.
58. a) Bandyopadhyay, K.; Patil, V.; Vijayamohanan, K. Sastry, M. *Langmuir* **1997**, *13*, 5244 .b) Gole, A.; Sainkar, S. R.; Sastry, M. *Chem. Mater* **2000**, *12*, 1234.
59. Sarathy, K. V.; Thomas, P. J.; Kulkarni, G. U.; Rao, C. N. R. *J. Phys. Chem. B* **1997**, *103*, 399.
60. Brust, M.; Bethell, D.; Kiely, C. J.; Schiffrin, D. J. *Langmuir* **1998**, *14*, 5425.
61. Musick, M. D.; Keating, C. D.; Keefe, M. H.; Natan, M. J. *Chem. Mater.* **1997,** *9,* 1499.
62. a) Decher, G. *Science* **1997**, *277*, 1232.b) Kotov, N. A.; IDe´ca´ny, I.; Fendler, J. H. *J. Phys. Chem.***1995**, *99*,13065. c) Liu, Y.; Wang, A.; Claus, R. *J. Phys. Chem. B* **1997**,*101*,1385.
63. a) Schneider, T.; Haase, M.; Kornowski, A.; Naused, S.; Weller, H.; Forster, S.; Antonietti, M. *Ber. Bunsen-Ges. Phys. Chem. Chem*. **1997**, *101*, 1654.b) Kitazawa, N. *J. Mater. Sci*. **1998**, *33*, 1441. c) De, G. T. *J. Sol.-gel. Sci. Technol*. **1998**, *11*, 289. d) Dante, S.; Hou, Z.; Risbud, S.; Stroeve, P. *Langmuir* **1999**, *15*, 2176.
64. Iler, R. K. *J.Colloid Interface Sci.* **1966**, *21*, 569.
65. a) Decher, G.; Hong, J.-D. *Makromol. Chem., Macromol. Symp.* **1991,** *46*, 321**.** b) Decher, G.; Hong, J. D. *Ber. Bunsen-Ges. Phys. Chem.* **1991,** *95*, 1430**.** c) Decher, G.; Hong, J.-D.; Schmitt, J. *Thin Solid Films* **1992,** *210/211,* 504**.** d) Decher, G.; Schmitt, J. *Prog. Colloid Polym. Sci.* **1992,** *89***,** 160. e) Decher, G.; Essler, F.; Hong, J.- D.; Lowack, K.; Schmitt, J.; Lvov, Y. *Polym. Prepr. (Am. Chem., Soc., Diu. Polym. Chem.)* **1993,** *34*,745**.** f) Decher, G. *Nachr. Chem., Tech. Lab.* **1993,** *41*,793**.** f) Lvov, Y.; Decher, G.; Mohwald, H. *Langmuir* **1993,***9***,**481**.** g) Lvov, Y .; Decher, G.; Sukhorukov, G. *Macromolecules* **1993,** *26*, 5396**.** h) Lvov, Y.; Hass, H.; Decher, G.; Mohwald, H.; Kalachev, A. *J . Phys. Chem.* **1993,** *97*, 12835**.** i) Lvov, Y.; Essler, F.; Decher, G. *J. Phys. Chem.* **1993,** *97*, 13773**.** *j)* Schmitt, J.; Griinewald, T.; Kjaer, K.; Pershan, P.; Decher, G.; Lbche, M. *Macromolecules* **1993,** *26*, 7058**.**
66. Caruso, F.; Niikura, K.; Furlong, D.N.; Okahata, Y. *Langmuir* **1997**, *13*, 3427.

67. Mamedov, A.; Ostrander, J.; Aliev, F.; Kotov, N. A. *Langmuir* **2000**, *16*, 3941.

68. Hao, E.; Yang, B.; Ren, H.; Qian, X.; Xie, R.; Shen, J.; Li, D. *Mater. Sci. Engg. C.* **1999**, *10*, 119.

69. Lvov, Y.; Ariga, K.; Onda, M.; Ichinose, I.; Kunitake, T. *Langmuir* **1997,** *13*, 6195.

70. a) Maya, L.; Muralidharan, G.; Thundat, T.G.; Kenik, E.A. *Langmuir* **2000**, *16*, 9151. b) Feldheim, D.L.; Grabar, K.C.; Natan, M.J.; Mallouk, T.E.; *J.Am.Chem.Soc.* **1996**, *118*, 7640. c) He, J.-A.; Valluzzi, R.; Yang, K.; Dolukhanyan, T.; Sung, C.; Kumar, J.; Tripathy, S. K.; Samuelson, L.; Balogh, L.; Tomalia, D. A. *Chem. Mater.* **1999**, *11*, 3268.

71. Cassagneau, T.; Mallouk, T.E.; Fendler, J.H. *J. Am Chem. Soc.* **1998**, *120*, 7848.

72. a) Caruso, F.; Mohwald, H. *J. Am. Chem. Soc.***1999**, *121,* 6039.b) Dong, A. G.; Wang, Y. J.; Tang, Y.; Ren, N.; Yang, W. L.; Gao, Z. *Chem. Commun.* **2002**, 350.c) Phadtare, S.; Kumar, A.; Vinod, V. P.; Dash,C.; Palaskar, D. V.; Rao, M.; Shukla, P. G.; Sivaram, S.; Sastry, M.; *Chem. Mater.* **2003,** *15,* 1944.

73. Steven W. Keller, Hyuk-Nyun Kim, and Thomas E. Mallouk' *J . Am. Chem. Soc.* **1994***,116,* 8817.

74. Gole, A.; Sainkar, S. R.; Sastry, M. *Chem. Mater.* **2000**, *12*, 1234.

75. Auer, F.; Scotti, M.; Ulman, A.; Jordan, R.; Sellergren, B.; Garno, J.; Liu, G.-Y. *Langmuir* **2000**, *16*, 7554.

76. Zamborini, F. P.; Murray, R. W. *J. Am. Chem. Soc.* **2000**, *122*, 4514.

77. a) Shenton, W.; Davies, S. A.; Mann, S. *Adv. Mater.* **1999**, *11*, 449. b) Connolly, S.; Fitzmaurice, D. *Adv. Mater.* **1999**, *11*, 1202.

78. Li, M.; Wong, K. K. W.; Mann, S. *Chem. Mater.* **1999**, *11*, 23.

79. a) Shenton, W.; Pum, D.; Sleytr, U. B.; Mann, S. *Nature* **1997**, *389*, 585. b) Shenton, W.; Douglas, T.; Young, M.; Stubbs, G.; Mann, S. *Adv. Mater.***1999**, *11*, 253.

80. Saenger, W. *Principles of nucleic acid structure,Springer-Verlag: Berlin,.* **1987**

81. Seeman, N. C. *Nano. Lett*. **2001**, *1***,** 22.

82. a) Coffer, J. L.; Bigham, S. R.; Pinizzotto, R. F.; Yang, H. *Nanotechnology* **1992**, *3*, 69. b) Bigham, S. R.; Coffer, J. L. *Colloids Surfaces A* **1995**, *95*, 211. c) Coffer, J. L.; Bigham, S. R.; Li, X.; Pinizzoto, R. F.; Rho, Y. G.; Pirtle R. M.;Pirtle, I. L. *Appl.Phys.Lett.* **1996**, *69*, 3851.

83. Brawn, E.; Elchen, Y.; Sivan, U.; Ben-Yoseph, G. *Nature* **1998**, *391*, 775.

84. Richter, J.; Seidel, R.; Kirsch, R.; Mertig, M.; Pompe, W.; Plaschke, J.; Schackert, H. K. *Adv. Mater.* **2000**, *12*, 507.

85. a) Mirkin, C. A.; Letsinger, R. L.; Mucic, R. C.; Storhoff, J. J. *Nature* **1996**, *382* 607. b) Mucic, R. C.; Storhoff, J. J.; Mirkin, C. A.; Letsinger, R. L. *J. Am. Chem. Soc.* **1998**, *120***,** 12674. c) Storhoff J J, Elghanian R, Mucic R C, Mirkin C A and Letsinger R L *J. Am. Chem. Soc.* **1998**, 120 1959. *d)* Storhoff J J and Mirkin, C. A. *Chem. Rev*. **1999**, 99, 1849. *e)* Storhoff J J, Mucic R C and Mirkin C A *J. Am. Chem. Soc.* **1997**, 8 179. f) Cao Y. W.; Jin, R. and Mirkin, C. A. *J. Am. Chem. Soc.* **2001**, 123 7961.

86. a) Kreibig, U.; Genzel, L. *Surf. Sci.* **1985**, *156*, 678. (b)Quinten, M.; Schonauer, D.; Kreibig, U. *Z. Phys. D* **1989**, *12*, 521. c)Yang, W.-H.; Schatz, G. C.; Van Duyne, R. P. *J. Chem. Phys.* **1995**, *103*, 869.

87. Taton, T. A.; Mucic, R. C.; Mirkin, C. A.; and Letsinger, R. L. *J. Am. Chem. Soc.* **2000,** *122,* 6305.

88. a) Alivisatos, A. P.; Johnsson, K. P.; Peng, X.;Wilson, T. E.; Loweth, C. J.;Jr, M. P. B.; Schultz, P. G.; *Nature* **1996**, 382, 607. b) Loweth, C. J.; Caldwell, W. B.; Peng, X; Alivisatos, A. P.; and Schultz, P. G. *Angew. Chem. Int. Ed.* **1999**, 38, 1808.

89. Niemeyer, C. M.; Burger, W.; Peplies, J. *Angew. Chem., Int. Ed. Engl.* **1998**, *37*, 2265.

90. Maeda, Y.; Tabata, H. and Kawai, T. *Appl. Phys. Latt.* **2001**, 79, 1181.

91. Torimoto, T.; Yamashita, M.; Kuwabata, S.; Sakata, T.; Mori, H.; and Yoneyama, H. *J. Phys. Chem. B* **1999**, 103, 8799.

92. Brust, M.; Walker, M.; Bethell, D.;Schiffrin, D. J.; Whyman, R. *J. Chem. Soc. Chem. Commu.* **1994**, 801.

93. a) Petit, C.; Talab A. Pileni, M. -P. *Adv. Mater* **1998**, *10*, 259. b) Wang, Z. L. *Adv. Mater* **1998**, *10*, 13. c) Andres, R. P.; Bielefeld, J. D.; Henderson, J. I.; Janes, D. B.; Kolagunta, V. R.; Kubiak, C. P.; Mahoney, W. J.; Osifchin, R. G. *Science* **1996**, *273*, 1690. d) Whetten, R. L.; Khoury, J. T.; Alvarez, M. M.; Murphy, S.; Vezmar, I.; Wang, Z. L.; Stephens, P. W.; Cleveland, C. L.; Luedtke, W. D.; Landman, U. *Adv. Mater.* **1996**, *8,* 428.

94. a) Motte, L.; Billoudet; F.;and Pileni, M. P. *J. Phys. Chem.* **1995**, *99*, 16425. b) Motte, L.; Billoudet; F.; Lacaze, E. and Pileni, M. P. *Adv. Mater*. **1996**, *8*, 1018.

95. a) Leff, D. V.; Ohara, P. C.; Heath, J. C.; Gelbart, W. M. *J. Phys. Chem.* **1995**, *99*, 7036. b) Hosteler, M. J.; Stokes, J. J.; Murray, R. W. *Langmuir* **1996**, *12*, 3604. c) Harfenist, S. A.; Wang, Z. L.; Alvarez, M. M.; Vezmar, I; Whetten, R. L. *J. Phys. Chem. B* **1996**, *100*, 13905. d) Heath, J. R.; Knobler, C. M.; Leff, D. V.; *J. Phys. Chem. B* **1997**, *101*, 189.e) Brust, M.;Fink, J.; Bethell, D.;Schiffrin, D. J.; Kiely, C. *J. Chem. Soc. Chem. Commu.* **1995**, 1655. f) Leff, D. V.; Brandt, L.; Heath, J. R. *Langmuir* **1996**, *12*, 4723. g) Templeton, A. C.; Hostetler, M. J.; Kraft, C. T.; Murray, R. W. *J. Amer. Chem. Soc.* **1998**, *120*, 1906.

96. a) Ohara, P. C.; Heath, J. R.; Gelbart, W. M. *Angew. Chem, Int. Ed. Engl.* **1997**, *36*, 1077. b) Vossmeyer, T.; Chung, S. –W.; Gelbart, W. M.; Heath, J. R. *Adv. Mater.* **1998**, *10*, 351.c) Ohara, P. C.; Gelbart, W. M. *Langmuir* **1998**, *14*, 3418.

97. a) Fink, J.; Kiely, C. J.; Bethell, D.;Schiffrin, D. J. *Chem. Mater.* **1998**, *10*, 922. b) Kiely, C. J.; Fink, J.; Brust, M.; Bethell, D.;Schiffrin, D. J. *Nature* **1998**, *396*, 444.

98. a) Sarathy, K.V.; Kulkarni, G.U.; Rao, C. N. R. *Chem. Commun.* **1997**, 537.b) Sarathy, K. V.; Raina, G.; Yadav, R.T.; Kulkarni, G. U.; Rao C. N. R. *J. Phys. Chem. B.***1997**, *101*, 9876. c) Thomas, J. P.; Kulkarni, G.U.; Rao, C. N. R. *J. Phys. Chem.* **2000***, 104,* 8138.

99. Zhao, S.-Y.;Shen-Hao Chen, S.-H.; Wang, S.-Y.; Li, D.-G.; Ma, H.-Y. *Langmuir* **2002**, *18,* 3315.

100.a) Andrews, M. P.; Ozin, G. A. *J. Phys. Chem*. **1986**, *90*, 2929. b) Nakao, Y.; Kaeriyama, K. *J. Colloid Interface Sci*. **1989**, *131*, 186.

101.a) Efrima, S. *Heterog. Chem*. Rev. **1994**, *1*, 339. (b) Mulvancy, P. *Langmuir* **1996**, *12*, 788.

CHAPTER II

Experimental Section

This chapter describes the different methods for synthesis and surface modification of nanoparticles. Experimental techniques used for characterization of nanoparticles and thin films during the course of the present work have also been discussed.

The present work mainly emphasizes on the hydrophobization and organization of inorganic nanoparticles. These inorganic nanoparticles have been synthesized and surface modified by different methods, which are discussed in this chapter. The characterization at different stages of synthesis and organization of nanoparticles have been probed by the following techniques: UV-visible spectroscopy, Fourier transform infrared spectroscopy (FTIR), X-ray photoelectron spectroscopy (XPS), X-ray diffraction technique (XRD), Transmission electron microscopy (TEM), Scanning tunneling microscopy (STM), Thermal gravimetric analysis (TGA), Differential thermal analysis (DTA), Differential scanning calorimetry (DSC), Nuclear magnetic resonance spectroscopy (NMR) and Quartz crystal microgravimetry (QCM). This chapter briefly deals with the experimental techniques used for different characterization of the nanoparticles synthesized in the present work.

2.1. Materials

2.1.1. Chemicals.

4-aminothiophenol (4-ATP:$NH_2C_6H_4SH$) and 4-mercaptobenzoic acid (4-CTP:$COOHC_6H_4SH$) were purchased from Sigma chemicals and used without any further purification. Chloroauric acid ($HAuCl_4$), amino acids valine [$(CH_3)_2CH(NH_2)(COOH)$] and lysine [$NH_2(CH_2)_4CH(NH_2)(COOH)$], octadecylamine (ODA: $CH_3(CH_2)_{17}NH2$), dodecylamine (DDA: $CH_3(CH_2)_{11}NH_2$), Sodium hydroxide (NaOH), were obtained from Sisco Research Laboratory Pvt. Ltd, India. Octadecanethiol (ODT: $CH_3(CH_2)_{17}SH$), Ethidium bromide, Cadmium chloride ($CdCl_2$), Sodium sulfide (Na_2S) were purchased from Merck, Germany. Silver sulfate (Ag_2SO_4), hydrazine (N_2H_4), Sodium chloride (NaCl), Sodium borohydride ($NaBH_4$), Hydrogen peroxide (H_2O_2), Citric acid, potassium dichromate ($K_2Cr_2O_7$) were from S. D. Fine-chem. Ltd. India.

2.1.2. Solvents:

Chloroform ($CHCl_3$), hexane (C_6H_{14}), benzene (C_6H_6), isopropanol (iso-C_3H_7OH), methanol (CH_3OH), ethanol (C_2H_5OH), acetone (CH_3COCH_3), of AR grade were purchased from Merck and used without any further purification. Laboratory grade

sulfuric acid (H_2SO_4), hydrochloric acid (HCl), nitric acid (HNO_3) was used for several experiments. Double distilled water was used wherever required.

2.1.3. Preparation of DNA:

In the present work, both synthetic DNA and calf thymus DNA were used as templates for the organization of the gold nanoparticles. Sixteen- and 30-mer oligonucleotide of sequences GGAAAAAACTTCGTGC (DNA 1) and CCTTAAGCTTTTGTAGAATCTATCTACATA (DNA 2) were synthesized by β-cyanoethyl phosphoramidite on a Pharmacia GA plus DNA synthesizer, purified by FPLC and rechecked by RP HPLC. The oligonucleotides were hybridized by heating an equimolar mixture of DNA 1 and DNA 2 (10^{-6} M concentration) with their complementary DNA strandds in 1 mM NaCl aqueous solution at 90 ^{o}C followed by slow cooling. Ethidium bromide was used as the fluorescent intercalator for both the DNA molecules.

2.2. Synthesis and modification of nanoparticles

2.2.1. Synthesis of 4-carboxythiophenol (4-CTP) modified silver nanoparticles

The silver nanoparticle solution was prepared by a method reported by Vukovic and Nedeljkovic[1] which involves borohydride reduction of Ag_2SO_4 salt solution. 100 ml of 10^{-4} M of silver sulfate solution was added into dry flask containing 0.01 g of sodium borohydride and stirred rigorously.

$$Ag_2SO_4 + NaBH_4 \leftrightarrow Ag + BH_4^- + NaOH$$

This procedure yielded a clear yellow solution at pH ~ 8.5. 100 ml of the sol was mixed with 10^{-3} M 4-CTP in absolute ethanol to give the final concentration of 10^{-5} M of 4-CTP, which was rigorously mixed. The UV-vis spectra of the silver nanoparticle solution before and after capping with 4-CTP is shown in Figure 2.1.

The solid line refers to the spectrum of as-prepared silver nanoparticle solution while the dashed line is the spectrum recorded 48 hours after capping the silver

nanoparticles. The resonance at ca. 380 nm in the UV-vis spectrum of the silver nanoparticles in water arises

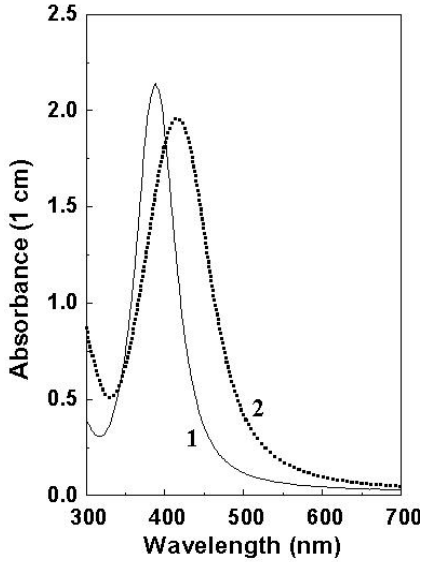

Figure 2.1: UV-vis spectra of silver nanoparticle solution before (solid line) and after 48 h of capping with 4-CTP (dashed line) at pH ~`8.5.

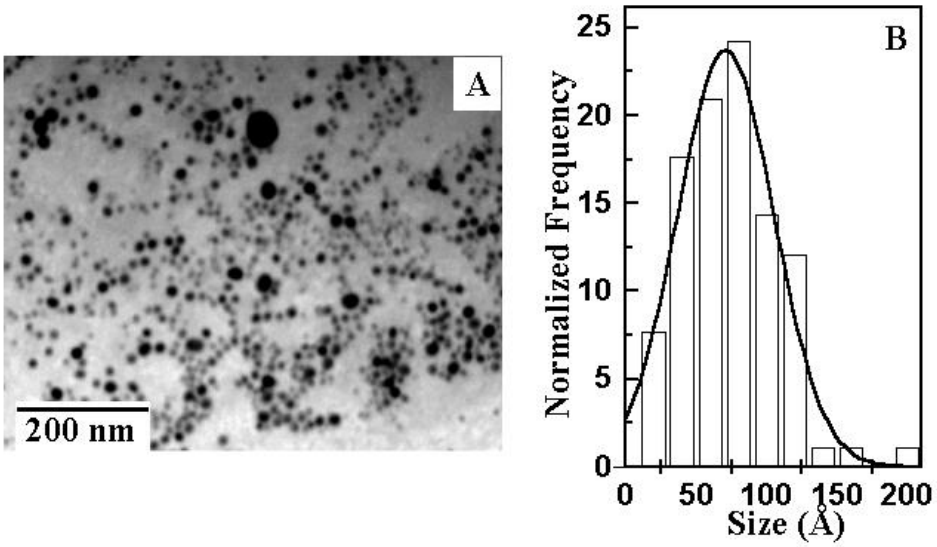

Figure 2.2: A) TEM image of drop-coated film of 4-CTP capped silver nanoparticles deposited on carbon coated TEM grid. B) Particle size distribution measured from figure A.

due to excitation of surface plasmon vibrations in the silver nanoparticles and is responsible for the striking yellow color of silver nanoparticle solutions. It is observed

that the surface plasmon resonance is broadened and shifted to ca. 415 nm (curve 2) after capping with 4-CTP of the nanoparticles indicating surface binding of the 4-CTP molecules to the silver nanoparticles surface.

Drop coated film from 4-CTP capped silver nanoparticle solution was formed on carbon coated copper grid and analyzed by TEM. Figure 2.2A shows a representative TEM image of 4-CTP capped silver nanoparticles while Figure 2.2B is a plot of the particle size distribution (PSD) histogram measured from an analysis of 150 particles in Figure 2.2A and other micrographs. A Gaussian fit to the PSD histogram yielded a particle size of 71 ± 34 Å.

2.2.2. Synthesis of gold nanoparticles

Similar to silver nanoparticle solution, gold nanoparticles were also prepared by reducing 100 ml of 1.25×10^{-4} M $HAuCl_4$ solution in water using sodium borohydride (0.01g). A clear red solution was obtained with pH~9. The optical absorption spectrum of the nanoparticle solution showed surface plasmon maxima at 530 nm.

2.3.2.1. Modification of gold nanoparticles with amino acid, valine.

The gold nanoparticles were thereafter capped with the amino acid, L-valine, by mixing a carefully weighed quantity of the amino acid to yield an overall valine concentration of 10^{-4} M. The pH of the valine-capped gold nanoparticle solution was adjusted to the values 8.5 and 3.5 by addition of dilute HCl. The PI (isoelectric point) of valine is ca. 6 and therefore, the gold nanoparticles are expected to acquire a net negative and positive charge above and below pH~6 respectively. The stability of the nanoparticle solution at these pH values is a good indicator of the surface binding of the valine molecules and was studied by UV-vis. spectroscopy.

Figures 2.3A and 2.3B show the spectra of valine-capped gold nanoparticle solutions at pH~8.5 and pH~3.5 respectively recorded as a function of time after capping with the amino acid. The spectra have been displaced vertically for clarity. It is seen from Figure 2.3A that there is little change in the spectrum of the gold nanoparticle solution even after aging for 48 h and indicates electrostatic stabilization of the gold nanoparticles

at both pH values. From the UV-vis. results presented in Figure 2.3, it is inferred that

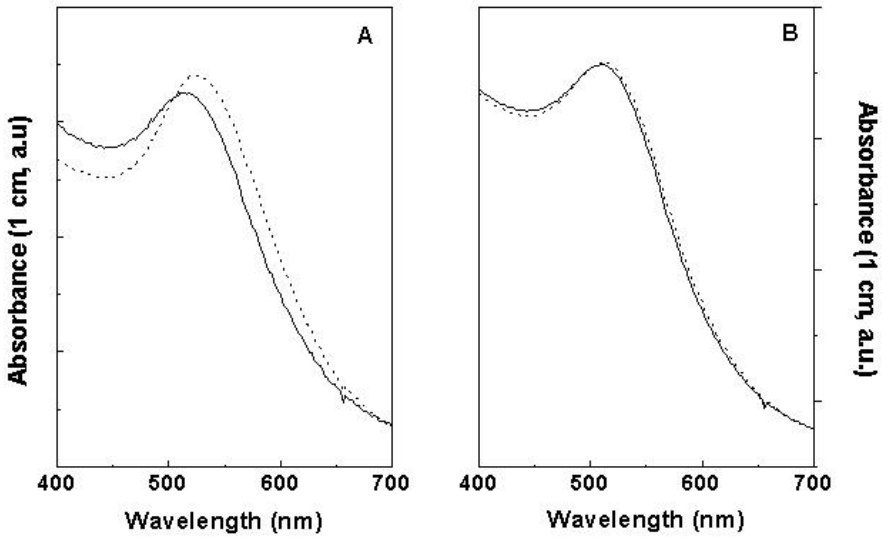

Figure 2.3: A) UV-vis spectra of aqueous solution of gold nanoparticles capped with valine monolayer at pH ~ 8.5 immediately after capping (solid line) and after 48 h of capping (dashed line). B) UV-vis spectra of aqueous solution of gold nanoparticles capped with valine monolayer at pH ~ 3.5 immediately after capping (solid line) and after 48 h of capping (dashed line).

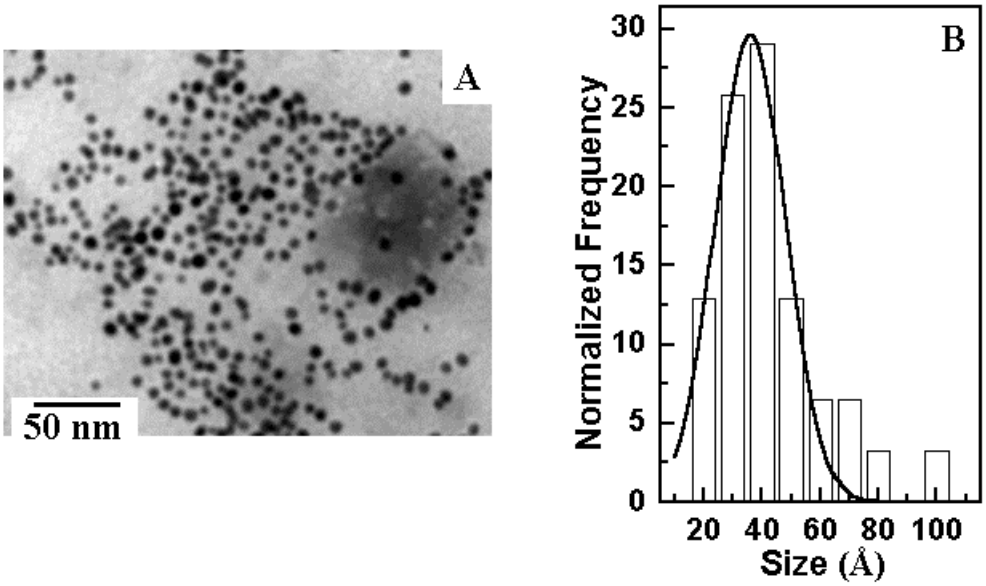

Figure 2.4: A) TEM image drop coated film of valine capped gold nanoparticles deposited on carbon coated grid. B) Particle size distribution measured from Figure A.

valine is bound to the surface of the gold particles and furthermore, that ionization of the carboxylic acid and amine functional groups at solution pH values of 8.5 and 3.5

respectively is responsible for the particle stability. The stabilization at low pH could occur through protonation of the amine groups via formation of a $-NH_2^+-Au^0$ complex and thus provides the necessary electrostatic stabilization.

Figure 2.4A shows a representative TEM image of valine capped gold nanoparticles while Figure 2.4B is a histogram showing the particle size distribution (PSD) measured from an analysis of 150 particles in Figure 2.4A and other micrographs. A Gaussian fit to the PSD histogram yielded a particle size of 36 ± 12 Å.

2.2.2.2. Modification of gold nanoparticles with amino acid, lysine.

The pH of the borohydride reduced gold nanoparticles solution was adjusted to 7 using dilute HCl following which the gold nanoparticles were modified with amino acid L-lysine molecules (PI ~ 8.5). Carefully weighed quantity of the lysine was mixed to the borohydride reduced gold nanoparticle solution to yield an overall lysine concentration of 10^{-5} M. Figure 2.5 shows the UV-vis spectra of the gold nanoparticle solution before

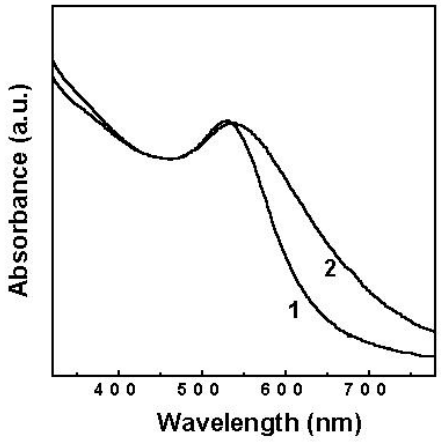

Figure 2.5: UV-vis spectra of gold nanoparticle solution before (curve 1) and after capping with lysine (curve 2).

capping (curve 1) and the spectrum measured after capping with amino acid lysine at pH ~ 7 (curve 2). A small red shift in the gold surface plasmon resonance from 530 nm to 538 nm was observed indicating surface co-ordination of the lysine molecules with gold nanoparticles.

Figure 2.6A shows a representative TEM image of lysine capped gold nanoparticles while Figure 2.6B is a plot of the particle size distribution (PSD) histogram

measured from an analysis of 150 particles in Figure 2.6A and other micrographs. A Gaussian fit to the PSD histogram yielded a particle size of 40± 7 Å.

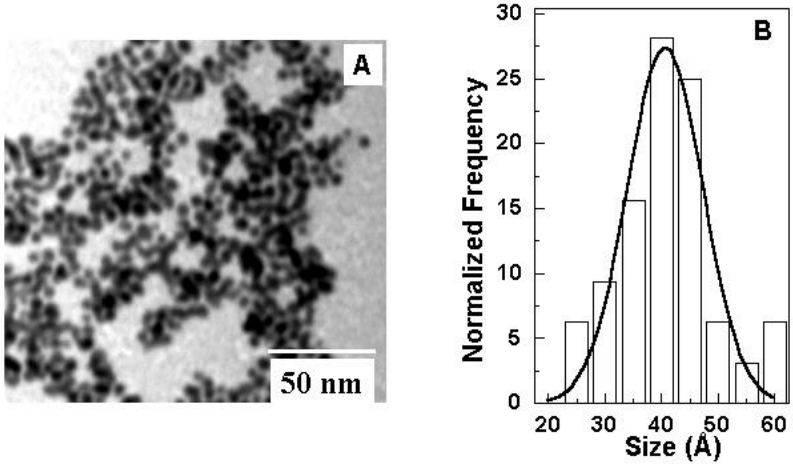

Figure 2.6: A) TEM images of lysine capped gold nanoparticles film formed on carbon coated grid by drop coating. B) Particles size distribution measure from figure A.

2.2.3. Synthesis of 4-ATP modified gold nanoparticles by citric acid

The gold colloid was prepared by a method reported by Lee and Maisel[4] which involves the reduction of chloroauric acid with citric acid. 240 mg of chloroauric acid ($HAuCl_4$) was dissolved in 500 ml of water and the solution was boiled after which, a solution of 1% sodium citrate (50 ml) was added with continued boiling for ~1 hour.

The particles were derivatized with 4-aminothiophenol (4-ATP) by mixing 1 ml ethanolic solution of 4-ATP to 9 ml of the citric acid reduced gold solution to yield an effective concentration of the 4-ATP in solution of 10^{-4} M. The pH of the gold nanoparticles solution was ca. 4 and capping with 4-ATP was effected at this pH in order to electrostatically stabilize the particles after capping. It is known that thiol groups covalently bind to gold particle surfaces and in analogy with the 4-CTP capping protocol which results in carboxylic acid derivatization of the nanoparticles,[5] surface-coordination of 4-ATP with the gold particles is expected to lead to amine functionalization of the gold nanoparticle surface. Figure 2.7 shows the UV-vis spectra of the gold nanoparticle solution before capping (solid line) and the spectrum measured 48 h after capping with 4-ATP at pH ~ 4 (dashed line). A small red shift of the gold plasmon resonance together with a weak damping of the resonance intensity is observed and indicates capping of the

gold nanoparticles with 4-ATP. It is important to note that the particles are stable in solution and no significant aggregation is detected from the UV-vis spectrum.

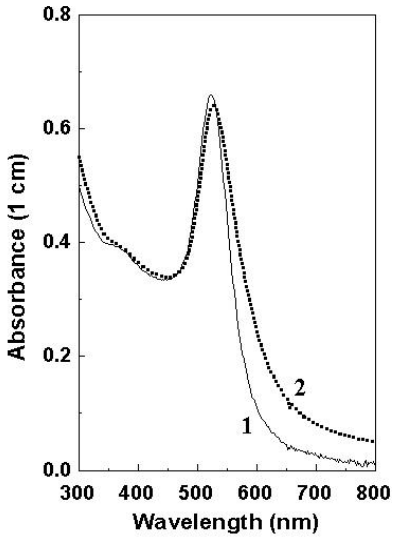

Figure 2.7: UV-vis spectra of gold nanoparticles solution before (solid line) and after 48 h of capping with 4-ATP (dashed line) at pH ~4.

Figure 2.8A shows representative TEM image recorded from solution-cast film of 4-ATP capped gold nanoparticles. It is clear from the TEM image that particles are well separated from each other. Figure 2.8B shows the particle size distribution (PSD) measured from the image shown in Figure 2.8A based on an analysis of 150 gold nanoparticles. A Gaussian fit to the PSD histogram yielded a particle size of 130± 27 Å.

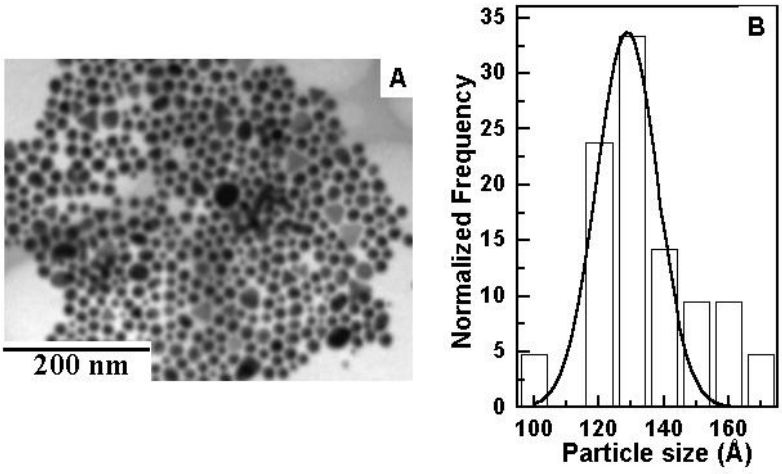

Figure 2.8: A) TEM images of 4-ATP capped gold nanoparticles film formed on carbon-coated grid by drop coating. B) Particles size distribution measure from figure A.

2.3. Characterization techniques:

2.3.1. UV-visible spectroscopy:

We have extensively used UV-vis spectroscopy for the characterization of metal nanoparticles (gold and silver) since they exhibit strong surface plasmon resonance absorption in the visible region, and are highly sensitive to surface modification.

All the UV-vis spectroscopy measurements were performed on a Hewlett-Packard HP 8542A diode array spectrophotometer operated at a resolution of 2 nm in transmission mode at ambient temperature either in solution or in the film form. The films were formed by simple drop coating technique on quartz substrate.

2.3.2. Fourier Transform Infrared spectroscopy (FTIR):

The IR characterization was carried out on a Shimadzu 8201 PC FTIR spectrometer or Perkins Elmer spectrophotometer spectrum 1 operated in the diffuse reflectance mode in the range of 4000-400 cm^{-1} at a resolution of 4 cm^{-1}. Generally, a total of 256 scans yielded a good signal to noise ratio of the IR spectra. Films formed on silicon substrates by solvent evaporation technique are preferred for these studies for a variety of reasons. Silicon is chemically very stable and generally not very reactive even at high temperatures. It has no strong lattice absorption bands in the useful regions of the infrared and thus can be used for transmission studies in this region. To correct for the lattice absorption bands in silicon, a blank silicon sample is used as a reference. All FTIR data presented in the thesis have been presented after the necessary baseline corrections.

2.3.3. NMR spectroscopy:

Nuclear magnetic resonance Spectroscopy (NMR) is very good tool for the determination of the structure and dynamics of monolayer on nanoparticles. It also gives information about the order –disorder transition and interaction between stabilizing agent and metal nanoparticles. Known quantities (~10 mg/ml) of the purified monolayer protected nanoparticles powders were dissolved in $CDCl_3$ and the solutions analyzed by ^1H NMR. ^1H NMR spectra of the nanoparticles solutions were recorded on a Bruker AC

200 MHz instrument and scanned in the range 0 to 15 ppm. By looking at the chemical shift of protons present in different chemical environment in the molecule, the structure of molecule and its interaction with nanoparticles can be determined.

2.3.4. Thermal analysis (TGA /DTA/DSC):

These techniques are very useful to study the physical properties related to phase transitions such as temperature of transition, energy of transition, stability, chemical reaction of material as a function of temperature etc. TGA /DTA of the purified nanoparticles powder was done on a TGA-7 Perkin Elmer instrument in the temperature range 0 - 800 ^{o}C at a scan rate of 10 ^{o}C/min. Differential scanning calorimetric measurements were carried out using DSC-7 Perkin Elmer unit from 25 to 325 ^{o}C at a heating rate of 10 ^{o}C/min under nitrogen environment.

2.3.5. X-Ray Diffraction:

Powder x-ray diffraction technique has been used to determine phase purity, crystal structure and to roughly estimate the size of the nanocrystallites. X-ray diffraction patterns have been obtained with a Philips-Norelco diffraction model PW1730 instrument using monochromatic high intensity CuK_{α} radiation (λ=1.54056 Å). A nickel filter is used to eliminate the K_{β} lines. All the XRD measurements were done with drop coated films of nanoparticles on Si (111) substrate. The average crystallite size of the nanoparticles can be obtained from the XRD pattern using the Deby-Seherrer formula.

$$t = \frac{0.9 \cdot \lambda}{\beta \cdot Cos\ \theta}$$

where t is the crystallize size, λ the wavelength of X-ray, β is the full width at half maxima and 2θ is the center of the peak.

2.3.6. Transmission Electron Microscopy (TEM):

We have used TEM analysis to estimate the size of the metal nanoparticles and their state of assembly. TEM samples were prepared by placing a drop of the nanoparticles solution onto a carbon coated copper TEM grid. After 5 minutes, the excess

amount of the solution was removed using a blotting paper. TEM measurements were performed on a JEOL Model 1200EX instrument operated at an accelerating voltage of 120 kV.

2.3.7. Scanning Tunneling Microscopy (STM):

This technique can be used to obtained surface structure and surface morphology. It is very sensitive technique and has the capability to provide a picture of the atomic arrangement of a surface. In the present work, STM was used to image the organization of nanoparticles in a drop-coated film of nanoparticles solution on a conducting silicon wafer. STM measurements were performed on home built STM. This STM was fabricated and constructed by Dr. C. V. Dharamadhikari at University of Pune.

2.3.8. Fluorescence spectroscopy:

The double helical structure of DNA molecule can be confirmed by introduction of the well known fluorescent dye, ethidium bromide.[6] Enhanced fluorescence signal from the ethidium bromide molecule occurs upon intercalation into the double helical DNA structure[7] and thus may be used to confirm the retention of the DNA double helical structure after binding with nanoparticles. In the present work, fluorescence measurements were done on a Perkin Elmer model LS 50-B spectrometer at 25 ^{0}C, with a slit width of 5 nm for the excitation at 460 nm and 10 nm for the emission monochromator.

2.3.9. X-Ray Photoelectron spectroscopy (XPS):

XPS is a surface characterization technique and useful for characterization of the nanoparticles, multilayer films of nanoparticles and to understand the interaction between nanoparticles and capping agent. The measurements were carried out on a VG MicroTech ESCA 3000 instrument at a pressure of better than 1 x 10^{-9} Torr. The general scan of desired core level spectra were recorded with un-monochromatized Mg K_α radiation (photon energy = 1253.6 eV) at a pass energy of 50 eV and electron takeoff angle (angle between electron emission direction and surface plane) of 60^o. The overall resolution was ~ 1 eV for the XPS measurements. The core level spectra were background corrected

using the Shirley algorithm[8] and the chemically distinct species resolved using a non-linear least squares procedure. The core level binding energies (BE) were aligned with the adventitious carbon binding energy of 285 eV.

2.3.10. Ellipsometry:

Ellipsometry is one of the most versatile techniques for the study of optical properties of thin films on either solid or liquid surfaces. We have used ellipsometry to calculate the packing density of nanoparticles in multilayer nanoparticles films. Ellipsometry measurements of the growth of the individual layers of nanoparticles on glass were performed using a manually operated Gaertner L 119 null ellipsometer operated in the polarizer-compensator-sample-analyzer (PCSA) mode at an angle of incidence of 60^{o}. One side of the glass substrate was made optically rough to prevent specular reflection of the laser beam from that surface and the other, optically flat surface, was exposed sequentially to the different colloidal solutions. The compensator was a quarter wave plate set with the optical axis at 45^{o} to the plane of incidence. The light source was a He-Ne laser (5 mW), the wavelength being 6328 Å. The ellipsometric angles Ψ and Δ were determined from a measurement of the polarizer and analyzer angles in four zones to correct for any instrument misalignment. A photomultiplier was used to determine the extinction (null) condition precisely.

2.3.11. Thermal evaporation of fatty lipid:

The lipid films used for DNA immobilization in the present work have been deposited using an Edwards E306 coating unit. The coating unit consists of a rotary pump, which can pump upto 10^{-3} Torr. Below this pressure, an oil diffusion pump is employed and can go upto 10^{-7} Torr. Both these pumps are used in conjunction for backing and roughing the deposition chamber. A liquid nitrogen trap was also used. Deposition of organic thin films is done under vacuum due to the following reasons: a) the quality of deposition is better due to the increased mean free path of a molecule under vacuum as compared to atmosphere. This result in a linear trajectory of the thermally evaporated molecule; b) the melting point is reduced under vacuum enabling low current requirements for thermal evaporation. The amphiphilic molecules required for deposition,

were taken in a molybdenum boat and subjected to a low tension DC of about 20 amps under 10^{-7} Torr vacuum. Different substrates such as Si (111), glass, quartz were kept at a suitable distance above the molybdenum boat. The molecules when heated evaporate and condense onto these substrates giving uniform films on each substrate with roughly the same thickness. The deposition was monitored *in situ* using an Edwards FTM5 quartz crystal microbalance. The films deposited were tested by IR for possible decomposition, and were found that the films did not decompose on deposition in vacuum.

2.3.12. Self-organized Multilayers (SOMs):

In earlier studies in this group, it has been shown that thermally evaporated films of fatty acids/amines can be spontaneously organized via selective ionic interaction of cations/anions by simple immersion of the film in a suitable electrolyte.[9] This leads to an organized lamellar film structure similar to c-axis oriented Y-type LB films, which is termed as self-organized multilayers (SOMs). Recognizing that this principle is general, it was extended to the electrostatic binding of surface modified colloidal nanoparticles[10], and intercalation of proteins/enzymes[11]/DNA. In our work, the intercalated DNA in lipid film has been used as a template for the growth of nanoparticles. The process has been explained in detail in Scheme 1.

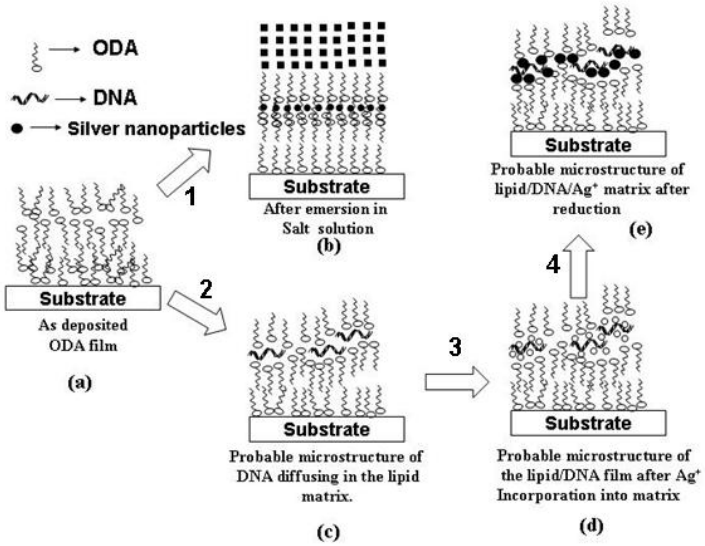

Scheme 1. Scheme showing the formation of the fatty acid salts, DNA-lipid composites by simple immersion protocols and growth of nanoparticles

Step1 involve the spontaneous organization of thermally evaporated fatty acid/amine films via selective ionic interactions of cations/anions by immersion of the film in a suitable electrolyte solution. This leads to an organized lamellar film structure similar to c-axis oriented Y-type LB films. This protocol was further extended towards the realization of DNA thin films (Step 2). This DNA composite film was then immersed in silver salt solution to incorporate silver ions (Step 3) and thereafter silver nanoparticles were formed on DNA backbone by reducing it in hydrazine atmosphere (step 4).

2.3.13. Quartz crystal microgravimetry:

Quartz crystal based microgravimetry is a powerful tool to study various adsorption processes and has been used to study adsorption of gases,[12a,b] self-assembled monolayers (SAMs),[12c-e] Langmuir-Blodgett films,[12f,g] nanoparticles,[12f-j] and biomolecules.[12k-n] For the work discussed in this thesis, QCM has been extensively used for calculating the amount of entrapped DNA and silver ions in the lipid film.

We have used gold-coated AT-cut 6 MHz quartz crystals in all the studies. The frequency counter used was an Edwards FTM5 instrument operating at a frequency stability and resolution of $\pm$ 1 Hz. At this frequency, the mass resolution would be 12 ng/cm^2. We have used QCM technique in the following way. Different thickness films of lipids were thermally evaporated on the QCM crystals. These crystals were immersed in DNA solutions and the frequency changes were measured *ex-situ* at different time intervals after thorough washing (in deionized water) and drying (in flowing nitrogen) of the crystals. The mass uptake was estimated from the observed frequency changes using the Saurbrey formula.[13]

2.4. References:

1. Vukovic, V. V.; Nedeljkovic, J. M. *Langmuir* **1993**, *9*, 980.
4. Lee, P. C.; Maisel, D. *J. Phys. Chem.* **1982**, *86*, 3391.
5. Mayya, K. S.; Patil, V.; Sastry, M. *Langmuir* **1997**, *13*, 2575.
6. Lepecq, J. B.; Paoletti, C. *J. Mol. Bio.* **1967**, *27*, 87.
7. Sastry, M.; Kumar, A.; Pattarkine, M.; Ramakrishnan, V.; Ganesh, K. N. *J. Chem. Soc. Chem. Commun.* **2001**,1434.

8. Shirley, D.A. *Phys. Rev. B.* **1972**, *5*, 4709.

9. a) Ganguly, P.; Pal, S.; Sastry, M.; Shashikala, M.N. *Langmuir* **1995**, *11*, 1078; b) Pal, S. Ph.D. Thesis, University of Poona, **1996**; c) Gole, A.; Sastry, M. *Inorg. Chem. Commun*., **2001,** *4*, 568.

10. a) Patil, V.; Mayya, K. S.; Sastry, M. *Langmuir* **1998,** *14*, 2707; b) Sastry, M.; Patil, V; Mayya, K.S. *Langmuir* **1997**, *13*, 4490; c) Sastry, M.; Patil, V.; Sainkar, S. R. *J. Phys. Chem. B.* **1998**, *102*, 1404; d) Patil, V.; Sastry, M. *Langmuir* **2000**, *16*, 2207; e) Patil, V.; Sastry, M. *Langmuir* **1997**, *13*, 5511; f) Patil, V.; Malvankar, R. B.; Sastry, M. *Langmuir* **1999**, *15*, 8197; g) Patil, V.; Sastry, M. *J. Chem. Soc., Faraday Trans.* **1997**, *93*, 4347; h) Sastry, M. *Curr. Sci.* **2000**, *72*, 1089.

11. a) Gole, A.; Dash, C.; Rao, M.; Sastry, M. *J .Chem. Soc. ,Chem. Commun.* **2000**, 297; b) Gole, A.; Dash, C.; Mandale, A. B.; Rao, M.; Sastry, M. *Anal. Chem.* **2000**, *72*, 4301; c) Gole, A.; Sastry, M. *Biotech. Bioeng.* **2001**, *74*, 172; d) Gole, A.; Chaudhari, P.; Kaur, J.; Sastry, M. *Langmuir* **2001**, *17*, 5646; e) Gole, A.; Vyas, S.; Sainkar, S. R.; Lachke, A. L.; Sastry, M *Langmuir* **2001**, *17*, 5964.

12. a) Burrell, M. C.; Armstrong, N. R. *Langmuir* **1986**, *2*, 37; b) Cheek, G. T.; O' Grady, W. E. *J. Electroanal. Chem.*, **1990**, *277*, 341; c) Wang, J.; Frostman, L. M.; Ward, M. D. *J.Phys.Chem.* **1992**, *96*, 5224; d) Buttry, D. A.; Ward, M. D. *Chem. Rev.* **1992**, *92*, 1356; e) Geddes, N. J.; Urquhart, R. S.; Furlong, D. N.; Lawrence, C. R.; Tanaka, K.; Okahata, Y. *J. Phys. Chem*., **1993**, *97*, 13767; f) Brust, M.; Etchonique, R.; Calvo, E. J.; Gordillo, G.J. *J. C. S. Chem. Commun.*, **1996**, 1949; g) Patil, V.; Mayya, K. S.; Pradhan, S. D.; Sastry, M. *J. Am. Chem. Soc*., **1997**, *119*, 9281; h) Bright, R. M.; Musick, M. D.; Natan, M. J. *Langmuir* **1998**, *14*, 5695; i) Sastry, M.; Patil, V.; Sainkar,

S. R. *J. Phys. Chem. B* **1998**, *102*, 1404; j) Gole, A.; Sainkar, S. R.; Sastry, M. *Chem. Mater*., **2000**, *12*, 1234; k) Caruso, F.; Niikura, K.; Furlong, D. N.; Okahata, Y. *Langmuir* **1997**, *13*, 3427; l) Caruso, F.; Rodda, E.; Furlong, N. D.; Niikura, K.; Okahata, Y. *Anal. Chem.* **1997**, *69*, 2043; m) Gole, A.; Dash, C.; Mandale, A. B.; Rao, M.; Sastry, M. *Anal. Chem.* **2000**, *72*, 4301; n) Gole, A.; Chaudhari, P.; Kaur, J.; Sastry, M. *Langmuir* **2001**, *17*, 5646.

13. Sauerbrey, G. *Z.Phys. (Munich)* **1959**, *155*, 206.

CHAPTER III

Organization of nanoparticles using two dimensional surfaces as a templates

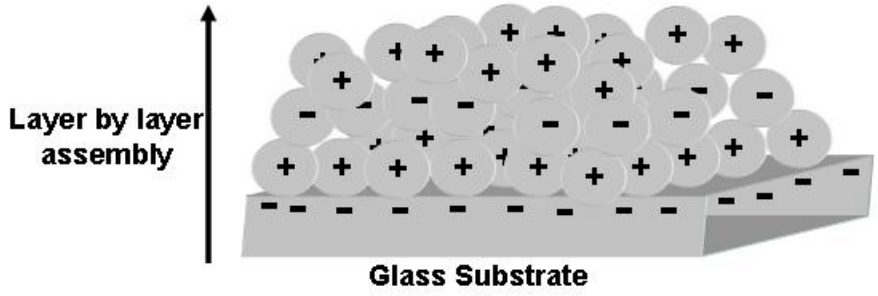

This chapter describes a simple immersion-based technique to organize nanoparticles on glass substrate using electrostatic interactions. Multilayer films of 4-aminothiophenol-capped gold and 4-carboxythiophenol-capped silver nanoparticles were formed by alternate immersion of glass substrates in different nanoparticle solutions. This technique was extended to form multilayers of amino acid (valine) modified gold nanoparticles on glass substrate. Valine derivatized gold nanoparticles are amphoteric i.e. negatively charged at pH greater than 6 (isoelectric point of valine) and positively charged below this pH. This property was used to obtain multilayers by immersion of the glass substrate alternatively into the valine-capped gold nanoparticle solutions maintained at pH = 3.5 and 8.5. The multilayer structures of nanoparticles on glass have been characterized by UV-vis, infrared spectroscopy, X-ray diffraction (XRD), X-ray photoemission spectroscopy and ellipsometry.

The work described in this chapter has been published: 1) Kumar, A.; Mukharjee, P.; Guha, A.; Adyantaya, S. D.; A. B. Mandale, A. B.; Kumar, R.; and Sastry, M. *Langmuir* 2000, *16*, 9775. 2) Kumar, A.; Mandale, A. B.; Sastry, M. *Langmuir* 2000, *16*, 6921.

3.1. Introduction

As discussed in chapter 1, a number of methods have been reported for the organization of nanoparticles in a two dimensional assembly with very good control over the spacing between the nanoparticles. However, only a few methods are known for the organization of nanoparticles along the direction normal to the plane of deposition or in a layer-by-layer (LBL) fashion for nanoparticles. Strategies known for the organization of nanoparticle multilayers in LBL fashion, based on electrostatic interactions or covalently bound linker molecules have already been discussed in section 1.5.4. This chapter describes our strategy and details of the LBL assembly of nanoparticles using electrostatic interactions on solid substrate such as glass. By manipulation of thecharges on the surface of nanoparticles we could grow multilayers of the same material and of two different materials in an alternating LBL fashion.

For assembling the positively charged gold and negatively charged silver nanoparticles on glass substrates in LBL fashion, we have utilized electrostatic interactions between the substrate and the particles as well as that between the particles. Gold and silver nanoparticles were derivatized by self-assembly of 4-aminothiophenol (4-ATP) and 4-carboxythiophenol (4-CTP) monolayers on the nanoparticles respectively. The particles upon subsequent ionization of the functional groups at appropriate pH values become charged. Glass substrate, which is negatively charged at pH > 3, is first immersed in the positively charged amine-derivatized gold nanoparticle solution leading to the formation of a monolayer of the gold nanoparticles and charge reversal of the glass surface. Thereafter, the glass surface covered with gold nanoparticles is immersed in the negatively charged carboxylic acid-derivatized silver nanoparticle solution and the silver nanoparticles self-assemble electrostatically on the glass surface. This process may be continued to yield multilayer structures of the nanoparticles.

Compared to the alternating LBL self-assembly of two different materials, the fabrication of multilayer of same material needs a different strategy as the particles with same surface charge will repel each other and hence resist self-assembly. Hence, we used amphoteric capping agent such as amino acids to modify the gold nanoparticles. The most important advantage of amino acid modified nanoparticles is that the sign and magnitude of charge on the nanoparticles can be changed with pH of the solution. This

amphotericity of nanoparticles can be used to organize nanoparticles in LBL fashion using electrostatic interactions. The amino acid, we employed here to modify the gold nanoparticles is, valine. The isoelectric point (PI) of valine is ca. 6. Therefore above pH or PI 6, the gold nanoparticles modified with valine acquire a net negative charge and are positively charged at pH value lower than 6. We used this charge reversibility to form multilayer of valine modified gold nanoparticles by immersing the glass substrate in valine capped gold nanoparticle solution at different pH. In the first step, negatively charged glass substrates are immersed in the valine-capped gold nanoparticle solution (pH ~ 3.5) and a gold nanoparticle monolayer electrostatically assembles on the glass surface. This leads to charge reversal of the glass surface and the possibility of electrostatically assembling a succeeding layer of negatively charged valine-capped gold nanoparticles (pH ~ 8.5). Thereafter, the process may be repeated to form multilayer structures of the gold nanoparticles**.** The stability of the valine-capped gold nanoparticle solutions at different pH values as well as the formation of the multilayer structure on glass has been characterized with UV-visible spectroscopy, Ellipsometry, Fourier transform infrared (FTIR) spectroscopy and X-ray photoemission spectroscopy (XPS). Presented below are the details of the investigation.

3.2. Layer-by-layer assembly of gold and silver nanoparticles

3.2.1. Experimental details

The synthesis and modification of the silver and gold particles were done as described in chapter 2. Multilayer of the nanoparticles was formed on borosilicate glass substrates by immersion in the different nanoparticle solutions as illustrated in Scheme 1. Step 1 involves the electrostatic assembly of positively charged 4-ATP capped gold nanoparticles on a negatively charged glass substrate during immersion in the 4-ATP capped gold nanoparticle solution at pH ~ 4. In the second step second layer of negatively charged silver nanoparticles was formed on positively charged gold nanoparticles covered glass following immersion in the 4-CTP capped silver nanoparticle solution at pH ~ 8.5. The process may be repeated to grow multilayer assemblies. The sequential

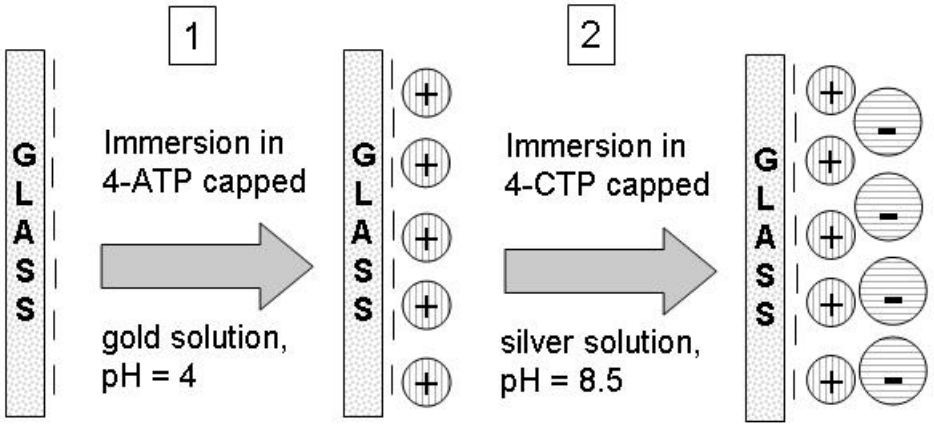

Scheme 1: Formation of electrostatically assembled alternating layers of gold and silver nanoparticles on glass substrate.

assembly of the 4-ATP capped gold and 4-CTP capped silver nanoparticles on glass was studied by UV-vis spectroscopy and ellipsometry. Care was taken to thoroughly wash the substrates with de-ionized water prior to measurement of the optical properties.

3.2.2. UV-visible study

The optical properties of 4-CTP capped silver and 4-ATP capped gold nanoparticles have been discussed earlier in chapter 2. The intense absorption in the visible region of the electromagnetic spectrum occurs due to excitation of surface plasmon oscillations and is responsible for the beautiful colors of the nanoparticle solutions.[1] Thus, electrostatically assembled films of 4-ATP-gold and 4-CTP-silver nanoparticles on glass are ideal candidates for study using UV-vis spectroscopy. In order to identify the optimum time scale for formation of a monolayer of 4-ATP capped gold nanoparticles on the glass surface, UV-vis spectroscopy measurements were carried out as a function of time of immersion in the gold nanoparticle solution at pH ~ 4 (step 1, Scheme 1). Prior to the UV-vis measurements, the film was washed with copious amounts of de-ionized water and dried. Figure 3.1A shows the spectra recorded from a glass substrate as a function of time of immersion in 4-ATP capped gold nanoparticle solution. The time of immersion is indicated next to the respective curves. Figure 3.1B shows the variation in the absorbance at 685 nm with time. A clear increase in the surface plasmon resonance intensity with time is observed and the nanoparticle adsorption

process is completed after ca.16 h of immersion. A uniform blue coloration of the glass surface was observed after formation of the gold nanoparticle monolayer. In the preparation of the Au/Ag nanoparticle films by the LBL self-assembly process, therefore, a time of immersion of 18 h in the gold and silver nanoparticle solutions was used. At pH ~ 4, the 4-ATP capped gold nanoparticles would be positively charged and it is known that a negative charge develops at the glass water interface due to ionization of surface-bound silanol groups.[2]

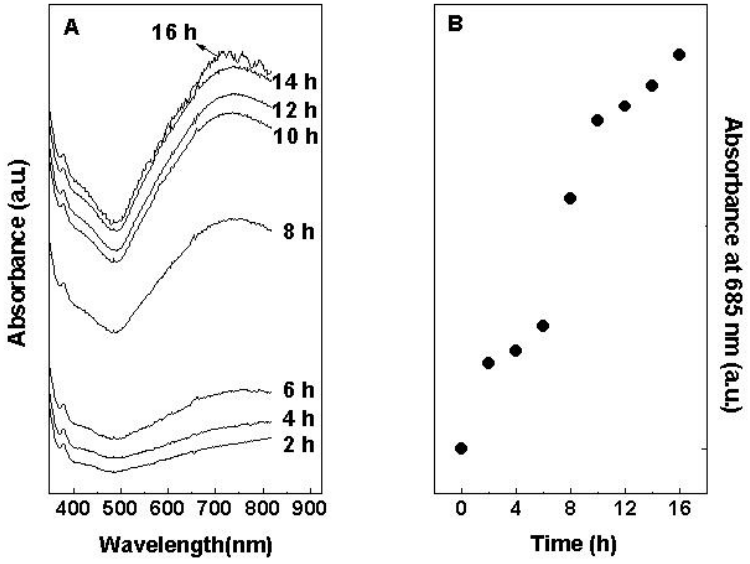

Figure 3.1: A) UV-vis spectra recorded as a function of time of immersion of a glass substrate in 4-ATP capped gold nanoparticle solution at pH ~ 4. The time of immersion is indicated next to the respective spectra. B) Absorbance at 685 nm plotted as a function of time of immersion for the UV-vis spectra shown in A.

Attractive electrostatic interaction between the glass surface and gold nanoparticles leads to self-assembly of the gold nanoparticles on the surface. In order to cross-check whether electrostatic interactions drive the self-assembly process, a glass film was immersed in the 4-CTP capped silver nanoparticle solution at pH ~ 8.5 for 18 h and the UV-vis spectrum recorded (solid line, lowest curve of Figure 3.2A). The presence of silver nanoparticles on the glass surface was below the detection limit of the UV-vis instrument used. Under the conditions of this control experiment, both the 4-CTP capped silver and glass surfaces would be negatively charged and thus, electrostatically driven

adsorption of the silver nanoparticles does not occur. The plasmon resonance in the monolayer of 4-ATP capped gold nanoparticles on glass is seen to occur at 685 nm and is considerably red-shifted with respect to the value of 530 nm for the gold nanoparticles in solution. Overlap of the dipole plasmon resonances between neighboring gold particles leads to the appearance of a longitudinal plasmon resonance at 685 nm and indicates close-packed regions of the gold particles on the glass surface.[3]

Figure 3.2 A is a plot of the UV-vis spectra recorded from films of Au/Ag on glass as a function of number of immersion cycles in the different nanoparticle solutions, the immersion time in the different solutions being 18 h. The number of immersion cycle is indicated next to the respective spectrum. In Figure 3.2 A, the solid lines are the spectra recorded after immersion in the gold nanoparticle solution and the dashed lines are for the film after formation of the succeeding layers of silver nanoparticles. The resonance at 685 nm and a weak shoulder at ca. 560 nm have been indicated in the Figure 3.2A. The resonance at 560 nm is the transverse plasmon resonance of the gold nanoparticles.[3] It is seen that the intensity of the absorption at 685 nm increases monotonically with number of immersion cycles in the different nanoparticle solutions quite clearly showing that the LBL electrostatic self-assembly process is operative. The increase in the resonance at 685 nm as a function of number of layers formed (these values are for the spectra recorded after formation of the gold nanoparticles layer in each of the cycles) is shown in Figure 3.2B. The solid line is non-linear least squares fit to the data. This result shows that the Au and Ag nanoparticles sequentially assemble onto glass substrate via electrostatic interaction with apparently little change in the nanoparticles density in each layer. As will be seen from the ellipsometry results discussed below, there is a small reduction in the nanoparticle density in each layer as the film is built up and this variation is below the detection limits of UV-vis spectroscopy.

In Figure 3.2A, it is observed that immersion of the gold particle coated glass substrates in the silver solutions leads to an increase in the resonance at 685 nm and a small overall variation in the UV-vis spectrum (dashed lines, Figure 3.2A). Close packing of the silver nanoparticles on the gold layer would result in the presence of a red-shifted longitudinal plasmon resonance and it is possible that it shifts to wavelengths within the broad envelope between 500 and 800 nm.[4] Thus, distinct UV-vis features due to silver

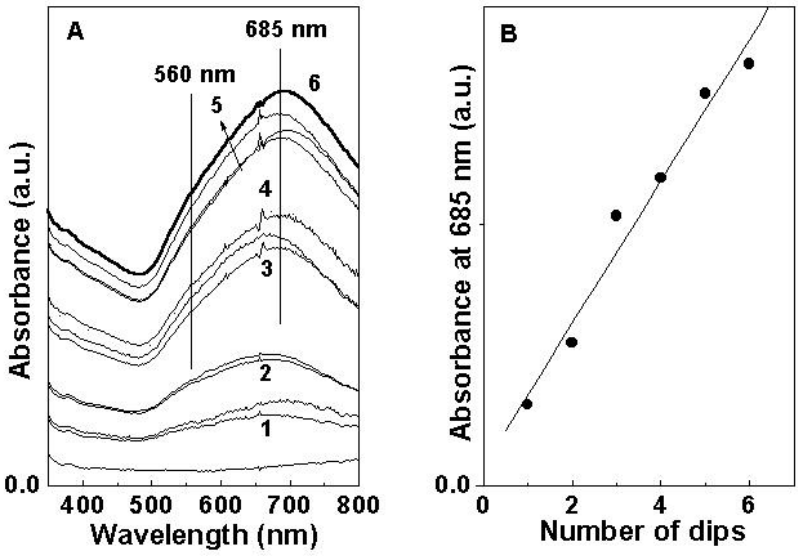

Figure 3.2: A) UV-vis spectra recorded from a glass substrate after each immersion cycle in 4-ATP capped gold (solid lines) and 4-CTP capped silver (dashed lines) nanoparticles; the number of immersion cycle is indicated next to the respective spectra. The unlabelled spectrum at the bottom of the figure corresponds to a film formed by immersion of the glass substrate in 4-CTP capped silver nanoparticle solution at pH ~ 8.5 for 18 h. B) Absorbance at 685 nm plotted as a function of number of immersion cycles; the spectra were measured after deposition of the 4-ATP capped gold layer each time. The solid line is a non-linear least square fit to the data.

and gold are not identifiable in the UV-vis spectra of the multilayer films and hence, XPS was used to unequivocally substantiate the presence of silver in the films (to be discussed below). However, the increase in the resonance at 685 nm during each immersion cycle indirectly points to the formation of the silver nanoparticles layer since without the charge reversal brought about by the adsorption of the negatively charged silver nanoparticles layer, it is not likely that the positively charged gold layer would form. By sequential immersing the substrate in 4-ATP capped gold and 4-CTP capped silver sol, 6 layer of Au/Ag particles film was prepared with outer layer consisting of silver nanoparticles.

3.2.3. Ellipsometric measurements

Though, the UV-vis spectroscopy measurements in Figure 3.2 show that the positively charged gold and negatively charged silver nanoparticles do adsorb

sequentially on glass substrates, information on the packing density of the particles in the individual layers may be more accurately obtained from ellipsometry. As in the case of the UV-vis measurements, the ellipsometric angles were recorded after immersion of the substrate in the respective nanoparticle solutions for 18 h and thoroughly washing and drying the substrates prior to measurement. Ellipsometry measurements of the Au and Ag layers sequentially adsorbed on a glass substrate were analyzed in terms of the Bruggeman effective medium model.[5] This effective medium formalism was chosen, since it is known to be applicable even for large filling fractions of the nanoparticles in the individual layers.[5] In the analysis, the sequentially adsorbed nanoparticles are considered to occupy layers of thickness equal to the size of the particle in that layer. The individual layers thus constitute a two-component mixture of the nanoparticles of dielectric function 'ε_C', filling fraction 'f' and air ($\varepsilon_M = 1$). For such a two-component system, the governing equation relating the effective medium (air + nanoparticles) dielectric function 'ε_{BR}' to the dielectric functions of the components and the filling fraction is[5]

$$f \cdot \frac{\varepsilon_C - \varepsilon_{BR}}{\varepsilon_C + 2 \cdot \varepsilon_{BR}} + (1 - f) \cdot \frac{\varepsilon_M - \varepsilon_{BR}}{\varepsilon_M + 2 \cdot \varepsilon_{BR}} = 0 \qquad \text{..... (1)}$$

The dielectric function for the gold and silver nanoparticles were taken from a compilation by Johnson and Christy[6] and are $(1.315 - 1.524i)^2$ and $(1.278 - 1.364i)^2$ respectively at 6328 Å (laser wavelength used in the ellipsometry measurements). After formation of the first gold nanoparticle layer on the glass surface, the dielectric function of the layer of thickness 130 Å (size of gold nanoparticles) was determined from the ellipsometric angles Ψ and Δ and thereafter, the filling fraction calculated by using equation (1). The substrate refractive index in this case was taken as 1.5, that of glass. Measurements were made on at least 5 different points of the film surface and averaged. For the first gold nanoparticle layer, an average filling fraction 'f' of 29.7% was calculated. This translates into a nanoparticle density of 3.36×10^{11} particles/cm^2 of the glass surface. Assuming an area/4-ATP molecule on the gold nanoparticles surface of 25 Å^2, the number of positive charges on each gold nanoparticle may be easily shown to be

2124 electronic charges. Assuming a typical value for the surface charge density on borosilicate glass (25 $Å^2$ per charge, 0.64 C/m^2)[2b], it is seen that for this concentration of gold nanoparticles on the surface, the positive charge density due to gold nanoparticles ($3.36 \times 10^{11} \times 2124 = 7.14 \times 10^{14}$ cm^{-2}) is larger than the negative charge density on the glass surface [$(25 \times 10^{-16})^{-1} = 4 \times 10^{14}$ cm^{-2}). Thus, there is clearly overcompensation of the negative charge on the glass surface due to adsorption of the positively charged gold nanoparticles and clearly supports the subsequent electrostatically controlled deposition of the silver nanoparticles. In a similar manner, the filling fraction for the next layer of silver nanoparticles of thickness 70 Å was calculated from the ellipsometric angles and Eq.1 taking the glass + layer of gold nanoparticles as the new substrate. The average filling factor for the first layer of silver nanoparticles was calculated to be 59.1% and it is easy to show that charge overcompensation occurs in this case as well. The filling fractions of the next cycle of gold and silver electrostatically assembled layers were also calculated and were 21.2% and 44.5% respectively. Thus, there is a small reduction in the particle density in succeeding layers. Lvov *et. al.*[7] have pointed out that electrostatic assembly of rigid, inorganic particles does not lead to efficient packing of the particles in the individual layers and a flexible polyelectrolyte 'glue' was observed to lead to better LBL growth. This may be one of the reasons for the reduction in particle density observed in this study. It is pertinent to point out that the model used for the ellipsometry analysis presented above is highly idealized. It is assumed that each successive layer of nanoparticles grows directly on top of the previous layer even though large voids (due to less that optimum packing of the particles in the layer below) exist in the substrate layer. From a purely electrostatic viewpoint, this growth mode does not appear to be unrealistic given that unfilled regions of the substrate would expose charges of the same sign as that of the incoming nanoparticles. Clearly, a better understanding of the results presented herein would require a more sophisticated model for the electrostatic assembly.

3.2.4. XRD study

XRD measurements were also carried out on the 6 layer gold/silver nanoparticle film on glass before and after heating at 250 ^{O}C for 1 h. The (111) Bragg reflection recorded from a 6 layer Au/Ag particle film on glass is shown in Figure 3.3 (curve 2). A

Lorentzian fit to the curve is also shown in the Figure 3.3. The 2θ value of this reflection is almost identical for silver and gold.

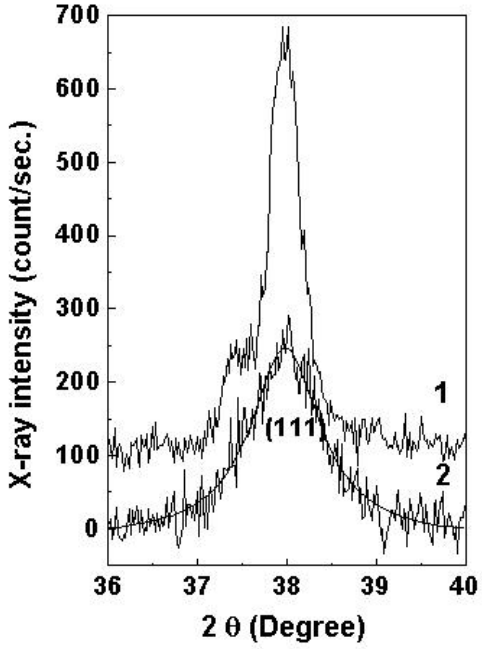

Figure 3.3: XRD pattern showing (111) Bragg peaks from a 6 layer Au/Ag film on glass before heating, curve 2 and after heating, curve 1 at 250 ^{o} C for 1 h. The Lorentzian fit to the (111) Bragg peak for curve 2 is also shown.

It is seen that this peak is quite broad and the particle size was calculated from the peak width using the Scherrer formula[8] to be 100 Å. This size is in fairly good agreement with the size of the particles estimated from TEM measurements of the silver (70 ± 13 Å)[9b] and gold particles (130 ± 30 Å)[9a].

3.2.5. XPS study

The film consisting of 6 alternating layers of gold and silver nanoparticles on glass was subjected to chemical analysis using XPS. The Ag 3d core level spectrum is shown in Figure 3.4. The upper curve is the as-recorded spectrum shown along with the background signal while the lower spectrum is after removal of the inelastic electron background. The background corrected Ag 3d spectrum was resolved into two spin-orbit components. The Ag $3d_{5/2}$ core level binding energy (BE) was 368.1 eV (the core levels were aligned with respect to the adventitious C 1s BE of 285 eV) and corresponds to that

of metallic silver.[10] There was no evidence for a chemically shifted component which may arise due to co-ordination of surface silver atoms to 4-CTP via thiolate linkages.

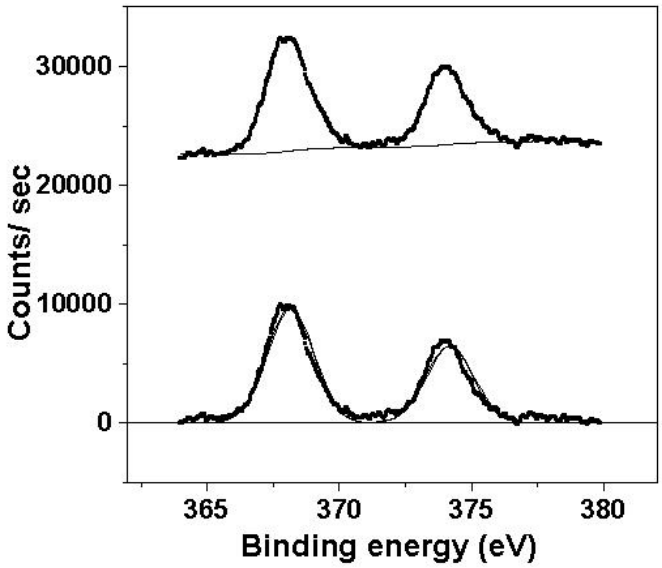

Figure 3.4: Ag 3d core level spectrum from a 6 layer Au/Ag film on glass before (upper curve) and after (lower curve) Shirley background subtraction. The spin-orbit components have been resolved and are shown in the lower spectrum.

Figure 3.5A shows the as-recorded Au 4f core level spectrum and is shown with the background signal simulated by the Shirley algorithm.[11] It is clear that the background function is much more intense and has a different form than that observed for the Ag 3d core level spectrum. Tougaard has shown that this background signal arises due to inelastic scattering of the core level photoelectrons during transport to the surface[12a] and furthermore, that this inelastically scattered electron background signal may be analyzed to obtain important information regarding the surface concentration profile of the various elements at the surface as well as the dielectric properties of the surface.[12a,b] The observation that the inelastic electron signal is more pronounced in the case of the Au 4f core level spectrum when compared to the Ag 3d core level spectrum indicates that the electrons emitted from the Au atoms are scattered much more strongly during transport in the surface as would be the case if the Au atoms were buried beneath a layer of Ag particles. Similarly, the electrons emitted from the Ag atoms in the outermost layer would be emitted almost directly into vacuum and therefore, the probability for

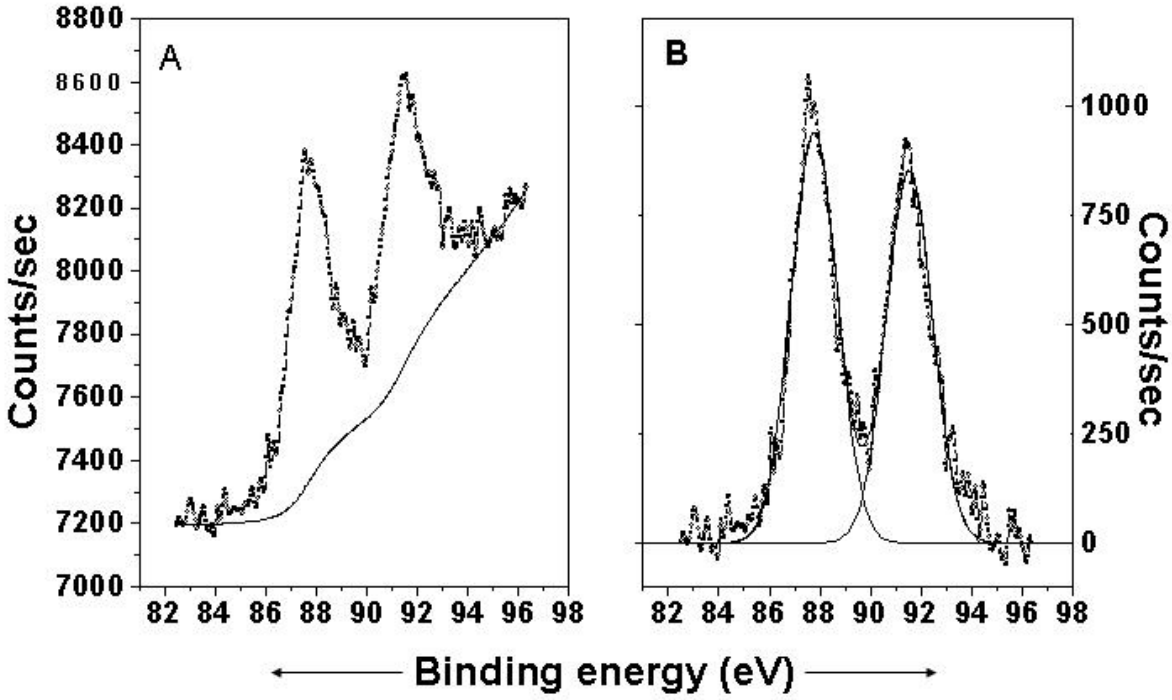

Figure 3.5: A) Au 4f core level spectrum from a 6 layer Au/Ag film on glass (as-recorded) along with the Shirley background signal. B) Au 4f core level spectrum from a 6 layer Au/Ag film on glass after Shirley background correction shown along with the spin-orbit components.

inelastic scattering is negligible resulting in a weak background signal. The XPS results shown in Figure 3.4 and 3.5 support the ellipsometry and UV-vis spectroscopy studies presented earlier for the LBL electrostatic assembly of the nanoparticles on glass in the manner shown in Scheme 1. The Au 4f spectrum after removal of the background signal was stripped into two spin-orbit components and is shown in Figure 3.5B. The Au $4f_{7/2}$ core level BE was determined to be 83.8 eV and corresponds to that of metallic gold.[10] In this case as well, there is no evidence of a chemically shifted peak due to thiolate linkage of surface Au atoms with 4-ATP.

The C 1s, O 1s, N 1s and S 2p core level spectra were also recorded and are shown in Figure 3.6 and 3.7. The C 1s spectrum could be resolved into two components at 285 and 288.4 eV BE (Figure 3.5A) and are assigned to carbons from the aromatic rings in 4-ATP and 4-CTP and carboxylate carbons (4-CTP) respectively.[13] The O 1s spectrum could also be resolved into two components centered at 531.5 and 535.0 eV

(Figure 3.5B) BE. These chemically shifted components are assigned to oxygen from the carboxylate groups in 4-CTP[14] and some adsorbed hydroxyl groups.

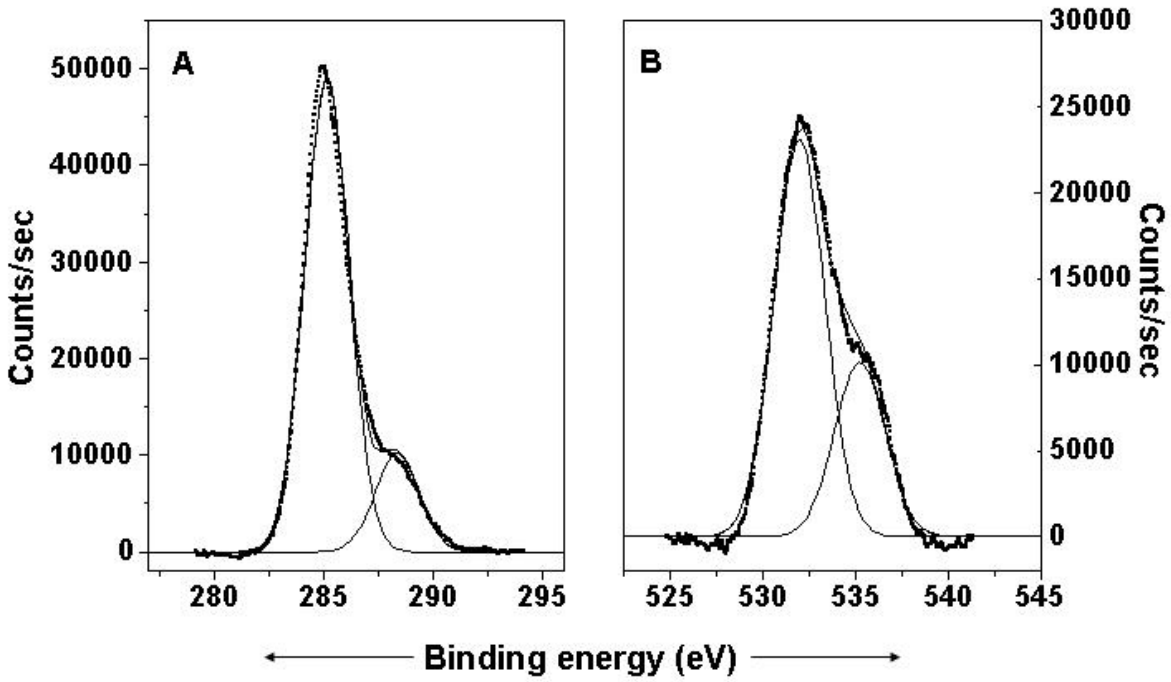

Figure 3.6: A) C1s core level spectrum from a 6 layer Au/Ag film on glass. B) O1s core level spectrum from a 6 layer Au/Ag film on glass shown along with the spin-orbit components.

The signal to noise ratio for the N 1s and S 2p spectra was not very good and therefore, a chemical analysis of these core levels was not possible. Both the N 1s and S 2p core levels were broad and centered at 399 eV (Figure 3.7A) and 168 eV (Figure 3.7B) BE respectively. The N 1s signal clearly originates from the amine group of 4-ATP. The large chemical shift in the S 2p BE (the S 2p BE in self-assembled monolayers of alkanethiols on gold thin films is ~ 163 eV)[15] indicates oxidation of a fraction of the thiolate linkages to sulfonate groups. We have observed a similar oxidation of the thiol groups in self-assembled monolayers of an aromatic dithiol on gold thin films by XPS and the S 2p BE agrees very well with that reported earlier.[16]

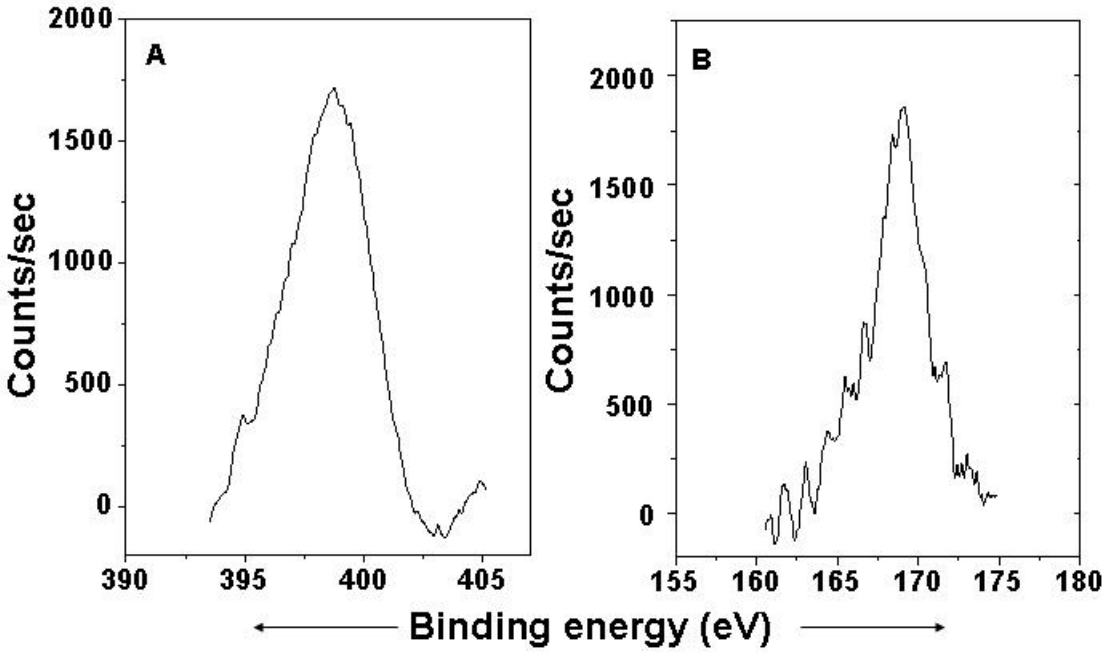

Figure 3.7: A) N1s core level spectrum from a 6 layer Au/Ag film on glass. B) S2p core level spectrum from a 6 layer Au/Ag film on glass.

3.2.6. Study of stability of multilayer film

The thermal stability of a 6 layer Au/Ag nanoparticle film on glass was investigated using UV-vis spectroscopy after heat treatment at different temperature. Figure 3.8 shows the spectra recorded for the 6 layer film after heating at 100, 150, 200 and 250 ^{o} C for 1 h at each temperature (the temperatures are indicated next to the respective spectra). At and above 150 ^{o}C, it observed that the longitudinal plasmon resonance, which was originally at 685 nm, shifts to the red with temperature clearly indicating aggregation of the particles in the film. It is likely that above 150 ^{O}C, there is desorption of both 4-ATP and 4-CTP molecules from the gold and silver nanoparticles respectively and this leads to sintering of the nanoparticles.

The film heated at 250 ^{O}C for 1 h was also analyzed by XRD and the pattern obtained is shown in Figure 3.3, curve 1. It is observed that there is considerable narrowing of the (111) Bragg reflection after heating. This supports the inference from the UV-vis spectroscopy data shown in Figure 3.8 that the particles sinter after the heating cycle. The particle size calculated using the line broadening of the (111) Bragg

reflection and the Scherrer formula is 250 Å and shows an increase from the 100 Å estimated for the as-prepared superlattice film.

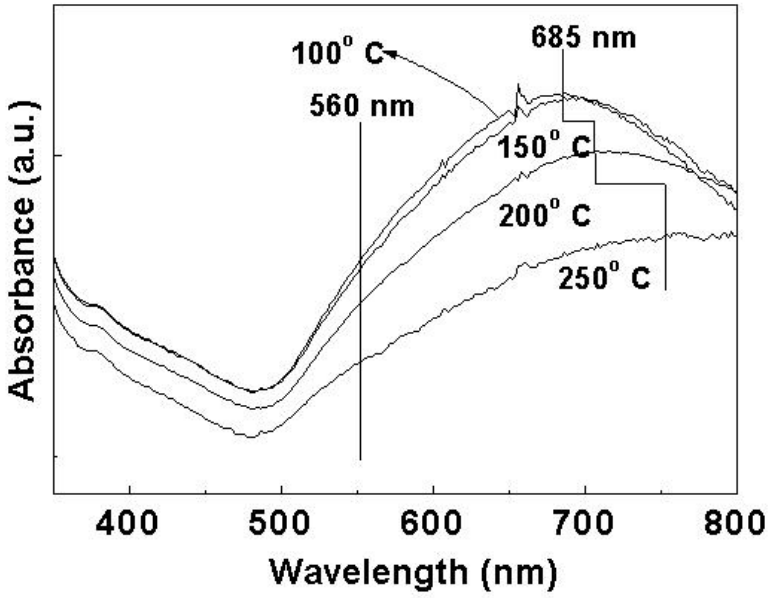

Figure 3.8: UV-vis spectra recorded from a 6 layer Au/Ag film on glass after heating for 1 h at different temperatures. The temperatures are indicated next to the respective spectra.

3.3. Layer-by-layer assembly of amphoteric gold nanoparticles

3.3.1. Assembly of valine capped gold nanoparticles

The gold nanoparticles were synthesized by sodium borohydride reduction and modified with valine as described in chapter 2. The valine is bound to the surface of the gold particles and furthermore, that ionization of the carboxylic acid and amine functional groups at solution pH values of 8.5 and 3.5 respectively is responsible for the nanoparticle stability. Leff, Brandt and Heath[17] have studied the stabilization of gold nanoparticles with alkylamine molecules and have concluded that a weak covalent interaction occurs between the amine group and the surface gold atoms. By comparison with earlier results on the self-assembly of alkylamine molecules on planar gold surfaces where the monolayer was found to be unstable,[18] they have shown that finite size effects present during adsorption on nanoparticle surfaces is responsible for the stability of the 3-

D self-assembled monolayer (SAM) of primary amines.[17] We believe that a similar covalent interaction between the amine group in the valine molecule and the gold surface leads to the capping postulated from the UV-vis measurements mentioned above. After capping and stabilization of the gold nanoparticles with valine, multilayers of the nanoparticles were formed on borosilicate glass substrates by sequential immersion of the substrate in the pH ~ 3.5 and pH ~ 8.5 gold nanoparticle solutions for 24 h as illustrated in Scheme 2. It is known that the negative charge at the glass-water interface is due to dissociation of surface silanol groups[2] and therefore immersion of the glass substrates in the valine-capped gold nanoparticle solution therefore immersion of the glass substrates in the valine-capped gold nanoparticle solution at pH ~ 3.5 should lead to electrostatic self-assembly of the gold nanoparticles on the glass surface (step 1, Scheme 2). Thereafter, the charge reversal on the glass surface due to adsorption of positively charged gold particles may be used to electrostatically assemble negatively charged valine-capped gold nanoparticles by immersion in the nanoparticle solution at pH ~ 8.5 (step 2, Scheme 2) and repeated to yield multilayer structures (Scheme 2). As in the previous section the sequential assembly of the valine-capped gold nanoparticles on glass was studied by UV-vis spectroscopy and ellipsometry. Care was taken to thoroughly wash the substrates with de-ionized water prior to measurement of the optical properties.

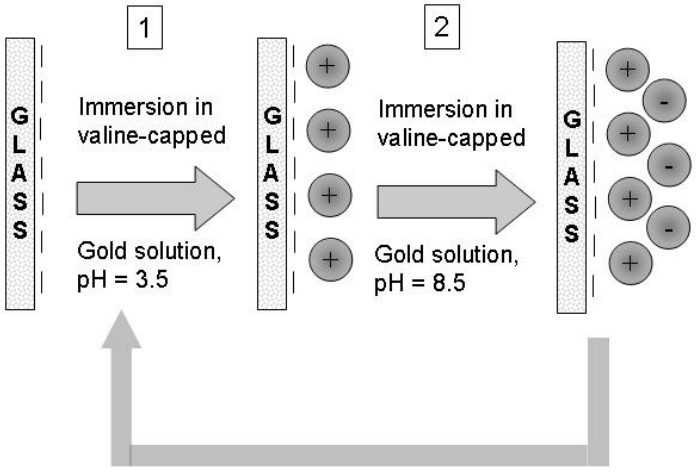

Scheme 2: Diagram showing the various stages in the sequential electrostatic assembly of valine-capped gold nanoparticles on glass.

A 4-layer valine-capped gold nanoparticle film was formed on oxidized Si (111) wafers in a manner similar to that adopted for the glass substrates and the film thus formed was analyzed by FTIR spectroscopy.

3.3.2. UV-vis. study

The optical properties and stability of valine capped gold solution have already been discussed in chapter 2. The multilayer formation was illustrated in Scheme 2, can be easily studied by UV-vis spectroscopy. The UV-vis spectra recorded from a glass substrate after the various immersion cycles mentioned above are shown in Figure 3.9. The spectrum recorded after the first immersion of the glass substrate in gold nanoparticle solution at pH ~ 3.5 for 24 h shows the presence of gold particles on the glass surface with a well defined resonance at ca. 590 nm (Figure 3.9, squares).

A blue coloration of the glass substrate was clearly visible to the naked eye at this stage. Comparison of the UV-vis spectrum recorded from the valine-capped gold nanoparticle solution at pH ~ 3.5 shows a large red shift in the surface plasmon resonance from the solution value of ca. 520 nm. The red shift in the surface plasmon resonance clearly indicates fairly close-packing of the gold nanoparticles on the glass surface.[19]

As a further test of the sign of the charge on the gold particles, a bare glass substrate was immersed in the valine-capped gold nanoparticle solution at pH ~ 8.5 for 24 h and the spectrum recorded is shown in Figure 3.9 (solid line). At this pH, both the glass and gold nanoparticle surfaces are expected to be negatively charged. The presence of gold on the glass surface is clearly below the detection limits of the UV-vis spectrophotometer for this control experiment and provides further support to the valine-induced amphotericity of the gold nanoparticles.

The formation of the second layer after immersion for 24 h now on the positively charged gold nanoparticle-glass surface in gold nanoparticle solution at pH ~ 8.5 can clearly be seen from the UV-vis spectrum (Figure 3.9, circles). The resonance at 590 nm has shifted to larger wavelengths indicating further close-packing of the gold particles and a new, well-defined plasmon resonance is observed at ca. 525 nm. The presence of a less-densely packed layer of gold nanoparticles is indicated during this cycle of immersion. Further immersion in pH ~ 3.5 (triangles, Figure 3.9) and pH ~ 8.5 (Figure

3.9, diamonds) gold nanoparticle solutions clearly shows the growth of the resonance at ca. 530 nm as well as a continued increase in the longer wavelength resonance intensity which is a good indication of electrostatic self-assembly of gold nanoparticles on glass surface. The UV-vis study also shows that the electrostatic self-assembly of gold nanoparticles on glass is due to amphoteric nature of valine-capped gold nanoparticles.

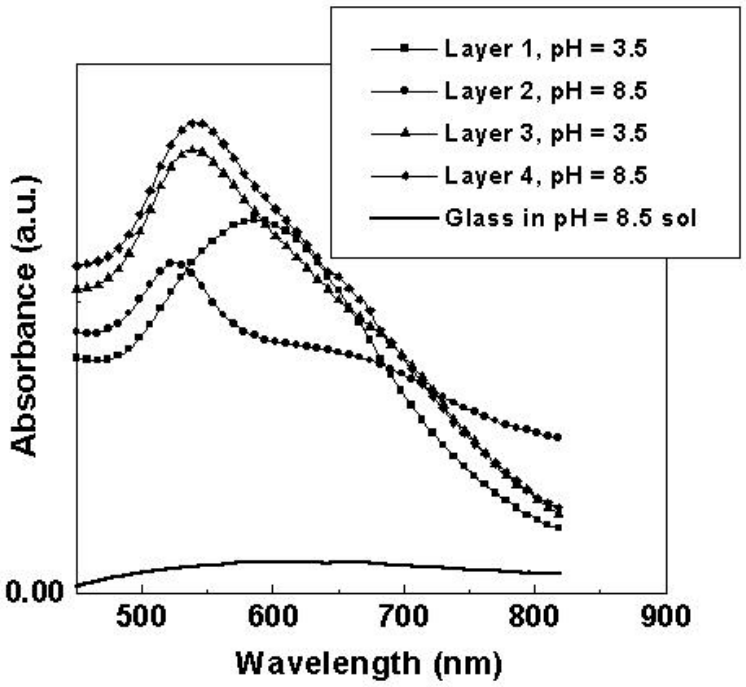

Figure 3.9: UV-vis spectra recorded from a glass substrate after immersion in the valine-capped gold nanoparticle solutions at different pH for 24 h. The different immersion cycles are identified in the legend shown in the Figure.

The UV-vis spectroscopy measurements shown in Figure 3.9 indicate that the valine-capped gold nanoparticles do adsorb sequentially on glass substrates at the pH ~ 3.5 and 8.5, the packing density of the particles in the individual layers was more accurately obtained from ellipsometry. As in the case of the UV-vis measurements, the ellipsometric angles were recorded after immersion of the substrate in the respective nanoparticle solutions for 24 h and thoroughly washing and drying the substrates prior to measurement.

3.3.3. Ellipsometric measurements

After formation of the first gold nanoparticle layer on the glass surface, the dielectric function of the layer of thickness 35 Å (size of gold nanoparticles) was determined from the ellipsometric angles Ψ and Δ and thereafter, the filling fraction calculated using Equation 1 (section 3.2.2.). For the first gold layer, an average filling fraction 'f' = 37.4 % was calculated. This translates into a particle density of 5.83 x 10^{12} particles/cm^2 of the glass surface. Assuming an area/valine molecule on the gold particle surface of 25 $Å^2$, the number of positive charges on each gold particle may be easily shown to be ca. 154 electronic charges. Assuming a typical value for the surface charge density on borosilicate glass (25 $Å^2$ per charge, 0.64 C/m^2),[2b] it is seen that for this concentration of gold nanoparticles on the surface, the positive charge density due to gold nanoparticles (5.83 x 10^{12} x 154 ≈ 8.98 x 10^{14} cm^{-2}) is larger than the negative charge density on the glass surface [(25 x 10^{-16})$^{-1}$ = 4 x 10^{14} cm^{-2}). Thus, there is clearly overcompensation of the negative charge on the glass surface due to adsorption of the positively charged valine-capped gold nanoparticles and clearly supports the subsequent electrostatically controlled deposition of the negatively charged gold nanoparticles at pH ~ 8.5 (step 2, Scheme 2). In a similar manner, the filling fraction for the next layer of gold nanoparticles was calculated from the ellipsometric angles and Equation 1 taking the glass + layer of gold nanoparticles as the new substrate. The average filling factor for the second layer of gold nanoparticles was calculated to be 28.6% and it is easy to show that charge overcompensation occurs in this case as well. The filling fractions for the next two gold nanoparticle layers were also calculated and were 21.6% and 22.5 % respectively. Thus, there is clearly a reduction in the particle density as the valine-capped gold nanoparticles multilayer film is built up by electrostatically on glass substrate. The ellipsometry calculations are in agreement with the UV-vis measurements of the valine-capped gold nanoparticles multilayer films shown in Figure 3.9 and discussed earlier.

3.3.4. FTIR study

FTIR spectra recorded from a 4-layer valine-capped gold nanoparticle film deposited on an oxidized Si (111) substrate in the spectral range 1400-1800 cm^{-1} and 2500-3550 cm^{-1} are shown in Figures 3.10A and B respectively. Figure 3.10A shows two

prominent resonances at 1642 cm^{-1} and 1544 cm^{-1}. The resonance at 1642 cm^{-1} arises due to excitation of the NH_3^+ deformation vibration mode (the "amino-acid I" band)[18] while the peak at 1544 cm^{-1} is assigned to absorption by the ionized carboxyl groups in the multilayer film.[20] The NH_3^+ resonance is also known to have a component in this frequency range (in the range 1485 – 1550 cm^{-1}, the "amino-acid II" band).[20] In addition to these bands, a relatively weaker resonance is observed at ca. 1740 cm^{-1}. This feature is attributed to absorption by un-ionized carboxyl groups in the film[20] and clearly confirms the amphoteric nature of the valine molecules in the multilayer gold film,

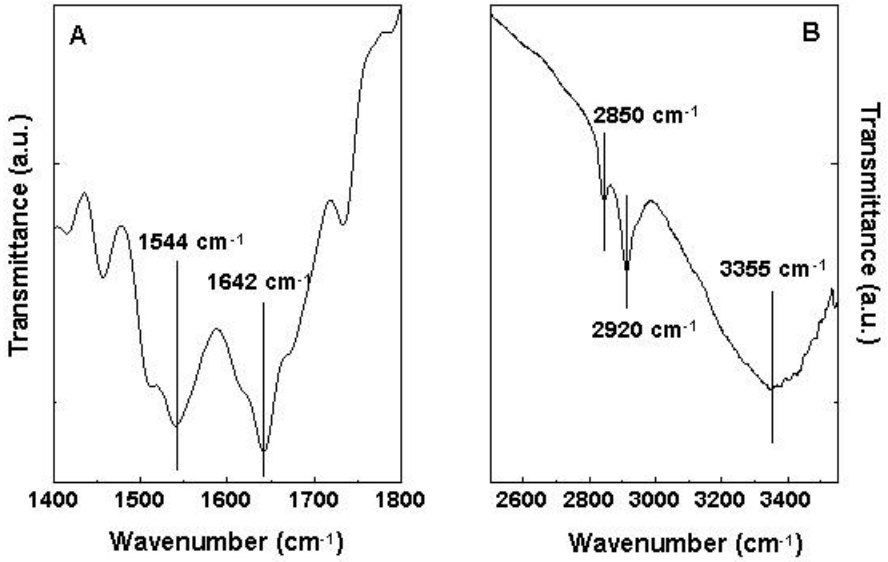

Figure 3.10: A) FTIR spectrum recorded from a 4-layer valine-capped gold nanoparticle film on an oxidized Si (111) substrate in the range 1400-1800 cm^{-1}. The main resonances are identified in the figure and discussed in the text. B) FTIR spectrum recorded from a 4-layer valine-capped gold nanoparticle film on an oxidized Si (111) substrate in the range 2500-3550 cm^{-1}. The main resonances are identified in the figure and discussed in the text.

Figure 3.10B shows the spectrum recorded from the 4-layer valine-capped gold nanoparticle film in the region of the N-H and C-H stretching vibrational modes. A broad and intense resonance centered at 3355 cm^{-1} is clearly seen in Figure 3.10B and is assigned to the N-H stretching vibration.[20,21] The fact that this peak is broad indicates that there may be some hydrogen bonding between amine and carboxylic acid groups of valine in successive layers in the multilayer valine-capped gold nanoparticles film. The methylene antisymmetric and symmetric vibration modes are observed at 2920 and 2850

cm^{-1}. The frequency of these resonances indicates that the valine molecules on the gold nanoparticle surface are in a close-packed state.[22] The features shown in Figure 3.10 are in agreement with reported values for amino acids and confirm the presence of an appreciable concentration of valine in the multilayer gold nanoparticle films. Furthermore, the valine molecules on the gold nanoparticle surface are in ionized states consistent with the electrostatic deposition protocol illustrated in Scheme 2.

3.3.5. XPS study

A film consisting of 4 layers of valine-capped gold nanoparticles grown on glass as well as drop-cast films of the nanoparticle solution at pH ~ 3.5 and pH ~ 8.5 on Si (111) wafers were subjected to chemical analysis using XPS. Figure 3.11A shows the N 1s core level spectra recorded from the drop coated films of gold nanoparticles solution at pH ~ 3.5 and 8.5, the spectra having been displaced vertically for clarity. The pH values of the nanoparticle solutions are given in the Figure 3.11A. It is clear that the N 1s core levels consists of two chemically distinct species in both the films and have been stripped into the individual components by a non-linear least squares procedure. The two components are shown in Figure 3.11A for the pH ~ 8.5 gold nanoparticle film and the parameters obtained from the fits are listed in Table 1 (for clarity, the components in the pH ~ 3.5 gold nanoparticle film have not been shown; the fitting parameters may be obtained from Table 1. The two components at ca. 399.0 and 403.5 eV BE (peaks 1 and 2 respectively in Figure 3.11A and Table 1) are assigned to electron emission from the un-ionized and ionized amine groups in the gold-surface bound valine molecules respectively. It is seen from Table 1 that the peak area ratios of the high BE component to the low BE component increases for the pH ~ 3.5 valine-capped gold nanoparticle film in comparison with the pH ~ 8.5 film (Figure 3.11A). The gold nanoparticle layers formed at pH ~ 8.5 would contain amine groups from valine in the predominantly un-ionized form while the amine groups in the layers self-assembled at pH ~ 3.5 would be, to a large extent, protonated. The N 1s core level XPS results shown in Figure 3.11A clearly provides chemical evidence of the amphotericity of the gold nanoparticles in the self-assembled multilayer film. Figure 3.11B shows the N 1s spectrum recorded from the 4

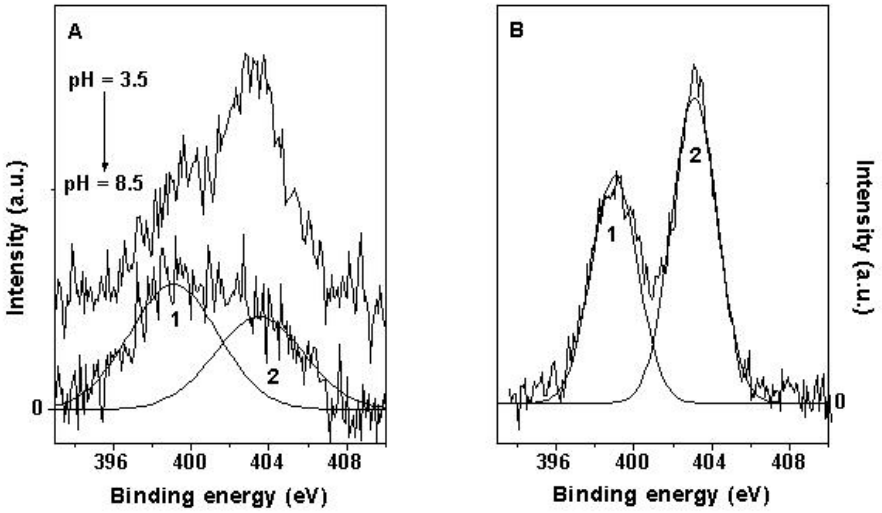

Figure 3.11: A) N 1s core level spectra recorded from drop-coated films of valine-capped gold nanoparticles on Si (111) substrates at pH ~ 3.5 and 8.5 (pH values indicated in the figure). The spectra have been displaced vertically for clarity. The chemically distinct components are shown for the pH ~ 8.5 films. B) N 1s core level spectrum recorded from a 4-layer valine-capped gold film deposited on a glass substrate.

Table 1

Parameters obtained from a non-linear least squares curve resolution analysis of the core levels from valine-capped gold particle films

Valine-capped Au Film	BE(1) eV)	BE(2) (eV)	BE(3) (eV)	A(2)/A(1)*	A(3)/A(2)*
pH = 8.5 (N 1s)	398.9	403.5	--	0.74	--
pH = 3.5 (N 1s)	398.5	403.7	--	2.05	--
4-layer gold film (N 1s)	399.0	403.3	--	2.08	--
pH = 8.5 (C 1s)	285.0	287.1	290	4.88	0.11
pH = 3.5 (C 1s)	285.0	287.3	290.1	1.10	0.19
4-layer gold film (C 1s)	285.0	287.5	290.5	4.04	0.17
4-layer gold film (Au 4f)	84.0	87.6	--	0.73	--
4-layer gold film (O 1s)	529.0	532.1	--	9.32	--

layer valine-capped gold nanoparticle film on glass along with the two chemically distinct species discussed above. The parameters obtained from a fit to the N 1s spectrum are listed in Table 1. It is clear that this spectrum shows the characteristics of the individual layers at pH ~ 3.5 and pH ~ 8.5 (Figure 3.11A).

The C 1s spectra recorded from the pH ~ 3.5 and pH ~ 8.5 valine-capped gold nanoparticle films on Si(111) are shown in Figure 3.12A and the chemically distinct components are shown for the pH ~ 3.5 film (Table 1 lists the parameters obtained from the fits to the C 1s core level for both films). The pH at which gold nanoparticle film was deposited is indicted next to the spectra. The C 1s spectrum could be satisfactorily deconvoluted into three components at ca. 285.0, 287.3 and 290.3 eV B.E. The 285 eV components is assigned to electron emission from the methyl groups in valine and adventitious carbon on the film while the components at 287.3 and 290.3 eV BE are assigned to the carbon coordinated to the amine group and carbon in the carboxylic acid group respectively.[23]

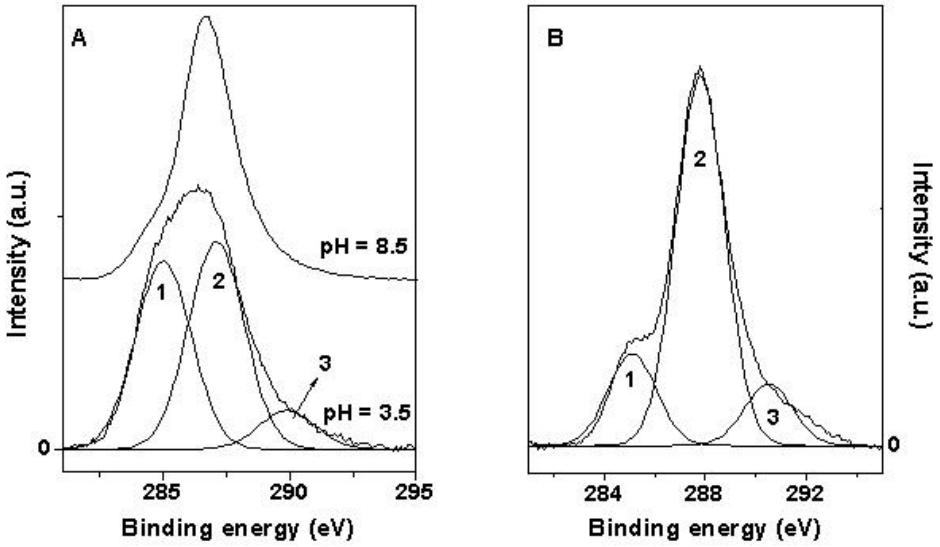

Figure 3.12: A) C 1s core level spectra recorded from drop-coated films of valine-capped gold nanoparticle film on Si (111) substrates from nanoparticle solution at pH ~ 3.5 and 8.5 (pH values indicated in the figure). The spectra have been displaced vertically for clarity. The chemically distinct components are shown for the pH ~ 3.5 film. B) C 1s core level spectrum recorded from a 4-layer valine-capped gold film deposited on a glass substrate. The chemically distinct species are shown in the figure and discussed in the text.

From stoichiometry considerations, the two higher BE components would be expected to have roughly the same intensities. We believe the 287.3 eV component may also contain contributions from carbons in the ionized carboxylic acid groups. That this is likely is indicated by the increase in intensity of component 2 (287.3 eV BE, Figure 3.12A) relative to component 3 (290.3 eV BE) at pH ~ 8.5 in comparison with the C 1s spectrum recorded at pH ~ 3.5 (see Table 1 for ratios of areas of the different components).

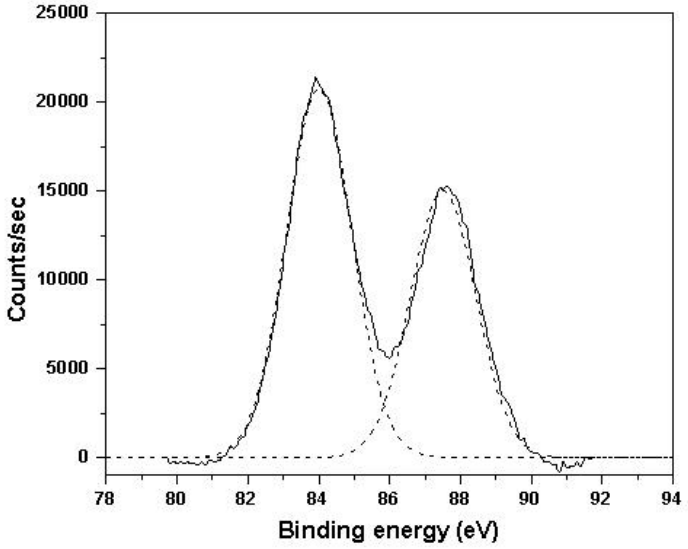

Figure 3.13: Au 4f core level spectrum from a 4-layer valine-capped gold film on glass substrate. The spin-orbit components are shown in dashed lines.

The C 1s core level spectrum recorded from a 4 layer valine-capped gold nanoparticles film on glass is shown in Figure 3.12B with the resolved components. That this spectrum is a superposition of the C 1s spectra from the individual layers (Figure 3.12A) is borne out by the coincidence in BEs of the individual components of the 4 layer gold nanoparticle film with the low and high pH valine-capped gold nanoparticle films as well as the peak area intensity ratio values which lie within the range determined by the individual layers (Table 1).

The Au 4f spectrum (Figure 3.13) recorded from the 4-layer valine capped gold nanoparticle film on glass showed the $4f_{7/2}$ component at 83.8 eV with a spin-orbit splitting of 3.7 eV. There was no evidence of additional components. This is in agreement with the XPS results of Leff, Brandt and Heath for alkylamines on gold[17] and

clearly shows that higher oxidation state gold ions do not exist in the clusters after co-ordination with valine. The O 1s spectrum from the multilayer gold nanoparticle film (Figure 3.14) on glass could be decomposed into two components at 528.6 and 532.3 eV and are assigned to electron emission from oxygen in the ionized and un-ionized carboxylic acid groups respectively. The higher BE component may also contain contributions from the glass substrate if the surface gold particle layers are sufficiently patchy.

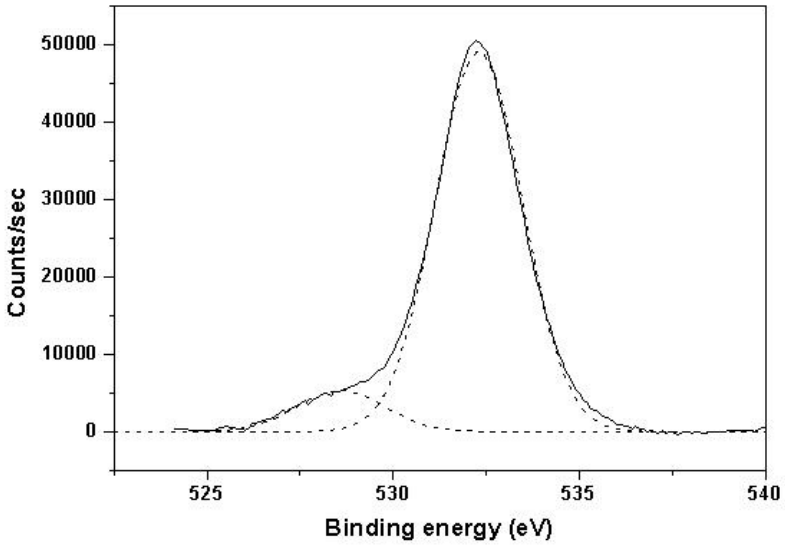

Figure 3.14: O 1s core level spectrum from a 4-layer valine-capped gold nanoparticles film on glass along with the chemically distinct species shown in dashed lines.

3.3.6. XRD study

XRD measurements were also carried out on the 4 layer gold nanoparticle film on glass before and after heating at 250 ^{O}C for 1 h. The (111) Bragg reflection recorded from a 4 layer Au nanoparticle film on glass is shown in Figure 3.15 (curve 1). A Lorentzian fit to the curve 1 is also shown in the Figure 3.15. It is seen that this peak is quite broad and the particle size was calculated from the peak width using the Scherrer formula[9] to be 122 Å. This size is bigger than valine capped gold nanoparticles. The increase in size of nanoparticles in the multilayer may be due to partial aggregation of nanoparticles on glass substrate.

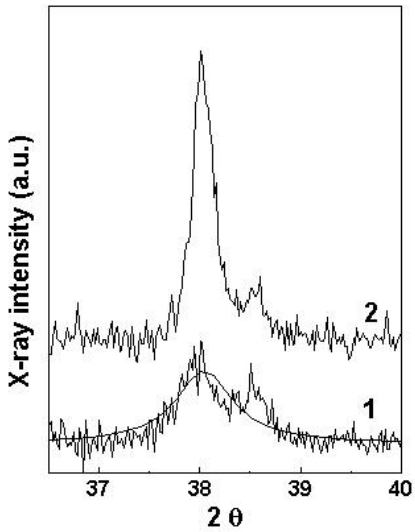

Figure 3.15 : XRD (111) Bragg peaks from a 4 layer Au film on glass – curve 1, before heating and curve 2, after heating at 250 ^{o} C for 1 h. The Lorentzian fit to the (111) Bragg peak for the multilayer film before heating (curve 1) is also shown.

3.3.7. Thermal stability of gold film

The thermal stability of a 4 layer Au nanoparticles film on glass was investigated using UV-vis spectroscopy after heat treatment at different temperatures. Figure 3.16 shows the spectra at 644 nm, become recorded from the 4 layer film after heating at different temperatures. Curves 1, 2, 3 and 4 correspond to the spectra recorded after heating the film at 100, 150, 200 and 250 ^{o} C for 1 h at each temperature. At and above 100 ^{o}C, it is observed that the longitudinal plasmon resonance, which was originally broader clearly indicating aggregation of the particles in the film. This broadening of plasmon of resonance is due to increase in longitudinal plasmon frequency of nanoparticles. It is likely that above 100 ^{O}C, there is desorption of valine molecules from the gold nanoparticles surface and this leads to sintering of the particles. The film heated at 250 ^{O}C for 1 h was also analyzed by XRD and the pattern obtained is shown in Figure 3.15, curve 2. It is observed that there is considerable narrowing of the (111) Bragg reflection after heating. This supports the inference from the UV-vis spectroscopy data shown in Figure 3.16 that the particles sinter after the heating cycle. The particle size calculated using the line broadening of the (111) Bragg reflection using Scherrer formula is 352 Å and shows an increase from the 122 Å estimated for the as-prepared superlattice film.

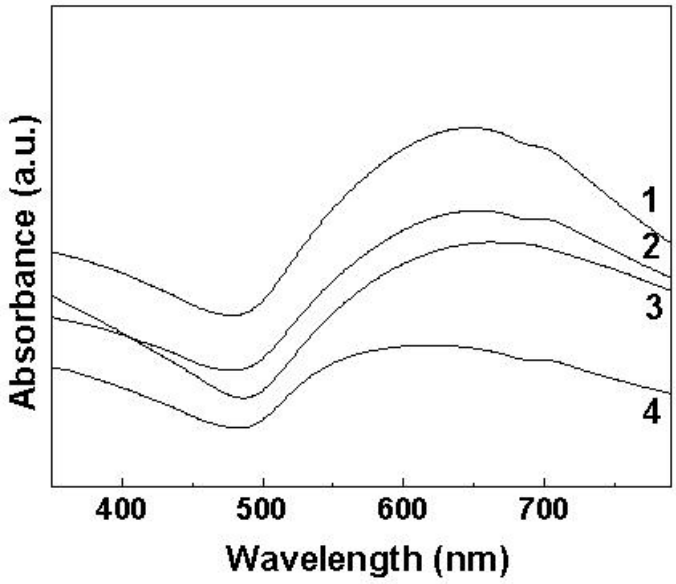

Figure 3.16: UV-vis spectra recorded from a 4 layer of Au film on glass after heating for 1 h at different temperatures. Curves 1, 2, 3 and 4 correspond to the film heated at temperatures 100, 150, 200 and 250 ^{0}C respectively.

3.4. Conclusions

- It has been shown that layer-by-layer electrostatic assembly of amine terminated gold and carboxylic acid terminated silver nanoparticles on glass substrates may be effected by a simple beaker-based immersion procedure and that fairly good quality multilayer structures are realized.
- Ellipsometry and XPS measurements indicated that a layered structure exists in the electrostatically assembled films.
- The nanoparticle multilayer films are stable up to 100 ^{O}C above which the nanoparticles sinter.
- The amphoterization of gold nanoparticles due to surface co-ordination of the amino acid, valine has been demonstrated.
- The valine-capped gold nanoparticle solution is extremely stable at both pH = 8.5 and 3.5 indicating electrostatic stablization via ionization of the carboxylic acid and amine functional groups respectively at these pH values.

- The gold nanoparticle surface charge reversal at two pH values on either side of the valine isoelectric point has been indirectly validated by electrostatically controlled sequential self-assembly of the gold nanoparticles on negatively charged glass substrates.
- Chemical analysis of the multilayer gold nanoparticle films on glass by XPS provides additional support to the valine-induced amphotericity of the gold nanoparticles.

3.5. References

1. Underwood, S.; Mulvaney, P. *Langmuir* **1994** , *10*, 3427.
2. a) Poptoshev, E.; Rutland, M.W.; Claesson, P.M. *Langmuir* **1999**, *15*, 7789; b) Cremer, P.S.; Boxer, S.G. *J.Phys.Chem.B.* **1999**, *103*, 2554.
3. Blatchford, C.G.; Campbell, J.R.; Creighton, J.A. *Surf.Sci.* **1982**, *120*, 435.
4. Creighton, J.A.; Blatchford, C.G.; Albrecht, M.G. *Trans.Faraday Soc.* **1979**, *75*, 790.
5. Granqvist, C.G.; Hunderi, O. *Phys.Rev.B.* **1977**, *16*, 3513.
6. Johnson, P.B.; Christy, R.W. *Phys.Rev.B.* **1972**, *6*, 4370.
7. Lvov, Y.; Ariga, K.; Onda, M.; Ichinose, I.; Kunitake, T. *Langmuir* **1997,** *13*, 6195.
8. Jeffrey, J.W. *Methods in Crystallography*; Academic Press : New York, 1971.
9. a) Mayya, K.S.; Patil, V.; Sastry, M. *Langmuir* **1997**, *13*, 2575 ; b) Sastry, M.; Mayya, K.S.; Patil, V.; Paranjape, D.V.; Hegde, S.G. *J.Phys.Chem.B.* **1997**, *101*, 4954;
10. Fadley, C.S.; Shirley, D.A. *J.Res.Nat.Bur.Stands.* **1970**, *74A*, 543.
11. Shirley, D.A. *Phys. Rev. B.* **1972***, 5*, 4709.
12. a) Tougaard, S. *J.Electron.Spectrosc.* **1990**, *52*, 243; b) Sastry, M.; Paranjape, D.V.; Ganguly, P. *J.Electron.Spectrosc.* **1992**, *59*, 243.
13. a) Davies, M.C.; Lynn, R.A.P.; Davis, S.S.; Hearn, J.; Watts, Vickerman, J.C.; Johnson, D. *Langmuir* **1994**, *10*, 1399; b) Sastry, M.; Ganguly, P. *J. Phys. Chem. A.* **1998**, *102*, 697.
14. Ganguly, P.; Paranjape, D.V.; Sastry, M.; Chaudhary, S. K.; Patil, K. R. *Langmuir* **1993**, *9*, 487
15. Laibinis, P.E.; Whitesides, G.M.; Allara, D.L.; Yu-Tai, T.; Parikh, A.N.; Nuzzo, R.G. *J. Am. Chem. Soc.* **1991**, *113*, 7152.

16. Bandyopadhyay, K.; Sastry, M.; Paul, V.; Vijayamohanan, K. *Langmuir* **1997**, *13*, 866.
17. Leff, D.V.; Brandt, L.; Heath, J.R. *Langmuir* **1996**, *12*, 4723.
18. Xu, C.; Sun, L.; Kepley, L.J.; Crooks, R.M. *Anal. Chem.* **1993**, *65*, 2102.
19. Mayya, K.S.; Patil, V.; Sastry, M. *Langmuir* **1997**, *13*, 3944.
20. Bellamy, L.J. *The Infra-red Spectra of Complex Molecules*, John Wiley, New York : 1960, Chapter 13, p.234.
21. Templeton, A.C.; Chen. S.; Gross, S.M.; Murray, R.W. *Langmuir* **1999**, *15*, 66.
22. Hostetler, M.J.; Stokes, J.J.; Murray, R.W. *Langmuir* **1996**, *12*, 3605.
23. a) Davies, M.C.; Lynn, R.A.P.; Davis, S.S.; Hearn, J.; Watts, Vickerman, J.C.; Johnson, D. *Langmuir* **1994**, *10*, 1399; b) Sastry, M.; Ganguly, P. *J.Phys.Chem.A.* **1998**, *102*, 697.

CHAPTER IV

Organization of nanoparticles using DNA as a template

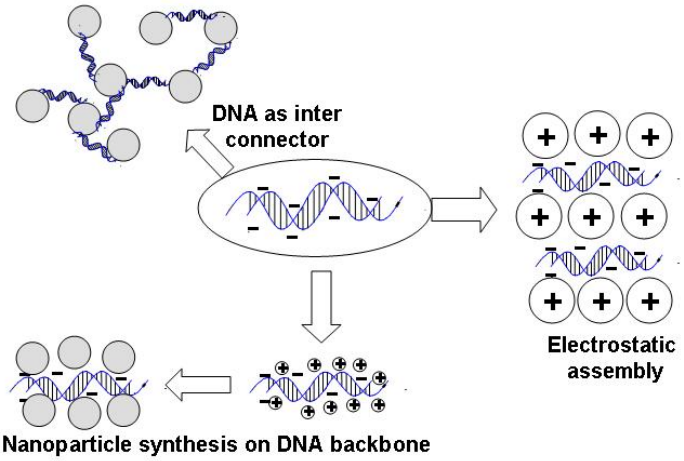

The assembly of nanoparticles using DNA as a template has been demonstrated in this chapter. Lysine-capped gold nanoparticles have been organized into linear superstructures by electrostatic complexation with DNA molecules in solution. Linear supercluster structures of nanoparticles have also been achieved by evaporation of lysine modified gold nanoparticle solution on drop-coated films of DNA. The assembly of gold nanoparticles in solution using phosphorothioate DNA as a structural interconnect has also been demonstrated. Sulfur-substituted DNA cross-links the gold nanoparticles in solution through thiolate linkages with the nanoparticle surface and organizes them in different geometries. The DNA-lipid composite film can also be used as a template for the synthesis of nanoparticles in an organized fashion. Synthesis of nanoparticles was done by incorporating DNA and silver ions in thermally evaporated fatty amine film and thereafter reduction of ions by hydrazine vapor. The synthesis and assembly of nanoparticles was confirmed by TEM, QCM, FTIR, fluorescence measurements.

The work presented in this chapter has been published:1) Kumar, A.; Pattarkine, M.; Bhadbhade, M.; Mandale, A. B.; Ganesh, K. N.; Datar, S. S.; Dharmadhikari, C. V.; and Sastry, M. *Adv. Mater* 2001, 13, 341.; 2) Kumar, A.; Ramakrishnan, V.; Gonnade, R.; Ganesh, K. N.; and Sastry, M. *Nanotechnology* 2002, 13, 597. 3) Sastry, M., Kumar, A.; Dater, S.; Dharmadhikari, C. V.; Ganesh, K. N.; *Appl. Phys. Lett.* 2001, 78, 2943.4) kumar, A.; Phadtare, S.; Pasricha, R.; Guga, P.; Ganesh, K. N.; and Sastry, M. *Current Science* 2003, 84, 71.

4.1 Introduction

We have discussed in the previous chapter that nanoparticles can be assembled in monolayer or multilayer form but certain applications may require the organization of nanoparticles in different geometry. Therefore, numbers of strategies have been developed to assemble nanoparticles in different kind of geometries, which have already been discussed in the chapter 1. Among these methods, the template-directed assembly of nanoparticles by using biomacromolecules such as DNA is of great interest.

Mirkin *et. al.*[1] and Alivisatos *et. al.*[2] have described the use of DNA for programmed assembly of nanoscale building blocks into periodic two and three dimensional structures. In all these approaches, gold nanoparticles are modified at 3' or 5'- thiolated ssDNA (single stranded DNA) sequences, which are complimentary to each other, and Watson-Crick's base pairing is used to control the relative spatial arrangement of nanoparticles. The limitation of this approach is that the duplex DNA is not sufficiently rigid to dictate a precise spatial arrangement of nanoparticles. So it is desirable to have such protocols, which are more DNA friendly with good control over spatial arrangement on nanoparticles. This chapter is based on those alternate approaches which deal with processes to organize the nanoparticles by using DNA as a cross linker as well as template.

In the first part of the chapter we demonstrate the use of DNA as a cross linker for the assembly of nanoparticles in a rigid superstructure. Simple addition of phosphorothioate DNA [sulfur-substituted DNA (S-DNA), Chart 1] to a gold hydrosol

Chart 1: Structure of phosphorothioate DNA

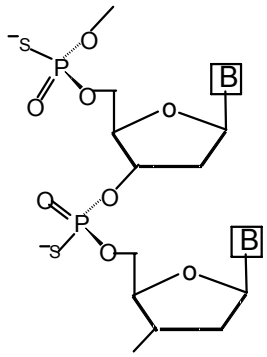

results in binding of the nanoparticles to the DNA via sulfur atoms in the DNA backbone and their cross-linking in solution. The use of small phosphorothioate DNA molecules (~ 40 Å long) renders them rigid and applicable as versatile connectors between the gold nanoparticles.

In the previous chapter, we have shown the layer-by-layer assembly of amino acid (valine) capped gold nanoparticles on the glass substrate using electrostatic interactions[3]. In this chapter we demonstrate the electrostatic self-assembly of gold nanoparticles capped with another amino acid, lysine, on synthetic and natural DNA double helical structures. Attractive Columbic interaction between the positively charged gold nanoparticles and the negatively charged phosphate backbone of the DNA molecules lead to the formation of linear, close-packed assemblies of the gold nanoparticles, the length of which can be tailored by varying the length of the DNA molecule template. While DNA molecules, or to be more precise, single stranded oligonucleotide sequences have been used for the organization of gold nanoparticles both in solution[1a,4] and as supramolecular nanoparticle structures,[1b,c] our process to assemble the nanoparticles in linear array is much simpler. In our approach, drop-dried films of synthetic DNA double-helical molecules were deposited on suitable substrates and thereafter, addition of lysine-capped gold nanoparticles to the film lead to spontaneous ordering of the gold nanoparticles into linear superstructures via attractive electrostatic interaction between the positively charged gold nanoparticles and the negatively charged phosphate groups of the DNA molecules. This relatively simple (and DNA-friendly) process for the realization of linear superstructure of gold nanoparticles shows promise for application to nanowire synthesis by stringing together metal nanoparticles as well as extension to topologically more intricate structures. This approach is very simple and different from other methods reported in the literature wherein ion exchange followed by reaction was used to assemble both semiconductor quantum dots (CdS)[4-6] and metal nanoparticles such as Pd[4] and Ag[6] on the surface of DNA molecules.

In this laboratory, a technique has been developed for the electrostatic immobilization of ions[7], charged nanoparticles,[8] proteins/enzymes[9a,b] and DNA/peptide nucleic acids (PNA)[9c,d] in thermally evaporated ionisable lipid films. Many applications in nanotechnology would require immobilization of the DNA-nanoparticles

superstructures on suitable supports and as a first step towards realizing such superstructures, we demonstrate herein the electrostatically controlled entrapment of calf-thymus (CT) DNA in thermally evaporated fatty amine films which can also be used as a template for growing the nanoparticles in an organized fashion. Entrapment of the negatively charged DNA molecules in the positively charged amine matrix leads to the possibility of binding metal cations such as Ag^+ to the surface of the immobilized DNA molecules. Reduction of the Ag^+ ions *in-situ* leads to the formation of silver nanoparticles on the backbone of the DNA molecules in a close-packed structure within the lipid matrix. We present the details of the investigation briefly introduced above.

4.2. Assembly of nanoparticles in solution using DNA as an inter-connector

4.2.1. Procedure

Gold nanoparticles were prepared by borohydride reduction of chloroauric acid as described in chapter 2. The pH of the gold nanoparticle solution was adjusted to 7 using dilute HCl. After formation of the gold nanoparticle solution, S-DNA was added to the solution to yield an overall DNA concentration of 10^{-7} M in the gold-DNA mixture. The sulfur-substituted oligonucleotides were obtained from Dr. Piotr Guga and the synthetic details can be found in references.[10] The base sequence and length of S-DNA were TTTTTTTTTTTT and roughly 40 Å respectively. The S-DNA-gold nanoparticle solution was kept for 2 hr to enable the assembly of the gold nanoparticles to reach completion following which drop-coated films of the S-DNA-gold nanoparticles complexes were formed on Si (111) substrates and carbon-coated copper grids for Fourier transform infrared (FTIR) spectroscopy and transmission electron microscopy (TEM) measurements respectively.

4.2.2. UV-vis. and FTIR studies

The gold nanoparticle-S-DNA solutions at various stages of preparation were subjected to UV-vis spectroscopy measurements and the spectra obtained are shown in Figure 4.1A. Curves 1, 2 and 3 in the Figure 4.1A correspond to spectra recorded from the gold nanoparticle solution, S-DNA-gold nanoparticle solution and pure aqueous S-DNA solution respectively. The spectrum of the gold nanoparticle solution before

addition of S-DNA shows a sharp resonance at 516 nm (curve 1) which broadens and shifts to the red upon complexation with S-DNA molecules (curve 2). The absorption band at 516 nm arises due to excitation of surface plasmon vibrations in the gold nanoparticles and is responsible for their lovely ruby-red color.[1a,8b] The red-shift in the surface plasmon resonance band clearly indicates surface co-ordination of the S-DNA molecules with the gold nanoparticles while the broadening of this absorption band suggests cross-linking of the gold nanoparticles in solution.[1a,11] We would like to mention that DNA solution is colorless and does not show any absorption in the visible region of the electromagnetic spectrum (curve 3). Figure 4.1B shows the FTIR

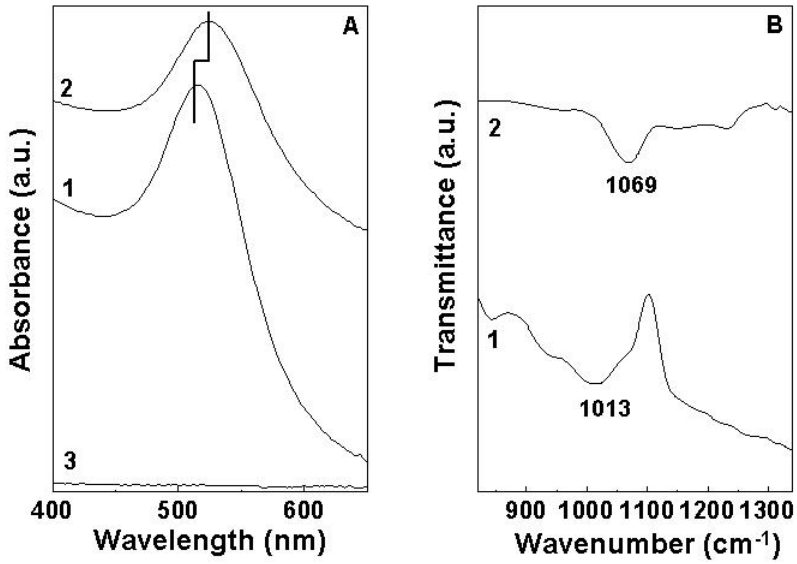

Figure 4.1. A) UV-Vis spectra of the borohydride reduced gold nanoparticle solution (curve 1) and the gold nanoparticle solution after addition of S-DNA and after aging for 2 h (curve 2). Curve 3 represents the spectrum recorded from pure aqueous S-DNA solution. B) FTIR spectra of drop-coated film of pure S-DNA (curve 1) and S-DNA-gold nanoparticle complexes (curve 2) on Si (111) substrate.

spectra recorded from drop-coated films of pure S-DNA (curve 1) and S-DNA-gold nanoparticle complexes (curve 2) on Si (111) wafers. The S-DNA film exhibits an absorption band centered at 1013 cm^{-1}, this band corresponding to the $P\text{-}S^-$ stretching vibration (curve 1). This band is broad and may be due to resonance between S and O atoms in the phosphate backbone. On complexation of S-DNA with the gold nanoparticles, this band becomes sharper and shifts to 1069 cm^{-1}. This clearly indicates

that S-DNA molecules bind to gold nanoparticles through the sulfur atoms as illustrated in Scheme 1.

Scheme 1: Binding of gold nanoparticles with S-DNA

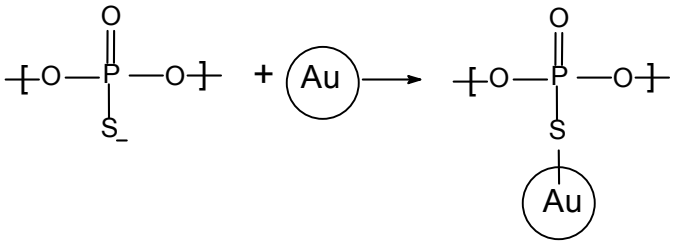

4.2.3. TEM study

Figure 4.2A and B show representative TEM pictures recorded from films of S-DNA-Au nanoparticles complexes prepared by drop-coating of the 2 hour old solution on a TEM grid. For comparison, the TEM micrograph obtained from a drop-coated film of gold nanoparticles before complexation with S-DNA molecules is shown in Figure 4.2C. From a comparison of Figure 4.2A and B with C, it is clear that the particles assemble into loose, open structures consequent to complexation with S-DNA. In the case of the parent gold nanoparticle solution (i.e., without S-DNA), the particles assemble into a

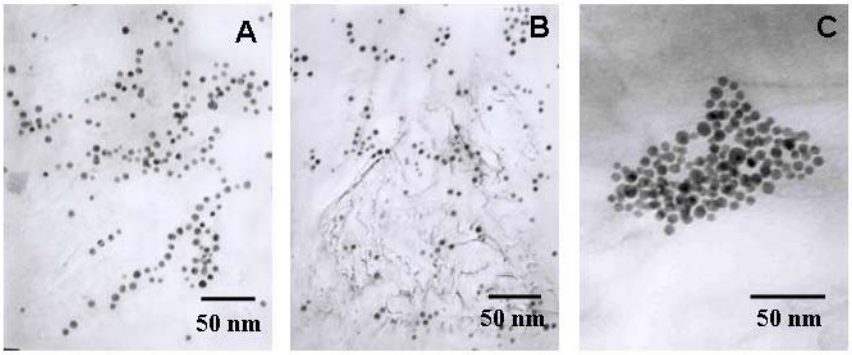

Figure 4.2. A and B - Representative TEM pictures of drop-coated films of gold – S-DNA complexes on carbon-coated grids. C) TEM picture of a drop-coated film of borohydride reduced gold nanoparticles before complexation with S-DNA on a carbon-coated TEM grid.

dense close-packed structure after evaporation of water (Figure 4.2C). This distinguishing feature indicates that the S-DNA molecules bound to the gold nanoparticles surface prevent their rapid assembly and hold them in place in quasi-linear open structures. In some regions, fairly long linear arrangement of nanoparticles is observed (Figure 4.2A).

Another important observation is the difference in separation between the gold nanoparticles before (Figure 4.2C) and after (Fig 4.2A and 4.2B) complexation with S-DNA molecules. The separation between the particles is larger (and more uniform) in the case of the S-DNA-Au nanoparticles sample (Figure 4.2A and B) than that observed for the gold nanoparticles before complexation with S-DNA (Figure 4.2C). Figure 4.3A and B show histograms of the gold nanoparticles edge-edge distances measured from the TEM micrographs shown in Figure 4.2 A, B and Figure 4.2C for the S-DNA-Au nanoparticles and starting gold nanoparticles samples respectively. A Gaussian fit to the histograms yielded an edge-edge distance of 32 ± 6 Å for S-DNA-Au nanoparticles complex and 12 ± 2 Å for gold nanoparticles before complexation with DNA.

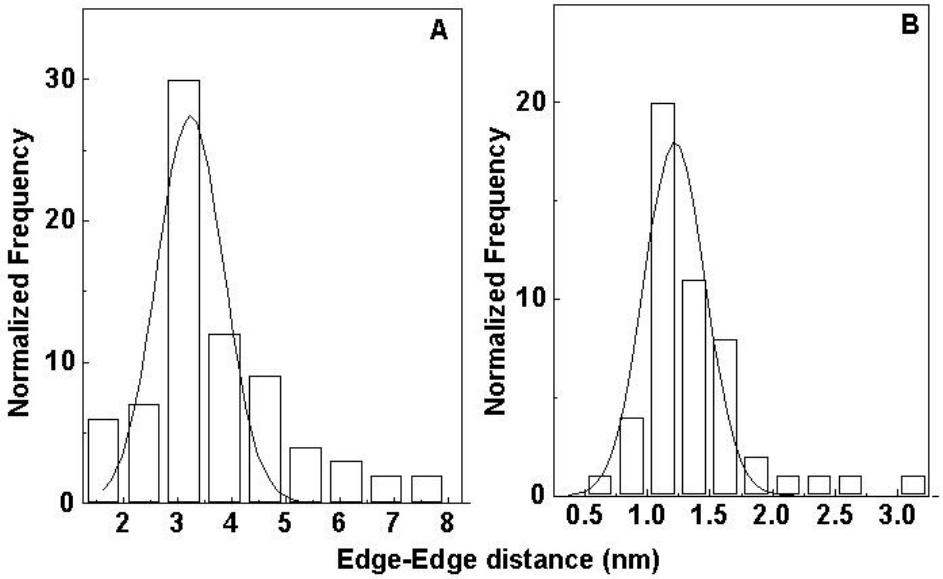

Figure 4.3. A) Histogram of edge-edge distances between gold nanoparticles cross-linked with S-DNA molecules. B) Histogram of edge-edge distances between gold nanoparticles before complexation with S-DNA. The solid curves in both figures represent Gaussian fits to the histograms.

The edge-edge separation between gold nanoparticles complexed with S-DNA is in good agreement with the length of S-DNA molecule of (~ 40 Å). We believe that the presence of a well-defined peak at 32 Å in the histogram showing inter particle edge-edge distance is a clear indication that the S-DNA molecules bind to the gold nanoparticles only through terminal sulfur atoms in the DNA as depicted in Figure 4.4.

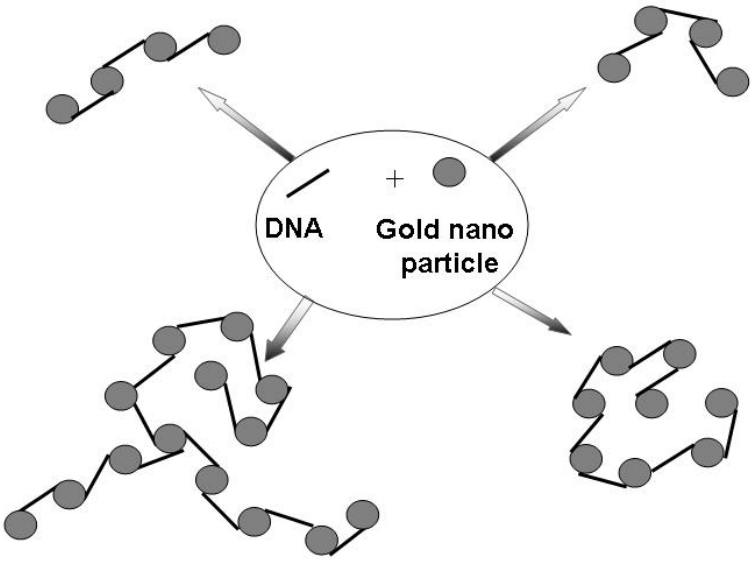

Figure 4.4. Schematic of possible gold nanoparticles superstructures formed in solution using S-DNA as a interconnector.

On the length scale of 40 Å, S-DNA acts like a rigid linker between the gold nanoparticles and the superstructures observed in Figure 4.2A and B may be easily constructed from the connector as illustrated in Figure 4.4. Unlike in the case of other DNA-based gold nanoparticle cross-linking strategies that rely on hybridization of complementary DNA molecules for super-structure formation, S-DNA covalently cross-links the gold nanoparticles and will conceivably lead to greater stability and possible electronic conduction between the nanoparticles via the covalently linked DNA backbone.

This covalent cross-linking assembles the nanoparticles in open structure. However it does not have any control to organize the nanoparticles in predefined geometry so it is desirable to have protocol, which has better control over the organization of nanoparticles. In an alternate approach presented below we used DNA as a template for the assembly of nanoparticles.

4.3. Assembly of nanoparticles in solution using DNA as a template

4.3.1. Procedure

The synthesis of double-helical DNA1 and DNA2 and lysine modified nanoparticle solution has already been discussed in chapter 2. After stabilization of the

lysine-capped gold nanoparticle solution, DNA was added to the solution to yield an overall DNA concentration of 10^{-6} M in the gold nanoparticle-DNA mixture.

On addition of DNA to the gold nanoparticle solution, the solution color changed rapidly to blue indicating aggregation of the gold nanoparticles.[12] The gold nanoparticle-DNA solutions were aged for 2 h to enable the assembly of the gold nanoparticles to reach completion after which the solutions were subjected to ultracentrifugation. The gold nanoparticles-DNA hybrid material was separated and redispersed in water at physiological pH thus resulting in the removal of un-coordinated DNA molecules in solution. Similar experiments were performed with calf thymus DNA. The gold nanoparticle-DNA solutions thus obtained were subjected to UV-vis and fluorescence spectroscopy.

4.3.2. UV-visible and Fluorescence studies

The UV-vis spectra obtained are shown in Figure 4.5A. Curves 1, 2, 3 and 4 in Figure 4.5A correspond to spectra recorded from the lysine-capped gold nanoparticle solution (before addition of DNA), synthetic DNA 1- and 2-gold nanoparticle solutions and calf thymus DNA-gold nanoparticle solution, respectively. It is observed that there is a broadening of the surface plasmon resonance of gold nanoparticles on coordination of gold nanoparticles with the DNA template. (compare curves 2, 3 and 4 with curve 1) and furthermore, the extent of broadening is considerably higher for the calf thymus DNA-gold nanoparticle solutions (curve 4). It is well known that the optical properties of gold nanoparticle solution change when the nanoparticles aggregate, the main feature being the growth of a long wavelength resonance (the longitudinal vibrational mode) due to overlap of the surface plasmon modes from neighboring particles.[11,12] The extent of red-shift in the longitudinal plasmon resonance indicates the degree of aggregation. The UV-vis spectra shown in Figure 4.5A thus show clearly that the gold nanoparticles are coordinated to the synthetic DNA molecules and also that the size of the supercluster structures formed is larger in the case of the calf thymus DNA-gold nanoparticle hybrids relative to synthetic DNA-gold nanoparticle hybrids. The role of Coulombic interactions in the creation of DNA-gold nanoparticle structures is underlined by the fact that bare

gold nanoparticles as well as carboxylic acid derivatized gold nanoparticles (which are negatively charged at

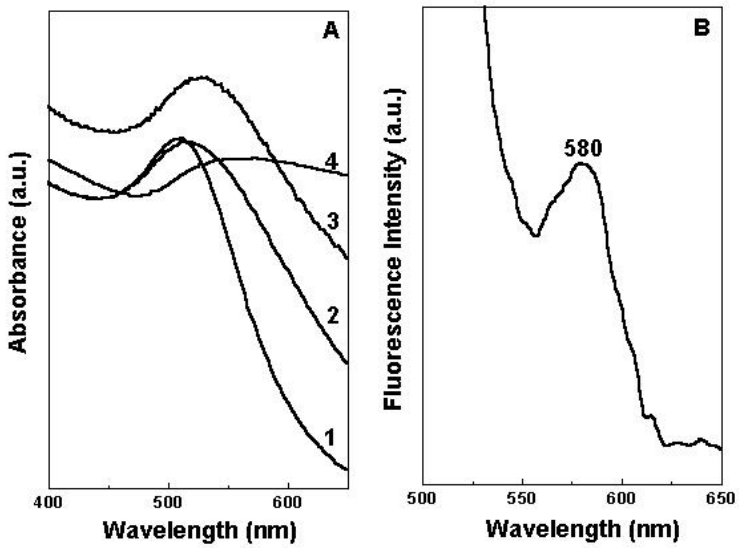

Figure 4.5. A) UV-vis spectra recorded from lysine-capped gold nanoparticle solution (curve 1), synthetic DNA 1- gold nanoparticle hybrid solution (curve 2), synthetic DNA 2- gold nanoparticle hybrid solution (curve 3), and calf thymus DNA-gold nanoparticle solution (curve 4). B) The fluorescence spectrum recorded from the synthetic DNA 1-gold nanoparticle solution by excitation of the ethidium bromide intercalator.

physiological pH) when mixed with either of the DNA solutions did not lead to a large change in the optical properties of the gold nanoparticle solution.

Figure 4.5 B shows the fluorescence spectrum recorded from the synthetic DNA 1-gold nanoparticle solution. A strong emission signal is observed at ca. 580 nm and arises from the ethidium bromide intercalator. Ethidium bromide is known to intercalate into the base pairs of DNA double helical structures and this process is readily detected by the enhanced fluorescence exhibited by this molecule on intercalation in DNA.[13] The presence and strength of this emission band indicates clearly that the double helical structure of the synthetic DNA molecules is retained[13] even after complexation of the lysine-capped gold nanoparticles. This aspect is important if successful templating action of such biomacromolecules is to be achieved in nanoparticle self-assembly.

4.3.3. Transmission electron microscopy (TEM) and scanning tunneling microscopy (STM) studies

Drop-coated films of synthetic DNA1-gold nanoparticle complexes were deposited on carbon-coated grids for transmission electron microscopy, and films of synthetic DNA 2-gold nanoparticles complexes were deposited on a highly conducting Si (111) wafer for scanning tunneling microscopy. Figure 4.6A shows the TEM picture of the synthetic DNA 1-gold nanoparticle film. Parallel dark bands are clearly observed with a high degree of order in the stacking of the chains over the surface of the film. Under higher (optical) magnification of the TEM micrograph, it was observed that each one of the band was composed of smaller black bands. The length of these bands was calculated to be ca. 80 Å in fairly good agreement with the length of the synthetic DNA 1 molecule of ca. 55 Å. While the individual gold nanoparticles could not be resolved in the TEM picture (attempts were made to increase the magnification in the TEM measurement but this resulted in melting of the DNA 1-gold nanoparticles film due to the higher energy electron beam), the dark bands are clearly due to electron scattering from the gold nanoparticles. A diffraction pattern corresponding to that of gold was observed and supports the above observation. The average separation between the longer black bands (measured as the distance between the centers of adjacent, parallel black bands) was ca. 90 Å in fairly good agreement with that expected from a gold nanoparticle-DNA 1 double helix-gold nanoparticles sandwich assembly. Figure 4.6B shows an STM image obtained from a film of DNA 2-gold nanoparticles complexes on a Si (111) wafer wherein the individual gold nanoparticles can be clearly seen. It is observed that the nanoparticles are arranged in a regular, linear fashion. Furthermore the surface height variation of DNA 2-gold nanoparticle assemblies, shown in Figure 4.6B is plotted in Figure 4.6C. Highly periodic variation in height occurs along this direction with a periodicity of ca. 4 nm. This periodicity is in excellent agreement with the size of gold nanoparticles and clearly indicates the arrangement of the gold nanoparticles in linear arrays.

The TEM and STM pictures indicate electrostatic assembly of the gold nanoparticles on the DNA molecule surface with the repetitive gold –DNA-gold-DNA- superstructures which is believed to be a consequence of an attempt to maximize the electrostatic interaction in the complex. The schematic shown in Figure 4.6D is the

expected structure of the DNA-gold nanoparticles-DNA-gold nanoparticles assembly and corresponds to a magnified view of the box drawn in the TEM (Figure 4.6A) and STM.

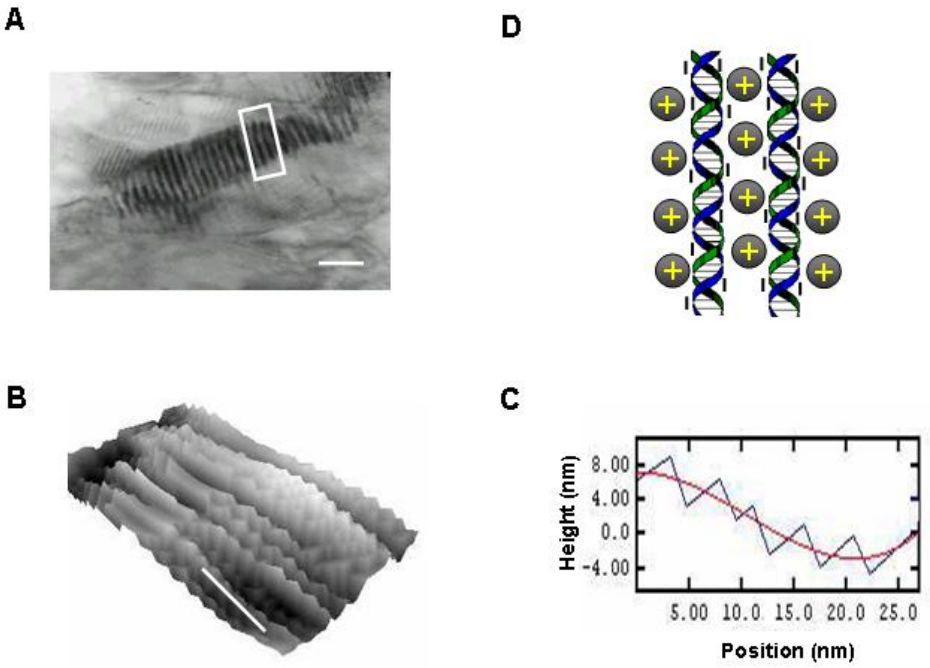

Figure 4.6. A) TEM picture of the synthetic DNA 1-gold nanoparticles complex film showing the linear gold supercluster assemblies mediated by the DNA template. The scale bar corresponds to 100 nm. B) STM image of a synthetic DNA 2-goldnanoparticles complex film drop coated on a highly conducting Si substrate showing the linear gold nanoparticles assemblies. The length of the line in this image corresponds to 27.5 nm. C) Surface height variation with distance along the line shown for the STM image in B. D) Schematic showing the expected templating action of the DNA double helical molecules leading to the condensed, layered gold-nanoparticles-DNA- gold nanoparticles-DNA…..structures observed in the TEM (A) and STM (B) image.

(Figure 4.6B) images. The TEM analysis of uncapped gold as well as carboxylic acid derivatized gold nanoparticles- DNA film did not reveal such ordered linear structure, thus highlighting the importance of electrostatic interactions in realizing the linear supercluster assemblies

4.3.4. Fourier Transform Infrared spectroscopy studies

Drop coated film of a DNA 1-gold nanoparticle complex was formed on Si (111) substrate for FTIR measurement. Figure 4.7 is the FTIR spectrum of that film in different spectral regions. FTIR measurements of the synthetic DNA 1-gold nanoparticle film showed the presence of bands at 1005 cm^{-1} and 1136 cm^{-1}. The resonances at 1136 and

1005 cm^{-1} (Figure 4.7A) correspond to the backbone PO_2 antisymmetric stretching and deoxyribose C-C stretching vibrations respectively.[14] The methylene antisymmetric and symmetric

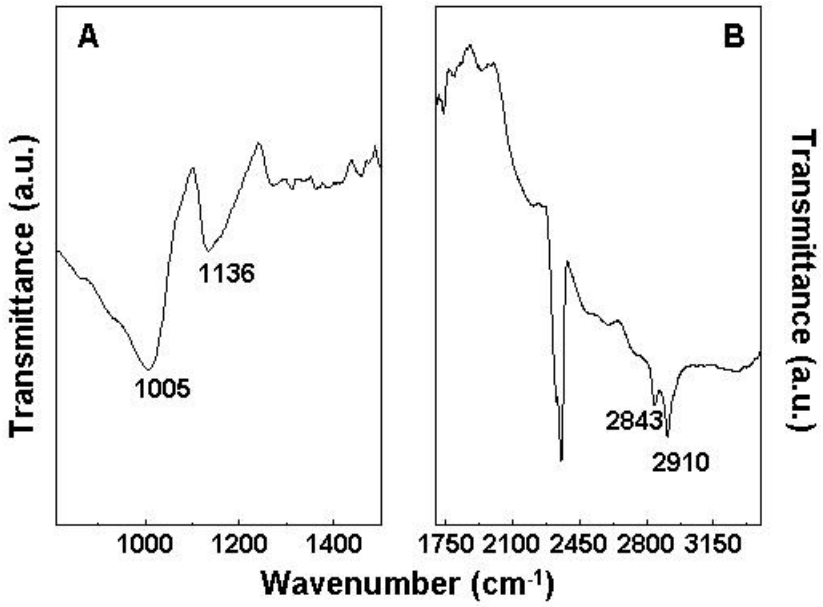

Figure 4.7. FTIR spectrum recorded from synthetic DNA-gold nanoparticle hybrid film formed on Si (111) substrate by solvent evaporation technique.

vibrations from the methylene group present in sugar bases are observed at 2910 and 2843 cm^{-1} (Figure 4.7B) respectively. The FTIR data clearly indicate that DNA is not degraded after forming the complex with the gold nanoparticles.

4.3.5. X-ray Photoemission studies

A chemical analysis of the DNA1-gold nanoparticle film formed by drop coating on Si (111) wafer was done using XPS and the Au 4f, P 2p, N 1s and C 1s XPS core level spectra were recorded. Figure 4.8A shows the Au 4f core level spectrum. The $4f_{7/2}$ and $4f_{5/2}$ spin-orbit components can clearly be seen with no evidence of a chemically shifted component indicating that the surface binding of lysine molecules is relatively weak. The binding energy (BE) of the $4f_{7/2}$ was 84 eV and is characteristic of metallic Au.[15]

A strong P 2p signal was recorded from the film (Figure 4.8B) and indicates the presence of DNA molecules in the film. This core level could be fit to the $2p_{3/2}$ (BE =

133.4 eV) and $2p_{1/2}$ spin-orbit components as shown in Figure 4.8B. The P $2p_{3/2}$ BE agrees fairly well with reported values of DNA films immobilized on self-assembled

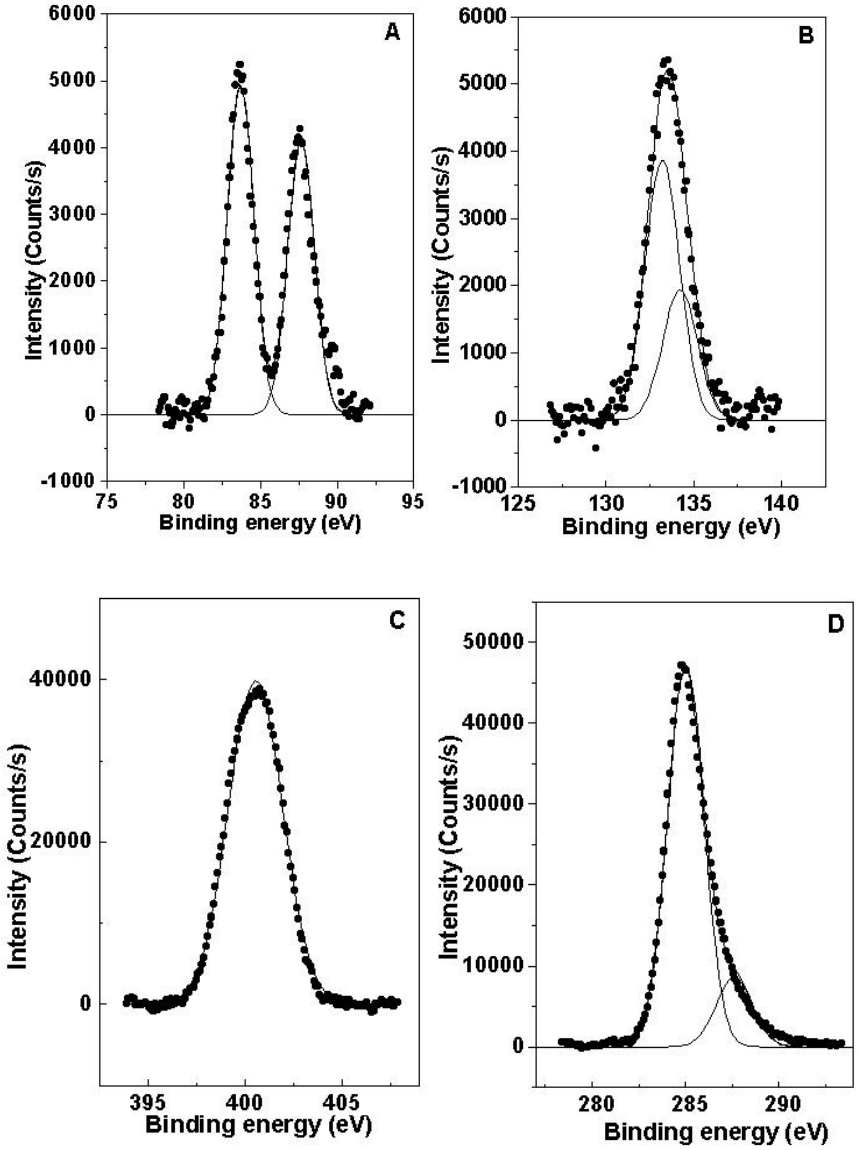

Figure 4.8. A) XPS spectrum of the Au 4f core level recorded from the synthetic DNA 1-gold nanoparticle hybrid film. The spectrum has been resolved into the $4f_{7/2}$ and $4f_{5/2}$ spin-orbit components and are shown in the figure. B) XPS spectrum of the P 2p core level recorded from the synthetic DNA-gold nanoparticle hybrid film. The spectrum has been resolved into the $2p_{3/2}$ and $2p_{1/2}$ spin-orbit components and are shown in the figure. C) XPS spectrum of the N 1s core level recorded from the synthetic DNA-gold nanoparticle hybrid film. D) XPS spectrum of the C 1s core level recorded from the synthetic DNA-gold nanoparticle hybrid film

monolayer surfaces[16] and indicates no degradation of the DNA molecules due to coordination with the gold nanoparticles. The N 1s spectrum shows the presence of a

single component (Figure 4.8C) at 400.5 eV and is assigned to the nitrogen in the bases of the DNA molecules[17] in the conjugate film as well as the nitrogen in the gold surface-bound lysine molecules while the C 1s spectrum (Figure 4.8 D) could be resolved into two chemically distinct components at 285 eV and 288.5 eV. The lower BE component in the C 1s spectrum is assigned to carbons in the DNA sugars and bases while the higher BE component arises due to electron emission from carbons coordinated to the phosphates in DNA as well as from carbons coordinated to amine and carboxylic acid functional groups in the gold-surface bound lysine molecules.

In next step we simplified the process in which we organized the nanoparticles by evaporating the lysine capped gold nanoparticles on drop dried DNA films and the process is as follows.

4.4. Assembly of nanoparticles on drop-dried film of DNA

4.4.1. Procedure

A 10^{-6} M solution of synthetic double-helical 30-mer DNA (sequence: CCTTAAGCTTTTGTAGAATCTATCTACATA) molecules was prepared and films of the DNA molecules were cast on quartz and highly conducting Si (111) wafers by placing drops of the DNA solution on different substrates and evaporation of the aqueous component. This process was repeated three times to get a fairly thick DNA film. After that, drops of lysine capped gold nanoparticle solution were added to the DNA films on quartz and Si wafers and allowed to dry. For comparison, a film of lysine capped gold nanoparticles was also cast on a bare quartz substrate.

4.4.2. UV-visible and FTIR studies

Figure 4.9A shows the UV-vis spectra recorded from the plain DNA film (curve 1), a film of lysine-capped gold nanoparticles (curve 2) and the DNA film after complexation with lysine-capped gold nanoparticles by simple drop-coating (curve 3). A number of interesting features are seen which may be interpreted as follows. A strong resonance is observed at 545 nm (indicated by an arrow in Figure 4.9A) in both the lysine-capped gold nanoparticle film (curve 2) as well as the DNA film complexed with lysine-capped gold nanoparticles (curve 3). This resonance is due to excitation of surface

plasmon vibrations in the gold nanoparticles and is responsible for the ruby-red color of the nanoparticle films and solutions.[8b,18] This resonance is clearly absent in the bare DNA film (curve 1). In addition to the resonance at 545 nm, the DNA film complexed with lysine-capped gold nanoparticles shows an additional resonance at 685 nm (indicated by an arrow in Figure 4.9A). It is well known that aggregation of noble metal nanoparticles such as silver and gold into quasi-linear superstructures leads to the appearance of a longitudinal surface plasmon resonance, red-shifted with respect to the transverse component (in this case, the 545 nm resonance).[12,19] The presence of the longitudinal plasmon resonance at 685 nm in the DNA – Au nanoparticle conjugate film (curve 3) is therefore strongly indicative the assembly of the gold nanoparticles in extended, open structures mediated by the underlying DNA template. Attractive electrostatic interaction between the positive charges in the lysine molecules bound to the gold nanoparticles and the negative charges on the phosphate groups of the DNA molecules drives the assembly

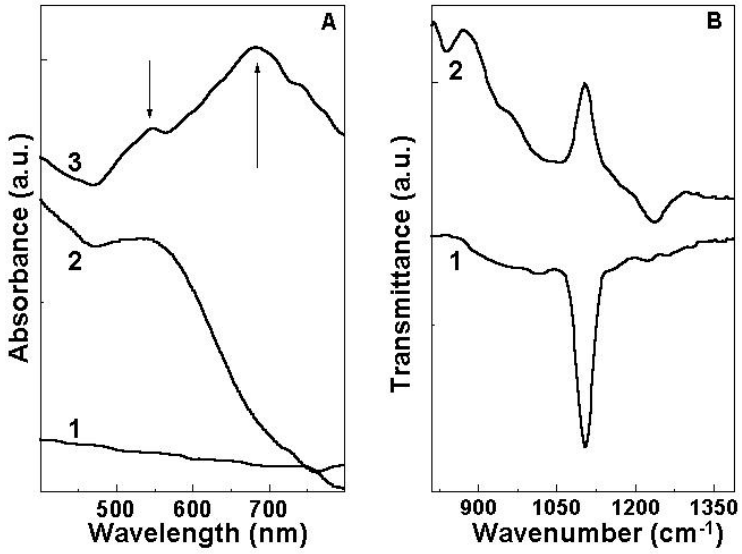

Figure 4.9: (A) UV-vis spectra recorded from a drop-dried DNA film deposited on quartz (curve 1); a lysine-capped gold nanoparticle film deposited by solution casting onto quartz (curve 2) and a drop-dried DNA film to which lysine-capped gold nanoparticles were added (curve 3). The transverse and longitudinal surface plasmon resonances are indicated in the Figure.(B) FTIR spectra recorded from a DNA film deposited on a Si (111) substrate by solution casting (curve 1) and from a drop-dried DNA film on Si (111) substrate after addition of lysine-capped gold nanoparticles (curve 2).

of the gold nanoparticles into close-packed, open structures inferred from the UV-vis measurements. The DNA molecules thus act like a counter ions and screen the repulsive interactions between the positively charged gold nanoparticles thus enabling their assembly into close-packed superstructures.

Figure 4.9B shows the Fourier transform infrared (FTIR) spectra recorded from the DNA film on a Si (111) wafer (curve 1) and the DNA film after complexation with lysine-capped gold nanoparticles (curve 2). A strong absorption band centered at 1105 cm^{-1} is clearly observed in the as-prepared DNA film (curve 1). This resonance is assigned to the deoxyribose band, the presence of which is known to be a strong indicator of the hybridization of the DNA molecules in a double-helical structure.[20] On complexation of the DNA film with lysine-capped gold nanoparticles, this resonance is broadened and shifted to smaller wave numbers. This indicates some destabilization of the double-helical structure consequent to electrostatic assembly of the gold nanoparticles. However, as will be seen from the microscopy studies below, this factor does not affect the linear gold nanoparticle superstructure formation, which is the goal of this protocol.

4.4.3. STM studies

The STM image obtained from the as-deposited DNA film is shown in Figure 4.10A. While the individual structural units such as the bases in the DNA molecules are not resolved in this image, it is observed that the molecules have organized themselves into aggregates with some indication of long-range order. Earlier STM studies of DNA films on highly oriented pyrolytic graphite[21] and Au (111) substrates[22] have revealed similar aggregated structures of DNA. The films were extremely stable in time and repeated scans did not result in the movement of the DNA molecules over the surface. This indicates fairly strong binding of the DNA molecules with the underlying Si substrate, possibly through interaction of the phosphate groups in the DNA with Si atoms on the surface of the substrate. Another possibility is the strong interaction of the adenine bases in the DNA molecules with Si, an aspect which has been observed in other STM related studies.[23] An estimate of the thickness of the DNA film deposited by drop-coating on a highly conducting Si wafer was made using ellipsometry. The film was fairly

uniform over the surface of the substrate with an average thickness of 5 nm. This thickness corresponds to roughly 2.5 DNA double-helical molecules stacked one on top of the other.

The STM image recorded from this DNA film after addition of lysine-capped gold nanoparticles and thorough drying of the film is shown in Figure 4.10B This image clearly shows highly organized, parallel linear assemblies of the gold nanoparticles. In order to ascertain whether the dimensions of the features seen in Figure 4.10B agree with expected sizes of the gold nanoparticles and the DNA molecular length, the surface height variation with distance along two nearly perpendicular directions (indicated in Figure 4.10B) was plotted and are shown in Figures 4.10.C and D. The surface height variation with distance along the length of one of the linear nanoparticle assemblies is plotted in Figure 4.10C and clearly shows the presence of a high degree of order in the supercluster. The average size of the structures along the length of the Au "nanowire" was estimated to be ca. 4 nm in excellent agreement with the size of the nanoparticles (3.5 nm). A plot of the surface height variation along a direction perpendicular to that of Figure 4.10C is shown in Figure 4.10D. In this case as well, a highly regular and periodic

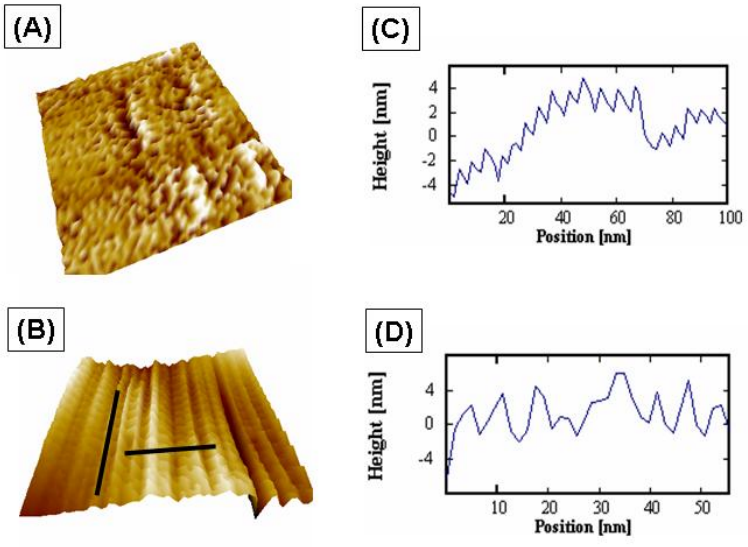

Figure 4.10: (A) STM image recorded from a drop-dried DNA film deposited on a conducting Si substrate. The extent of this image is 100 nm X 100 nm.(B) STM image recorded from a drop-dried DNA film deposited on a conducting Si substrate after addition of lysine-capped gold nanoparticles. The extent of this image is 100 nm X 100 nm.(C) Surface height variation with distance along the vertical line shown in the STM image of the DNA-gold nanoparticle film (B).(D) Surface height variation with distance along the horizontal line shown in the STM image of the gold nanoparticle-DNA film (B).

assembly of structures is seen. The average size of these structures is ca. 10 nm. The length of a 30-mer DNA molecule is ca. 11 nm and indicates that the DNA molecules are organized parallel to the direction of measurement of Figure 4.10D. We would like to add that STM images of films of lysine-capped gold nanoparticles deposited by drop-coating on bare Si substrates did not show any ordering into superstructures. The STM results thus provide unequivocal evidence for the templating action of the DNA molecules by a simple drop-coating method described above. We believe that the DNA molecules which are locked into a fairly rigid structure prior to addition of lysine-capped gold nanoparticles (Figure 4.10A) are rendered sufficiently mobile due to solvation by water during addition of drops of the lysine-capped gold nanoparticle solution on the DNA film surface. This process facilitates reorganization into highly regular linear nanoparticle superstructures during electrostatic complexation. The reorganization of the DNA molecules by electrostatic interaction with the gold nanoparticles may be viewed as the in-plane analogue of the well-known electrostatically driven layer-by-layer assembly of nanoscale systems along a direction normal to the substrate surface.[24] A sandwich structure consisting of alternate layers of positively charged gold nanoparticles and negatively charged DNA molecules constrained to grow along a plane parallel to the surface of the substrate would lead to an energetically stable situation as seen in the STM images (Figure 4.10B).

4.5. Assembly of nanoparticles by using electrostatically entrapped DNA molecules in lipid thin film as templates

4.5.1. Process

Thin films of octadecylamine of ca. 25 nm thickness were deposited by thermal evaporation in a vacuum coating unit at a pressure better than 1 x 10^{-7} Torr. The films were deposited onto gold-coated quartz crystals (for quartz crystal microgravimetry (QCM) measurements), carbon-coated transmission electron microscopy (TEM) grids and quartz substrates (for UV-vis spectroscopy studies). The ODA film deposited on the 6 MHz QCM crystal was then immersed into a 10^{-6} M synthetic DNA and calf-thymus DNA (CT-DNA, ca. 1000 base pairs long) solution in water at physiological pH and the

mass uptake due to DNA diffusion into the ODA film was monitored *ex-situ* after thorough washing and drying of the films. The ODA-DNA composite film was then immersed in 10^{-4} M $AgNO_3$ solution in water (pH ~ 7) and the mass uptake due to incorporation of Ag^+ ions was monitored *ex-situ* in a similar fashion. The metal ions in the ODA-DNA-Ag^+ composite film on quartz were reduced *in-situ* by placing the film in hydrazine vapor for a period of 1 h and the excitation of surface plasmon vibrations in the silver nanoparticles formed in the film was monitored by UV-vis spectroscopy. Direct evidence of the nature of the Ag nano-structures formed due to DNA templating is obtained from TEM measurements of a 25 nm thick ODA-DNA-(Ag nanoparticle) film after removal of the ODA matrix. The lipid matrix was removed by placing the TEM grids bearing the ODA-DNA-Ag nano composite film (one cycle of silver ion exchange and reduction) in hexane and soaking the film for 15 minutes. The grid was then carefully removed, dried gently in flowing nitrogen and analyzed by TEM.

4.5.2. Quartz crystal micro gravimetric and UV-visible spectroscopy studies

Figure 4.11A and 4.12A show the QCM measurements of the kinetics of diffusion of CT-DNA and 30-mer synthetic DNA into a 25 nm thick ODA film (region 1). From the QCM measurements, an equilibrium mass uptake of CT-DNA and synthetic DNA in the lipid film of ca. 6570 and 2200 ng/cm^2 is observed within ca. 20 minutes of immersion. The diffusion of DNA into the ODA matrix is driven by attractive electrostatic interaction between the protonated ODA molecules (pK_B ~ 10.5) in the film and the negative charges due to the phosphate groups in DNA. As mentioned in the introduction, such electrostatic interactions have been used with success in this group to immobilize surface-modified gold nanoparticles[8a], enzymes[9a,b,c] and DNA[9d] in thermally evaporated lipid films.

From the mass of the ODA film and intercalated DNA molecules and accounting for the charges on the DNA duplexes, it was observed that the positive charge in the lipid film was overcompensated by the negative charge on the DNA molecules by a factor of ~ 2.8 and 7 for CT-DNA and 30mer synthetic DNA respectively. Such charge overcompensation effects have been observed in the layer-by-layer assembly of polyelectrolytes and DNA[24] and indeed, forms the basis of this electrostatic assembly

protocol. The ODA-DNA composite film was then immersed in 10^{-4} M $AgNO_3$ solution in water (pH ~ 7) and the mass uptake due to incorporation of Ag^+ ions was monitored *ex-situ* in a similar fashion (Figure 4.11A and Figure 4.12A, region 2). The entrapment of the Ag^+ ions, driven by attractive Coulombic interaction between the metal cations and the immobilized anionic DNA molecules, is rapid and an equilibrium mass loadings (Ag^+ ions alone) of 14,550 and 11000 ng/cm^2 are attained within 40 and 75 minutes of immersion for CT-DNA and synthetic DNA respectively.

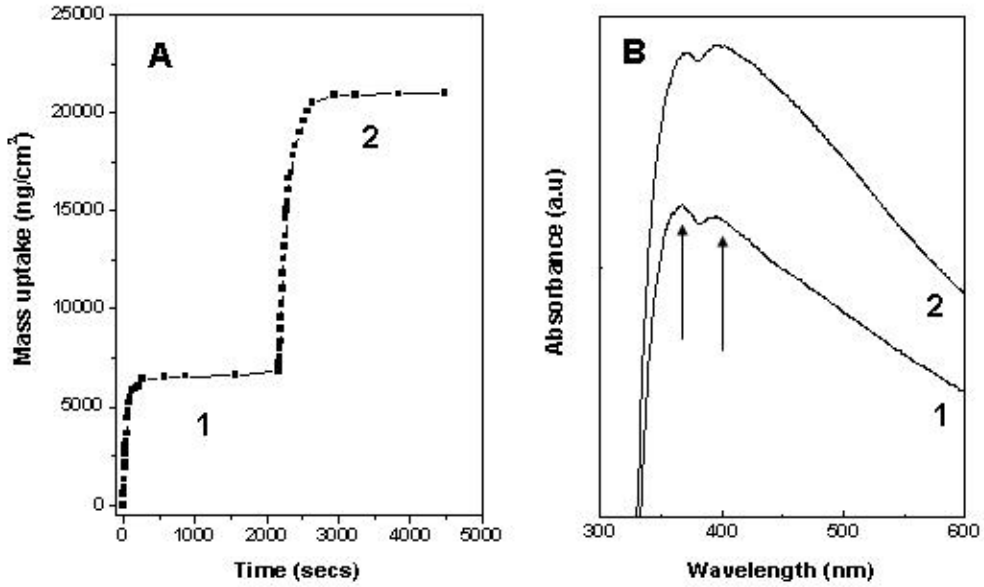

Figure 4.11: (A) QCM mass uptake kinetics data of the sequential diffusion of calf-thymus DNA (region 1) and Ag^+ ions (region 2) into a 25 nm thick ODA film. (B) UV-vis spectra recorded from a 25 nm thick ODA-DNA-(Ag nano) composite film on quartz after the first cycle of silver ion entrapment and reduction (curve 1) and the ODA-DNA-(Ag nano) film after an additional cycle of Ag^+ entrapment and reduction (curve 2). The transverse and longitudinal surface plasmon resonances are indicated in the figure.

The entrapment of Ag^+ ions in the CT-DNA-ODA film leads to overcompensation of the negative charge on the DNA by a factor of 4.6. Nearly 100 % compensation of the negative charge on the DNA molecules by the diffusing Ag^+ ions was calculated from this QCM experiment. The optimum times of immersion determined from the QCM measurements just discussed were used in the preparation of the ODA-DNA-Ag^+ composite films on the other substrates for additional analysis.

A yellowish brown color could clearly be seen in the film after the first cycle of Ag^+ incorporation and reduction indicating the formation of Ag nanoparticles in the film. A strong resonance is seen at ca. 400 nm due to excitation of surface plasmon vibrations in the silver nanoparticles[8b,25] formed in the film (UV-vis spectrum in Figure 4.11 B,

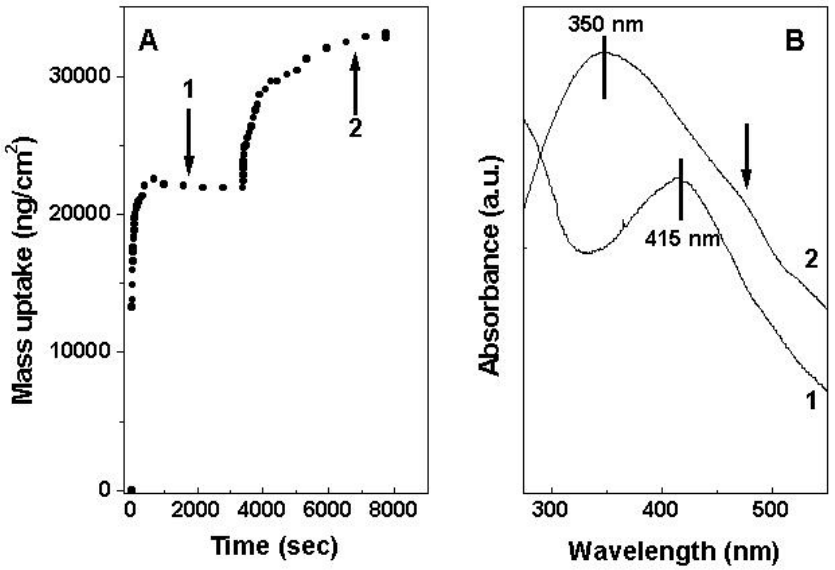

Figure 4.12: (A) QCM mass uptake kinetics data of the sequential diffusion of 30mer DNA (region 1) and Ag^+ ions (region 2) into a 25 nm thick ODA film. (B) UV-vis spectra recorded from a 25 nm thick ODA-DNA-(Ag nano) composite film on quartz after the first cycle of silver ion entrapment and reduction (curve 1) and the ODA-DNA-(Ag nano) film after an additional cycle of Ag^+ entrapment and reduction (curve 2). The transverse and longitudinal surface plasmon resonances are indicated in the figure.

curve 1) and is responsible for the characteristic color. It is observed that this resonance is broad and is accompanied by another component at shorter wavelengths (indicated by arrows in the Figure 4.11B). The broadening of the plasmon resonance and the presence of a low wavelength component at ca. 370 nm indicates aggregation of the silver nanoparticles in the lipid matrix and the generation of a close-packed structure of the nanoparticles.[25] Reduction of the Ag^+ ions enables an additional cycle of Ag^+ incorporation in the film (by immersing the film in $AgNO_3$ solution), which upon reduction with hydrazine, leads to an increase in the surface plasmon resonance intensity in the film (Figure 4.11B, curve 2). This clearly attests to the generation of additional silver nanoparticles in the film.

Figure 4.12B is the UV-vis absorption spectrum recorded from the synthetic DNA-Ag nanoparticle film, A strong resonance is seen at 415 nm (curve 1) and arises due to excitation of surface plasmon vibrations in the silver nanoparticles.[8b,25] A weak longitudinal surface plasmon vibration can be seen at ca. 500 nm and indicates fairly close-packing of the silver particles on the DNA surface within the lipid film. Soaking the ODA-DNA-(Ag nano) film in toluene for 1 h and carefully removing the solvent after this time period enables dissolution of the ODA matrix molecules and to an improvement in the degree of aggregation of the DNA-(Ag nano) super-assemblies. Curve 2 in Figure 4.12B corresponds to the UV-vis spectrum of the ODA-DNA-(Ag nano) film after removal of the lipid matrix. A large blue shift in the transverse surface plasmon resonance to ca. 350 nm is clearly seen to occur and is accompanied by the longitudinal plasmon component at 475 nm (indicated by an arrow in Figure 4.12B). Such a behavior in the optical properties of the film clearly indicates considerable increase in the packing density of the DNA-(Ag nano) assemblies' consequent to removal of the stabilizing (and separating) influence of the ODA matrix. The large blue shift in the transverse surface plasmon vibration from 415 nm to 350 nm is consistent with earlier reports on the organization of silver nanoparticles on thiol-functionalized glass and quartz surfaces.[26]

4.5.3. FTIR study

Incorporation of synthetic 30mer DNA and Ag^+ in ODA film was monitored by FTIR spectroscopy. Figure 4.13 shows the FTIR spectra recorded from the 250 Å thick ODA film on a Si (111) wafer after entrapment of DNA (curve 1) and after incorporation of Ag^+ ions in the ODA-DNA composite film (curve 2) and after reduction of silver ions (curve 3). Two bands centered close to 1100 cm^{-1} and 1250 cm^{-1} can clearly be seen in the spectra and are assigned to the deoxyribose and the backbone PO_2 antisymmetric stretching vibrations respectively[27] and clearly indicate the presence of DNA in the lipid film. The ODA film containing CT-DNA, Ag^+ and silver nanoparticles also shows similar spectra. FTIR measurements are in good agreement with QCM data and further study was done by TEM.

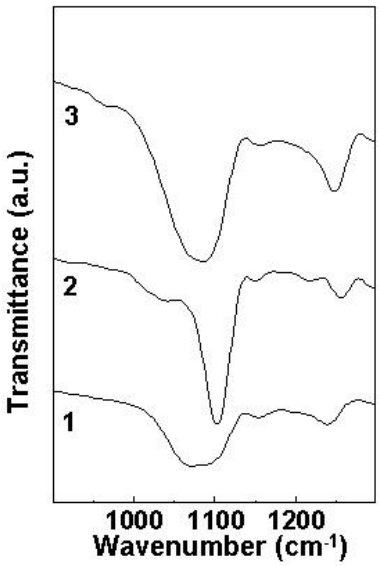

Figure 4.13: The FTIR spectra recorded from a sequentially formed ODA-DNA-Ag composite film, the ODA film after incorporation DNA (curve 1), ODA-DNA film after entrapment of Ag^+ ions (curve 2) and the ODA-DNA-Ag^+ film after *in-situ* reduction of the metal cations to form Ag nanoparticles (curve 3).

4.5.4. Transmission electron microscopy studies

Figure 4.14A-C show representative TEM images recorded from different regions of the ODA-DNA-Ag nano film surface formed after one cycle of Ag^+ ion exchange and reduction. As mentioned earlier, the lipid matrix was removed by careful soaking of the composite film in hexane for 15 min. The individual silver nanoparticles can clearly be seen in all the images and furthermore, a large percentage of the particles are arranged in a highly regular fashion.

The arrows in Figure 4.14 indicate regions of the film where the silver nanoparticles are assembled on the DNA backbone in a quasi-linear fashion. As mentioned above, discrete, randomly organized silver nanoparticles are also observed in the central region of Figure 4.14A and are a consequence of non-specific binding of the Ag^+ ions within the lipid matrix. Figure 4.14B and C show two regions where the silver nanoparticles are assembled on the DNA backbone in roughly circular structures. Selected area diffraction measurements of one of the nanoparticles clearly showed characteristic spots from nanocrystalline silver. The TEM results may be interpreted as follows.

During immersion of the CT-DNA-ODA film in Ag^+ ion solution, the metal cations are entrapped in the matrix both on the surface of the negatively charged DNA backbone by electrostatic interaction as well as non-specifically in the lipid matrix due to purely entropic factors. During reduction of the silver ions with hydrazine, the ions on the surface of the DNA aggregate to form nanoparticles being faithful to the underlying

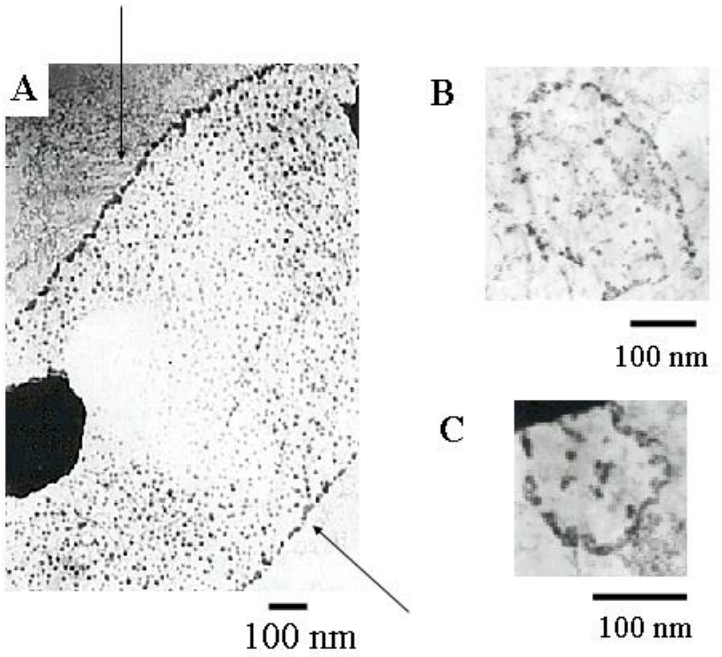

Figure 4.14: TEM pictures (A-C) of different regions of a 25 nm thick ODA-DNA-(Ag nano) film grown on a carbon-coated TEM grid after removal of the lipid matrix (see text for details). The arrows in (A) indicate quasi-linear silver nanoparticle assemblies on the immobilized CT-DNA backbone.

template (and are thus ordered) while the randomly placed ions do not yield nanoparticles with any particular positional order. In order to understand the organization of silver nanoparticles, same experiment was done with synthetic DNA (30mer) of length 100 A.

Figure 4.15A shows the TEM picture of the synthetic DNA-silver nanoparticle film. Parallel dark bands are clearly observed with a high degree of order in the stacking of the chains over the surface of the film. Under higher (optical) magnification of the TEM micrograph, it was observed that each one of the bands was composed of smaller black bands. The length of these bands was calculated to be ca.80 Å in fairly good

agreement with the length of the synthetic DNA molecule of ca. 55 Å. While the individual silver particles could not be resolved in the TEM picture (attempts were made to increase the magnification in the TEM measurement but this resulted in melting of the DNA-silver nanoparticle film due to the higher energy electron beam), the dark bands are clearly due to electron scattering from the silver particles. A diffraction pattern corresponding to that of silver was observed and supports the above observation.

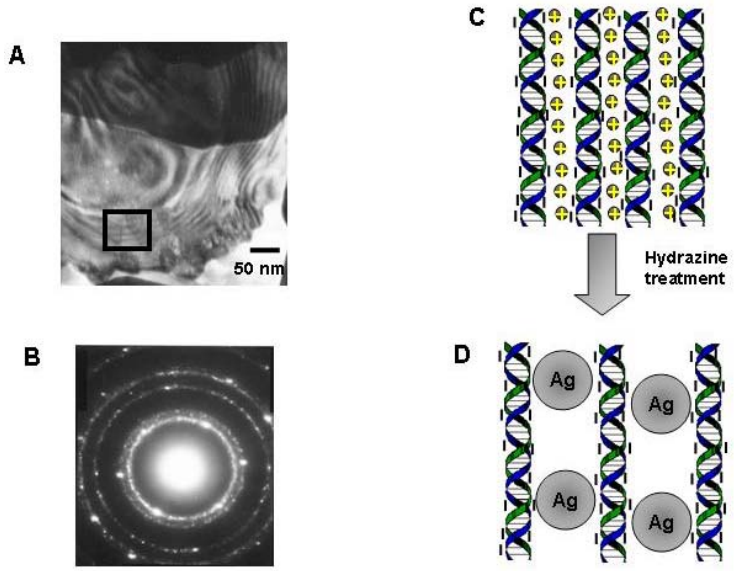

Figure 4.15: A) TEM picture of 25 nm thick ODA-DNA-(Ag nano) film grown on a carbon-coated TEM grid after removal of the lipid matrix. B) The diffraction pattern of selected area from Figure A. C and D) The schematic diagram of formation of silver nanoparticles.

4.6. Conclusions

- The electrostatic assembly of positively charged gold nanoparticles on the negatively charged phosphate backbone of DNA molecules has been demonstrated.
- The use of DNA templates in this DNA-friendly approach yields linear superstructures of the gold nanoparticles in a lamellar assembly.
- A simple procedure based on drop-casting films of DNA followed by lysine-capped gold nanoparticles on solid supports has been described which leads to the spontaneous ordering of the nanoparticles into linear superstructures.

- The above ordering is mediated by electrostatic interaction between the positively charged gold nanoparticles and the negatively charged DNA template molecules.
- This approach shows promise for extension to topologically more intricate structures based on rational DNA design as well as in the generation of nano-wires.
- The electrostatic entrapment of calf-thymus DNA molecules in thermally evaporated fatty amine films and their use as templates for the *in-situ* growth of Ag nanoparticles by an ion exchange/reduction process has been described.
- This approach thus combines the simplicity of a solution based nanoparticle synthesis procedure with the ability to immobilize suitable templates for nanoparticle assembly in thin film form.

4.7. References

1. a) Mirkin, C. A.; Letsinger, R. L.; Mucic, R. C.; Storhoff, J. J. *Nature* **1996**, *382*, 607 b) Mucic, R. C.; Storhoff, J. J.; Mirkin, C. A.; Letsinger, R. L. *J. Am. Chem. Soc.* **1998**, *120***,** 12674. c) Storhoff, J. J.; Elghanian, R.; Mucic, R. C.; Mirkin, C. A.; Letsinger, R. L. *J. Am. Chem. Soc.* **1998**, *120*, 1959. d) Storhoff, J. J.; Mirkin, C. A. *Chem. Rev*. **1999**, *99*, 1849. e) Storhoff, J. J.; Mucic, R. C.; Mirkin, C. A. *J. Am. Chem. Soc.* **1997**, *8* 179. f) Cao, Y. W.; Jin, R.; Mirkin, C. A. *J. Am. Chem. Soc.* **2001**, *123*, 7961.
2. Alivisatos, A. P.; Johnsson, K. P.; Peng, X.; Wilson, T. E.; Loweth, C. J.; Jr, M. P. B.; Schultz, P. G. *Nature* **1996**, *382*, 607.
3. Kumar; A.; Mukharjee, P.; Guha, A.; Adyantaya, S. D.; Mandale, A. B.; Kumar, R. Sastry, M. *Langmuir* **2000**, *16*, 9775.
4. Richter, J.; Seidel, R.; Kirsch, R.; Mertig, M.; Pompe, W.; Plaschke, J.; Schackert, H. K. *Adv. Mater.* **2000**, *12*, 507.
5. Coffer, J. L.; Bigham, S. R.; Li, X.; Pinizzoto, R. F.; Rho, Y. G.; Pirtle, R. M.; Pirtle, I. L. *Appl. Phys. Lett.* **1996**, *69*, 3851.
6. Brawn, E.; Elchen, Y.; Sivan, U.; Ben-Yoseph, G.; *Nature* **1998**, *391*, 775.
7. Ganguly, P.; Sastry, M.; Pal, S.; Shashikala, M. N. *Langmuir* **1995**, *11*, 1078.

8. a) Sastry, M.; Patil, V.; Sainkar, S. R. *J. Phys. Chem. B.* **1998**, *102*, 1404. b) Patil, V.; Malvankar, R. B.; Sastry, M. *Langmuir* **1999**, *15*, 8197.
9. a) Gole, A.; Dash, C.; Mandale, A. B.; Rao, M.; Sastry, M. *Anal. Chem.* **2000***, 72* 1401. b) Gole, A.; Sastry, M. *Biotech.Bioeng.* **2001**, *74*, 172. c) Sastry, M. *Trends in Biotech.* **2002,** *20*, 158. d) Ramakrishnan, V.; Sable, M.; D'Costa, M.; Ganesh, K. N.; Sastry, M. *Chem. Comm.* **2001**, 2622.
10. a) Ravikumar, V. T.; Cheruvallath, Z. S. *Nucleosides and Nucleotide* **1996**, *15***,** 1149. b) Battistini, C.; Brasca, M. G.; Fustinoni, S.; Lazzari, E. *Tetrahedron* **1992**, *48***,** 3209.
11. Mayya, K. S.; Patil, V.; Sastry, M. *Langmuir* **1997**, *13*, 3944.
12. Storhoff, J. J.; Lazarides, A. A.; Mucic, R. C.; Mirkin, C. A.; Letsinger, R. L. Schatz, G. C. *J. Am. Chem. Soc.* **2000**, *122*, 4640.
13. LePecq, J. B.; Paoletti, C. *J. Mol. Biol.* **1967**, *27*, 87.
14. Neault, J. F.; Tajmir-Riahi, H. A. *J. Phys. Chem. B.* **1998**, *102*, 1610.
15. Johnson, S. R.; Evans, S. D.; Mahon, S. W.; Ulman, A. *Langmuir* **1997**, *13*, 51.
16. Higashi, N.; Takahashi, M.; Niwa, M. *Langmuir* **1999**, *15*, 11.
17. Herne, T. M.; Tarlov, M. J. *J. Am. Chem. Soc.* **1997**, *119*, 8916.
18. Henglein, A. *J. Phys. Chem.* **1993**, *97*, 5457.
19. Kreibig U.; Genzel, L. *Surf.Sci.* **1985**, *156*, 678.
20. Taillandier, E.; Liquier, J. *Methods in Enzymology* **1992**, *211*, 307.
21. Beebe, T. P.; Wilson, T. E.; Ogletree, D. F.; Katz, J. E.; Balhorn, R.; Salmeron, M. B. Siekhaus, W. J. *Science* **1989**, *243*, 370.
22. Tano, T.; Tomyo, M.; Tabata, H.; Kawai, T.; *Jpn. J. Appl. Phys., Part1* **1998**, *37*, 3838.
23. Akiyama, R.; Matsumoto, T.; Kawai, T. *J. Phys. Chem. B.* **1999**, *103*, 6103.
24. G. Decher, *Science* **1997**, *277*,1232.
25. Henglein, A *J. Phys. Chem.* **1991**, *97* 5457.
26. a) Chumanov, G.; Sokolov, K.; Gregory, B. W.; Cotton, T. M. *J. Phys. Chem.* **1995**, *99*, 9466; b) Chumanov, G.; Sokolov, C.; Cotton, T. M. *J. Phys. Chem.* **1996**, *100*, 5166.
27. Neault, J-F.; Tajmir-Riahi, H. A. *J. Phys. Chem. B.* **1998**, *102*, 1610.

CHAPTER V

Hydrophobization or Phase Transfer of nanoparticles: from aqueous to organic phase

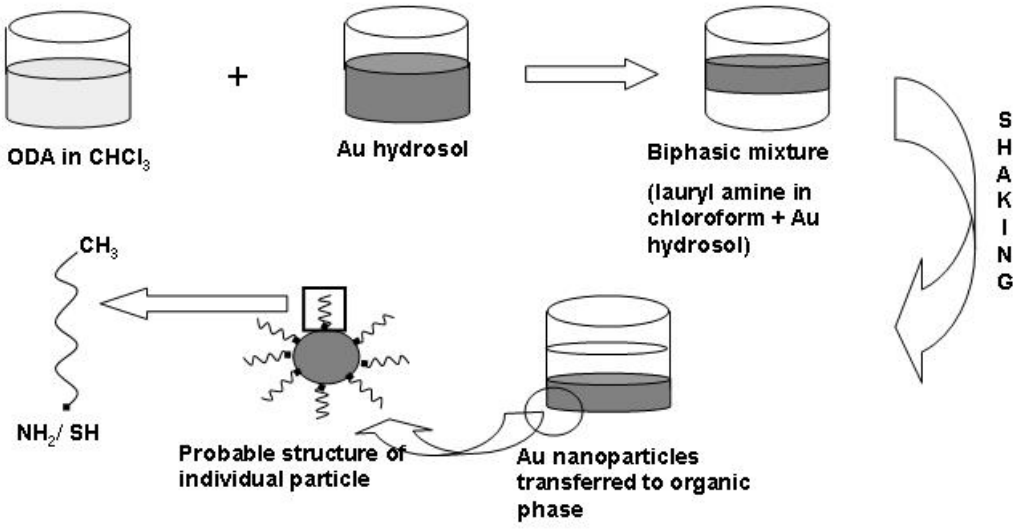

The phase transfer of nanoparticles, synthesized in an aqueous environment, into organic phase by direct co-ordination of the nanoparticles with laurylamine or octadecylamine (ODA)/octadecanethiol (ODT) molecules is described. Hydrophobization of the nanoparticles due to surface co-ordination of ODA/ ODT facilitates the phase transfer process. The hydrophobized nanoparticles can be stored in the form of powder and redispersed in different non-polar organic solvents without any apparent distortion in the particle size distribution. Close-packed nanoparticles thin films were formed by evaporation of the organic component on suitable substrate. The nanoparticles have been characterized at different stages of the synthesis procedure using UV-vis spectroscopy, Fourier transform infrared (FTIR) spectroscopy, X-ray diffraction, thermogravimetry, X-ray photoemission spectroscopy (XPS) and contact angle measurements.

The work described in this chapter has been published: 1) Sastry, M.; Kumar, A.; Mukherjee, P. Colloids Surf. A **2001**, 181, 255. 2) Kumar, A.; Mandale, A. B.; Sastry, M. *Langmuir* **2000,** *16*, 9299. 3) Kumar, A.; Joshi, H.; Pasricha, R; Sastry, M. J. *Colloid. and interface science* **2003**, *264*, 396 4) Kumar, A.; Mandal, S.; Selvakannan, PR.; Pasricha, R.; Mandale, A. B. and Sastry, M. *Langmuir* **2003**, *19*, 6277.

5.1. Introduction

The advantage of phase transfer protocols has already been discussed in Chapter 1. A number of protocols have been developed for the phase transfer of nanoparticles in different physicochemical environments. The first report of phase transfer of silver nanoparticles from water into several non hydroxylic organic solvents of low polarity occurred as byproducts of the preparation of silver metal liquid-like film (MELLF).[1] It was also demonstrated that silver and gold nanoparticles stabilized by oleate molecules can be extracted into various organic solvents by adding relatively large concentrations of salts (in the hundreds of mmoles per liter range).[2] Another report was by Underwood and Mulvaney in which they showed the phase transfer of gold nanoparticles from water to an organic solvent such as butyl acetate. In this study, the authors showed that aqueous gold nanoparticles synthesized by the Turkevich method[3] could be quantitatively transferred into butyl acetate by complexation of the particles with a 'comb stabilizer' present in the organic phase.[4] The comb stabilizer used was a co-polymer consisting of a backbone of methyl methacrylate and glycidyl methacrylate with poly(12-hydroxystearic acid) as pendant side chains. Gold nanoparticle solution possess lovely pink to ruby red color[4] and therefore, the phase transfer of the gold nanoparticles from one phase to another is seen as a dramatic transfer of color between phases.

Rao and coworkers cleverly used gold-alkanethiol interaction and demonstrated the acid-facilitated phase transfer of aqueous gold, silver and platinum nanoparticles into organic solvents such as toluene.[5] In a typical experiment, they took biphasic mixture of aqueous solution of nanoparticles and alkanethiol molecules in organic phase. To this biphasic mixture little amount of HCl was added under stirring condition resulting in a remarkably swift movement (within 3 min) of the nanoparticles to the hydrocarbon layer containing the alkanethiol. This could be seen vividly by the complete transfer of color across the interface.[5] This method has also been applied to the acid facilitated transfer of oleate stabilized silver nanoparticles by Wang, Efrima and Regev.[6] They have shown that silver nanoparticles can be phase transferred from water to organic solvents by binding the nanoparticles to sodium oleate present in cyclohexane/dodecane.[6] Similar to the acid facilitated phase transfer of gold nanoparticles using alkanethiols,[5] the phase transfer of

silver nanoparticles occurs when a small amount of orthophosphoric/perchloric acid is added to the reaction medium.[6]

Dr Sastry`s group also showed the phase transfer of platinum nanoparticles by modifying them with poly vinylpyrrolidone (PVP)[7a] as a capping agent. In a different approach they used electrostatic interaction to transfer the nanoparticles from aqueous to organic phase. This strategy involves the electrostatic complexation of negatively charged lauric acid modified CdS[7b] nanoparticles and 4-carboxythiophenol (4-CTP) capped gold nanoparticles[7c] with octadecylamine (ODA) molecules. After complexation, the nanoparticles become sufficiently hydrophobic and dispersible in organic solvent. Similar approach was followed by Caruso`s group and showed the complete phase transfer of carboxylate and sulfonate-derivatized gold nanoparticles from aqueous phase to organic phase containing single-chain primary amines by utilizing electrostatic interactions.[7d]

Cyclodextrins (CDs) which are cyclic oligosaccharides consisting of six, seven or eight glucopyranose units (α-, β- and γ-CDs respectively), are versatile host molecules for 'guests' such as alkanethiols, forming what are known as 'inclusion complexes'. Inclusion complexes of CD and alkanethiols in water have been self-assembled on gold thin films[8a] as well as on gold nanoparticles.[8b] Sastry and co-workers have shown recently that gold nanoparticles may be capped with ODT molecules threaded with cyclodextrin and furthermore that during vigorous shaking of a biphasic mixture of this hydrosol with chloroform, the gold nanoparticles were rapidly transferred to the organic phase.[9]

This chapter deals with the phase transfer of nanoparticles from aqueous phase to organic phase. Taking a cue from the acid mediated phase transfer methods above,[5,6] we envisioned that a slightly similar protocol could be applied to the phase transfer of aqueous CdS nanoparticles which are known to covalently bind thiol molecules.[10] Here, we demonstrate that CdS nanoparticles synthesized in water can be quantitatively transferred to petroleum ether (pet ether) by co-ordination to octadecanethiol (ODT) molecules present in the organic phase.

Apart from the details of phase transfer of CdS nanoparticles, this chapter details our efforts on the phase transfer (from aqueous phase to organic phase) of gold

and silver nanoparticles using amines. In most of the protocols available, nanoparticles have been generally modified with alkanethiols,[11] ω-functionalized alkanethiols,[12] aromatic thiols[13] and other thiol derivatives[14] because the thiol chemistry as a means for surface modification is very well understood. On the other hand, the reports on the synthesis of organic solutions of gold and silver nanoparticles derivatized with alkylamine[15a-f] and amine derivatives[15g] are very few. As in the case of alkanethiols, the self-assembly of alkylamine molecules was first investigated on thin films of gold.[16] Xu *et al*. showed that under certain conditions, vapor phase deposition of octadecylamine (ODA) molecules on gold thin films resulted in the formation of ordered monolayers of the alkylamines. However, attempts to self-assemble ODA from solution on gold thin films was not very successful due to competition of the Au^0-amine interaction with the amine-solvent interaction.[16] In an important shift to nanoscale gold surfaces, Heath and co-workers showed that primary amines form partially covalent bonds with gold nanoparticles and that the stability of amine-capped gold nanoparticles is a finite-size effect which is largely kinetic, rather than thermodynamic in origin.[15a] Most of the reports on surface derivatization of gold nanoparticles with alkylamine and other amine derivatives, however, qualitatively agree that the interaction of the amines with gold is strong and similar in this respect to thiolate bonds. As compared to gold, the reports for the modification of silver nanoparticles and its phase transfer into organic phase using fatty amine molecules has not been studied so far. Also the exact nature of interactions through which amines assemble on gold/silver surfaces is not clearly explained. So the detailed investigation into the chemistry of the interaction of amine molecule with coinage metal has been lacking and we address this issue also in this chapter.

We accomplished the hydrophobization of the nanoparticles with a fatty amine at liquid-liquid interface during vigorous shaking of a biphasic mixture of an aqueous solution of nanoparticles and organic solvent containing the fatty amine molecules. Complexation of nanoparticles with surfactant renders the particles hydrophobic and results in their phase transfer into organic phase. Presented below are details of the investigations.

5.2. Phase transfer of CdS nanoparticles

5.2.1. Experimental section

In a typical experiment, 50 ml each of 10^{-4} M aqueous $CdCl_2$ solution (pH ~ 5.8) and 5 x 10^{-3} M octadecanethiol (ODT) solution in petroleum ether were taken in conical flask and the biphasic mixture was vigorously shaken. As the biphasic mixture was stirred, H_2S gas was bubbled through the mixture for a period of ca. 20 minutes. As the reaction proceeded, a yellow coloration was observed in the solution and on cessation of the stirring, the two phases separated out with the CdS nanoparticles now present in the organic phase. We would like to point out two observations at this stage. In order to achieve near complete transfer of the CdS nanoparticles to the organic phase, excess ODT [excess (in relation to the Cd^{2+} ion concentration in water) by at least a factor of 20] in pet ether had to be taken. Apparently, the surface coverage of the ODT molecules covalently bound to the CdS nanoparticle surface determines a certain minimum hydrophobicity required for complete phase transfer below which the nanoparticles were observed to be immobilized at the water-pet ether interface. The process for the phase transfer of CdS nanoparticles is illustrated in Figure 5.1 which shows pictures of a test-tube before (test-tube on the left) and after (test-tube on the right) phase transfer of the CdS nanoparticles from the biphasic mixture. The phase transfer was observed by the yellow coloration of the organic phase and a corresponding almost complete loss of color from the aqueous phase when the two layers separated out as shown is Figure 5.1.

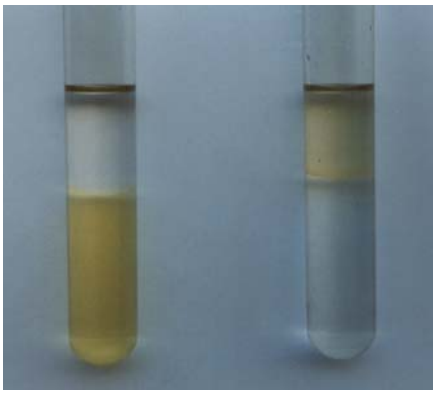

Figure 5.1: Picture showing test-tubes containing the biphasic mixture of aqueous CdS and ODT in pet ether before (test-tube on the left) and after (test-tube on the right) phase transfer of the CdS nanoparticles into the organic phase.

We have also observed that reaction of the Cd^{2+} ions with Na_2S instead of H_2S gas in the above experiment did not result in the transfer of the CdS nanoparticles to the organic phase, even under excess ODT conditions. After phase transfer of the CdS nanoparticles into pet ether had been accomplished, the CdS solution was rotary evacuated leading to a dark yellow powder. This powder was washed with ethanol to get rid of the powder of un-coordinated ODT molecules and could be readily redispersed in different organic solvents such as toluene, benzene and chloroform. Thin films of the CdS nanoparticles were formed on Si (111) substrates by immersion of the substrates in CdS solution in chloroform and evaporation of the solvent for different characterizations.

5.2.2. UV-vis. study

The ODT-stabilized CdS nanoparticles powder was redispersed in different organic solvents and showed clear yellow color with little evidence of flocculation. Figure 5.2 shows the UV-vis spectra recorded from the CdS nanoparticles in water (before phase transfer, curve 1); ODT-capped CdS nanoparticles in toluene (curve 2); ODT-capped CdS nanoparticles in chloroform (curve 3) and ODT-capped CdS nanoparticles in benzene

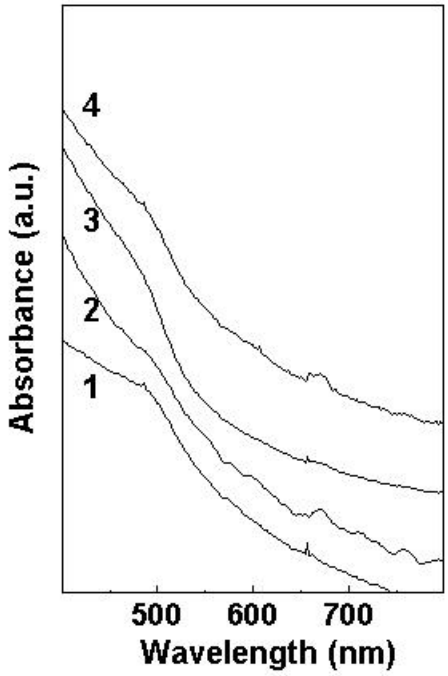

Figure 5.2: UV-vis spectra recorded from CdS nanoparticles dispersed in different solvents. Curve 1: as-prepared CdS nanoparticle solution in water; curve 2 : ODT-stabilized CdS nanoparticles in toluene; curve 3 : ODT-stabilized CdS in chloroform and curve 4 : ODT-stabilized CdS in benzene.

(curve 4). The onset of absorption occurs at ca. 475 nm (determined by taking the derivative of the UV-vis spectra) in each of the spectra and indicates little aggregation of the CdS nanoparticles after dissolution in the different solvents. This wavelength corresponds to a particle size of ca. 60 Å.[17] Tailing of the UV-vis spectra towards longer wavelengths is observed in the four CdS nanoparticle solutions shown in Figure 5.2. This tailing of the spectra is known to arise due to the presence of impurity states in and near the band-edge in such semiconductors.[18]

5.2.3. XRD study

The drop coated film of ODT-stabilized CdS nanoparticles was formed on Si (111) substrate and analyzed by XRD. XRD patterns of the ODT-stabilized CdS nanoparticle film on Si (111) substrates showed prominent Bragg reflections at 2θ values of 26.2^0 and 28.2^0 and correspond to the (002) and (101) Bragg reflections respectively.[19] The experimentally measured (101) Bragg reflection along with a Lorentzian fit to the data is shown in Figure 5.3 and a particle size of 70 Å was estimated from the line broadening of this peak using the Scherrer formula.[20] This value is in good agreement with the particle size of 60 Å estimated from the UV-vis absorption edge of the ODT-

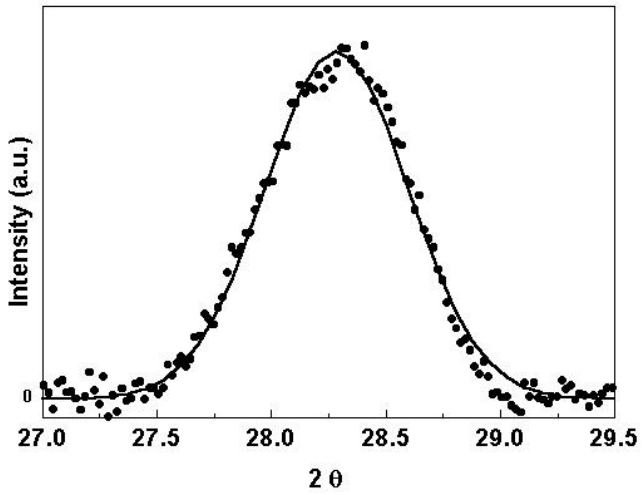

Figure 5.3: XRD pattern of a drop-coated ODT-stabilized CdS nanoparticle film formed on a Si (111) substrate showing the (101) Bragg reflection. The solid line is a fit to the experimental data.

stabilized CdS nanoparticle solutions (Figure 5.2). The XRD results also indicate that there is little sintering of the nanoparticles, most probably due to steric stabilization by the ODT monolayer covalently bound to the CdS nanoparticle surface. Contact angle measurements of the ODT-stabilized CdS nanoparticle film yielded an average value of 115^{o} over the film surface. This indicates a very hydrophobic surface and can only arise from effective capping of the CdS nanoparticle surface by the ODT monolayers. The contact angle of 115^{o} is to be contrasted with the value of 20^{0} measured for the bare Si (111) surface. This result lends further support to the stable particle size distribution deduced from the XRD measurements and clearly underlines the role played by the CdS nanoparticle surface-bound ODT molecules in hydrophobizing the nanoparticles and rendering them soluble in non-polar organic solvents.

5.2.4. TGA/DTA study

Carefully weighed amounts of the ODT-stabilized CdS nanoparticle powders were subjected to TGA/DTA and chemical analysis. Figure 5.4 shows a plot of the TGA data (left curve) and the DTA data (right curve) as a function of sample temperature. Two prominent weight losses are observed at 250^{0} C and 325^{0} C (TGA data, Figure 5.4) and are endothermic and exothermic processes respectively (DTA data, Figure 5.4). The weight loss at 250^{0} C is ca. 55% of the overall weight of the ODT-stabilized CdS nanoparticle sample and is attributed to desorption of surface-bound ODT molecules. This temperature agrees well with TGA data reported in the literature on the desorption of alkanethiols covalently bound to gold nanoparticles.[15a,21] The percentage weight contribution of the surface bound ODT molecules agrees fairly well with the figure of ca. 40 % estimated from chemical analysis of the ODT-stabilized nanoparticle powder. The exothermic feature at 325^{0} C corresponding to a weight loss of ca.25% is attributed to sintering of the CdS nanoparticles and desorption of the nanoparticles from the TGA/DTA crucible. The sintering of the CdS nanoparticles leading to the exothermic feature observed is likely given that the stabilizing ODT monolayer desorbs at 250^{0} C. By the time the sample is heated to $500\ ^{0}$ C, almost complete weight loss in the sample occurs and negligible residue was found in the TGA/DTA crucible. We would like to

point out an endothermic feature at ca. 50^0 C which is accompanied by a negligible weight loss of 0.7 % (Figure 5.4).

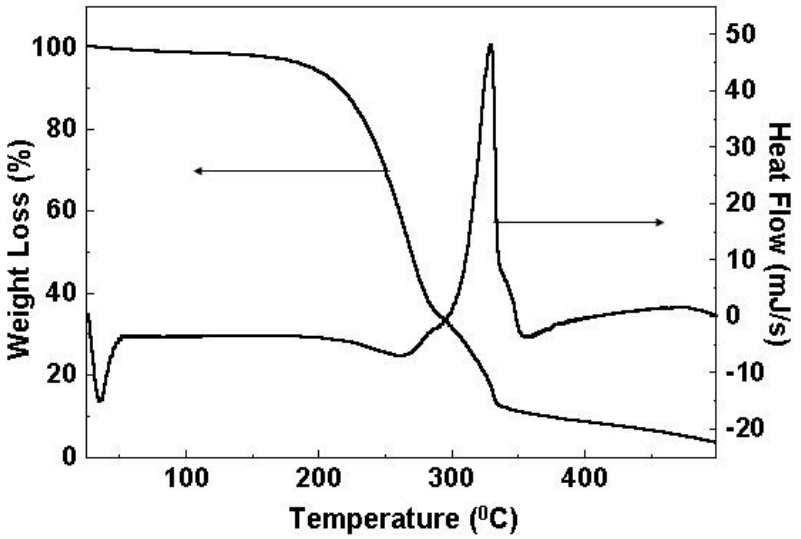

Figure 5.4: TGA (left axis) and DTA (right axis) plots of ODT-stabilized CdS nanoparticle powder as a function of temperature of heating.

This feature is attributed to melting of ordered regions in hydrocarbon chains from neighboring CdS nanoparticles, possibly in an interdigitated state and has been observed previously in alkylamine/alkanethiol stabilized gold colloidal particles[15a,21] as well as in fatty acid stabilized silver particle films.[22]

5.2.5. XPS study

An ODT-stabilized CdS nanoparticle film formed on Si (111) substrate was analyzed by XPS. The general scan spectrum showed the presence of the principal C 1s, S 2p and Cd 3d core levels with no evidence of impurities. The film was sufficiently thick and therefore, no signal was observed from the substrate (Si 2p core level). The C 1s, Cd 3d and S 2p core levels recorded from this film are shown in Figures 5.5, 5.6 and 5.7 respectively. The spectra have been background corrected using the Shirley algorithm[23] prior to curve refitting.

The C 1s core level could be stripped into two components at 285 eV and 287.8 eV (Figure 5.5) and are assigned to electron emission from the hydrocarbons in the ODT

molecules and the carbons co-ordinated to sulfonate groups respectively in the film. The presence of the higher binding energy (BE) component at 287.8 eV will be dealt with below during discussion of the S 2p core level signal. At this stage, we would like to point out that the thiol group is very weakly polar and therefore, the carbon co-ordinated to the thiol group in the ODT molecules is not expected to lead to such a large shift in the C 1s core level.

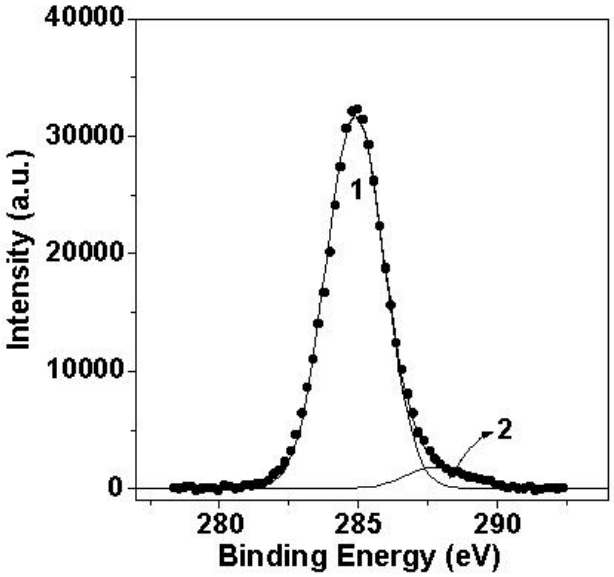

Figure 5.5: C 1s core level spectrum recorded from the ODT-stabilized CdS nanoparticle film grown on a Si (111) substrate. The spectrum has been resolved into two components by a non-linear least squares procedure.

The Cd 3d core level (Figure 5.6) could be satisfactorily fit to a single spin-orbit pair at 406.6 eV (3 $d_{5/2}$) and 413.3 eV (3 $d_{3/2}$). These values are in good agreement with published values for CdS nanoparticles.[24] There is no evidence for a chemically shifted component that could arise due to co-ordination of ODT molecules with Cd^{2+} ions at the surface.

The S 2p core level spectrum for the ODT-stabilized CdS nanoparticle film is shown in Figure 5.7. It is clear that there are two chemically distinct species in the spectrum and they have been individually fit to the 2 p spin orbit components as shown in the figure. The 2 $p_{3/2}$ - $2p_{1/2}$ separation has been taken in the fits to be 1.15 eV[25,26] while the ratios in intensity of the two components was 2 : 1. The fits lead to the two chemically distinct components of $p_{3/2}$ BEs at 163.3 and 167.9 eV. The low BE value is

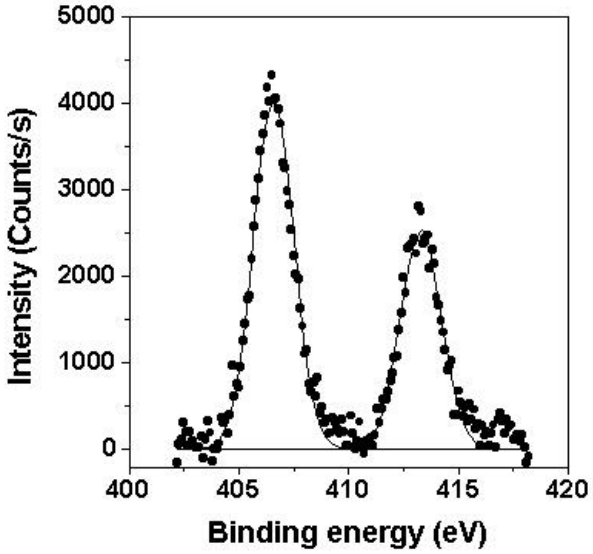

Figure 5.6: Cd^{2+} 3d core level spectrum recorded from the ODT-stabilized CdS nanoparticle film grown on a Si (111) substrate. The spin-orbit components are shown in the figure.

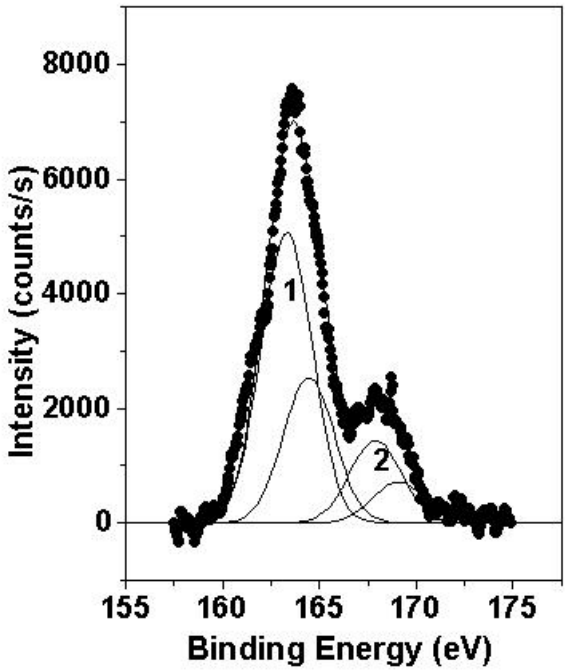

Figure 5.7: S 2p core level spectrum recorded from the ODT-stabilized CdS nanoparticle film grown on a Si (111) substrate. Two chemically distinct components are shown and have been individually resolved into the spin-orbit components (see text for details).

in excellent agreement with published values for the S 2p signal from self-assembled monolayers of alkanethiols[25] and aromatic thiols,[26] for alkanethiols on silver nanoparticles as well as from CdS nanoparticles themselves.[24] The higher BE component is assigned to sulfur in a sulfonate moiety and could occur by oxidation of the thiol group in ODT molecules. This value is in agreement with earlier XPS measurements on SAMs of aromatic thiols on a silver/platinum alloy surface.[26]

The co-ordination of the sulfur to electronegative oxygen atoms thus leads to a substantial chemical shift in the carbon co-ordinated to the sulfonate groups as observed in the C 1s spectrum discussed earlier (Figure 5.5, the component at 287.8 eV). As an additional test of the assignment of the high BE component in the C 1s spectrum, we performed a quantitative comparison of this component with the higher BE S 2p component. The peak areas were calculated from the fits, corrected for variation in ionization cross-section as well as the inelastic scattering length variation with electron kinetic energy (assuming an inelastic scattering length kinetic energy dependence of $E^{0.75}$)[27] and the ratios taken. The S 2p / C 1s higher BE component quantitative analysis yielded a value of 1.23 in good agreement with the expected value of 1. Thus, the XPS analysis of the film is consistent with ODT-stabilized CdS nanoparticles in the film with some degree of oxidation of the thiol groups in ODT.

5.2.6. FTIR study

ODT-stabilized CdS nanoparticle film on Si (111) substrate was analyzed with FTIR spectroscopy along with a film of ODT deposited by solution casting onto Si (111). The methylene antisymmetric and symmetric vibrational modes occurred at 2920 and 2850 cm^{-1} respectively.[28] The only noticeable difference in the FTIR spectra in the two films was the loss of the S-H stretch feature at 2550 cm^{-1} in the ODT-stabilized CdS nanoparticle film which was present in the as-prepared ODT film.[28] This clearly indicates co-ordination of the ODT molecules to the CdS nanoparticle surface.

5.2.7. TEM study

A drop-coated film of ODT modified CdS nanoparticles dispersed in petether was

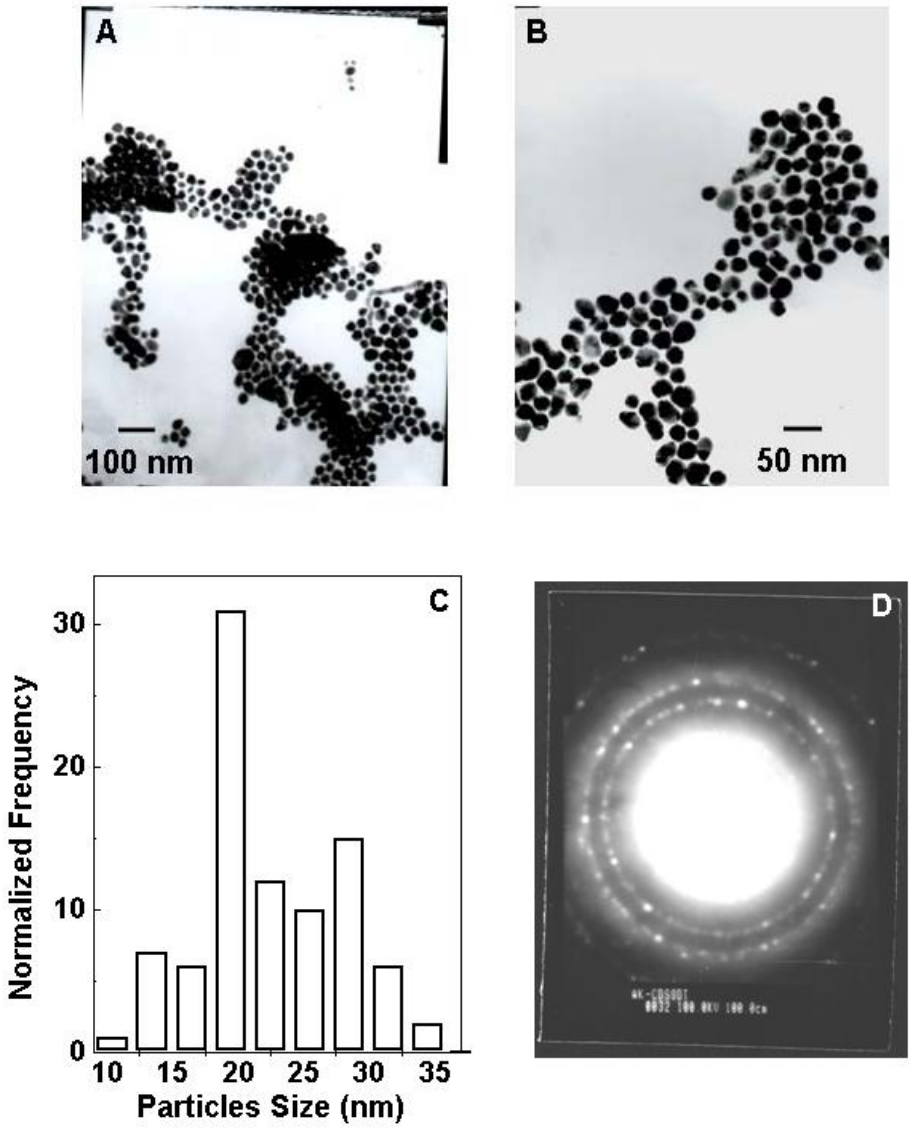

Figure 5.8: A)TEM images of ODT capped cadmium sulfide nanoparticles film formed on carbon coated grid by drop coating at lower magnification **B)** TEM images of ODT capped cadmium sulfide nanoparticles film formed on carbon coated grid by drop coating at higher magnification **C)** Particle size distribution of ODT capped cadmium sulfide nanoparticles measured from figure A. **D)** Selected area electron diffraction pattern of cadmium sulfide nanoparticles.

formed on carbon-coated copper grid by solvent evaporation and analyzed by transmission electron microscopy (TEM).

Figure 5.8A and B are the TEM pictures of CdS nanoparticles at lower and higher magnification respectively. It is clear from the TEM picture that particles are discrete and well defined. However, these particles were noticed to be composed of smaller particles

which are closely packed. Attempts to image the individual cadmium sulfide nanoparticles in the aggregates failed due to melting of the structures under the electron beam at higher magnifications. Figure 5.8C is the histogram measure from the figure 5.8 A which shows that the size of discrete spherical clusters is in the range from 10 nm to 35 nm. Figure 5.8D is the electron diffraction pattern recorded from single cadmium sulfide cluster, the spot array of which indicates the crystalline nature of individual CdS nanoparticles.

5.3. Phase transfer of gold nanoparticles

5.3.1. Experimental section

The gold nanoparticles of size 35 Å were synthesized by sodium borohydride reduction of chloroauric acid as described in the chapter 2. To two separate 100 ml batches of the gold nanoparticle solutions, 100 ml of a 2 x 10^{-4} M solution of laurylamine (LAM) and 100 ml of a 2 x 10^{-4} M solution of ODA in chloroform was added to yield immiscible layers of the red colored gold hydrosol on top of the colorless organic solution (Figure 5.9, test-tube on the right). Vigorous shaking of the test-tubes resulted in the extremely rapid transfer (within 30 s) of the gold nanoparticles into the organic phase as was observed by the red coloration of the organic phase and a corresponding loss of color from the aqueous phase (Figure 5.9, test-tube on the left) when the two layers separated out.

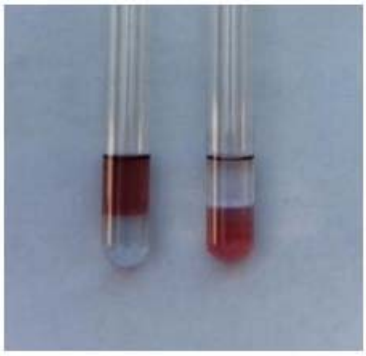

Figure 5.9:A) Picture showing the biphasic mixture of aqueous solution of gold particles and ODA containing chloroform layer before (test tube on the left) and after (test tube on the right) phase transfer of the gold particles into chloroform.

As mentioned earlier, this occurs spontaneously and did not require addition of acid, which is an essential ingredient in the alkanethiol coupled phase transfer protocol. We would like to point out that in order to achieve near complete transfer of the gold nanoparticles to the organic phase, excess ODA/LAM (excess in relation to the chloroaurate ion concentration in water by at least a factor of 2) in chloroform had to be taken. Apparently, the surface coverage of the ODA/LAM molecules bound to the gold nanoparticle surface determines a certain minimum hydrophobicity required for complete phase transfer below which the nanoparticles were observed to be immobilized at the water-chloroform interface. After phase transfer of the gold nanoparticles into chloroform had been accomplished, the ODA-Au and LAM-Au solutions were rotavapped leading to a dark brownish powder. This powder was washed repeatedly with ethanol to get rid of un-coordinated ODA/LAM molecules in the powder. Thin films of the gold nanoparticles were formed on Si (111) substrates by immersion of the substrates in gold nanoparticles-amine solution in chloroform and evaporation of the solvent for different characterization techniques.

5.3.2. UV-vis. study

As mentioned briefly in the experimental section, purified powders of Au-LAM and Au-ODA nanoparticles could be readily redispersed in different organic solvents. Curves 1 and 2 in Figure 5.10 correspond to UV-vis spectra recorded from Au-LAM and Au-ODA nanoparticle solutions in chloroform respectively. A strong resonance at ca. 520 nm is seen in both the spectra, this absorption band arising due to excitation of surface plasmon vibrations in the gold nanoparticles. The UV-vis spectra of these two nanoparticle solutions remained unchanged with time indicating the particle size distribution in the organic phase was extremely stable.

Curves 3 and 4 in Figure 5.10 correspond to UV-vis spectra recorded from Au-LAM and Au-ODA nanoparticle solutions in toluene respectively and as in the case of the nanoparticles in chloroform, a strong plasmon absorption band at 520 nm appears in both solutions. The UV-vis studies thus demonstrate that the alkylamine capped gold nanoparticles may be stored in the form of powder and dispersed in toluene/chloroform with little indication of aggregation of the nanoparticles.

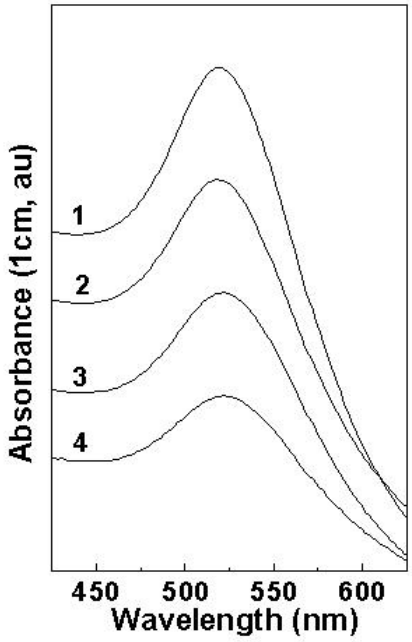

Figure 5.10. UV-vis spectra of laurylamine (LAM) and ODA-capped gold nanoparticles after redispersion in different organic solvents. Curves 1 and 3 : LAM-capped gold nanoparticles in chloroform and toluene respectively; curves 2 and 4 : ODA capped gold nanoparticles in chloroform and toluene respectively.

5.3.3. NMR study

Purified powders of Au-LAM and Au-ODA were dispersed in $CDCl_3$ and characterized by ^1H NMR spectroscopy. Curves 1, 2 and 3 in Figure 5.11 correspond to the ^1H NMR spectra recorded from the pure amine, Au-LAM and Au-ODA respectively. The NMR spectra of pure amine (curve 1) shows the prominent resonances at 2.7, 1.72, 1.26 and 0.85 which are correspond to the proton of α-CH_2, β-CH_2, methylene and methyl group from hydrocarbon chain respectively.

The spectra of Au-LAM (curve 2) and Au-ODA (curve 3) look similar and show broad multiplets at 1.55, 1.26 and 0.89 δ which correspond to β-CH_2, methylene and methyl group from hydrocarbon chain. It is clear from the comparison of spectra of pure amine and amine modified gold that the resonance at 2.7 δ of typical α-CH_2 proton in a pure amine (curve 1) is not observed in amine modified gold nanoparticles. This resonance seems to have been shifted from 2.7 δ in pure lauryl amine (curve 2) to 2.0- 0.5 δ in gold- amine complex due to the coordination of amine to gold nanoparticle through nitrogen atom. Such kind of large shift is due to presence of metal core in liquid

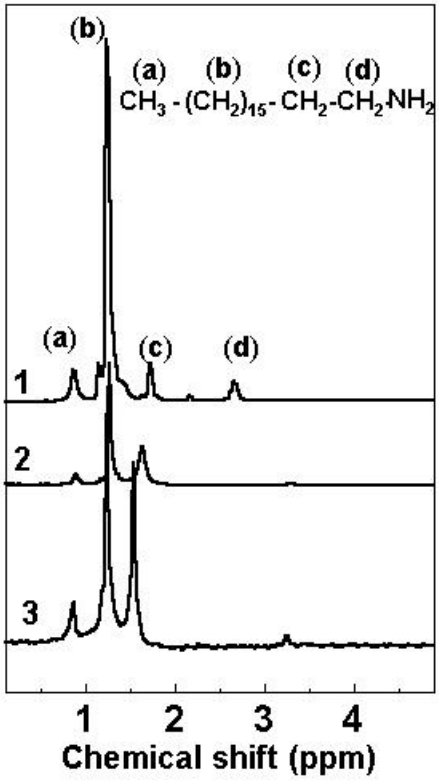

Figure 5.11. ^{1}H NMR spectra of pure amine (curve 1), Au-LAM (curve2) and Au-ODA nanoparticles (curve 3) dispersed in $CDCl_3$.

phase which can create large in-homogeneities in the magnetic field about local chemical environments. Similar observation was also reported by Heath and co-workers[15a] and they attribute it to the ligation of amine to the gold surfaces. Earlier ^{13}C NMR study of alkane thiol monolayer on gold surface also shows the broad resonance of carbon next to sulfur[29] (head group) which is indication of strong interaction of sulfur atom with gold surface. Broadening and absence of resonance at 2.7 δ in gold- lauryl amine complex indicates that the hydrophobized particle is free from uncoordinated amine molecule.

5.3.4. Transmission electron microscopy study

As mentioned briefly in the introduction, one of the advantages of the synthesis of hydrophobized gold nanoparticles in volatile organic solvents is that the nanoparticles spontaneously assemble into hexagonally ordered close-packed structures on solvent evaporation. Figures 5.12 and 5.13A show representative TEM images recorded from solution-cast films of LAM and ODA-capped gold nanoparticles respectively. The TEM

micrographs show that the particles of size 5.3 ± 0.7 A assemble into reasonably ordered 2-D structures that are in many regions in hexagonally close- packed. The fairly large

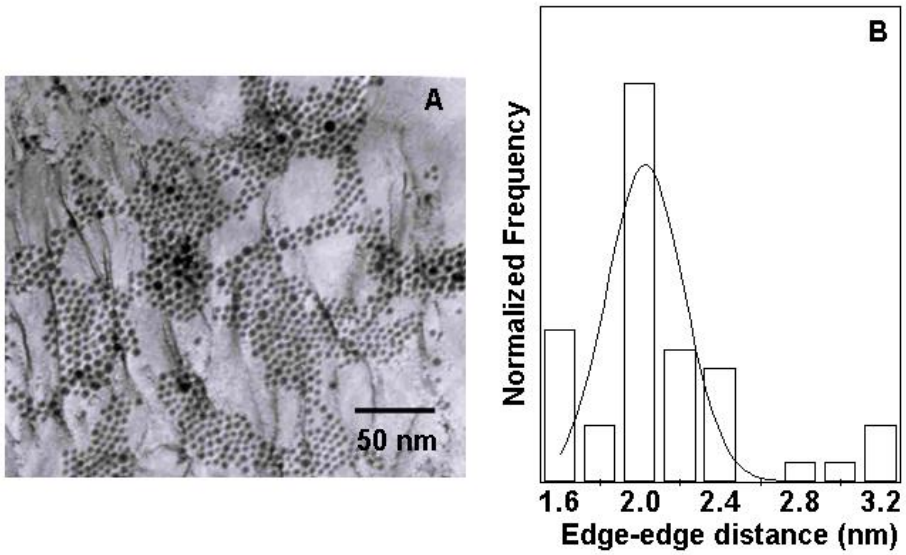

Figure 5.12: A) TEM image of lauryl amine capped gold nanoparticle film formed on carbon coated grid by drop coating. B) Edge to edge distance of lauryl amine capped gold nanoparticles measured from figure A.

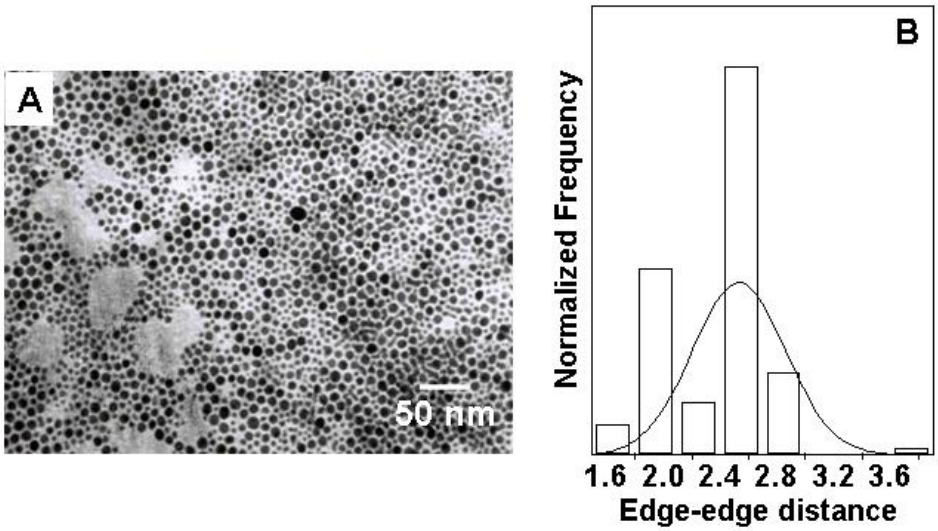

Figure 5.13: A) TEM image of octadecyl amine capped gold film formed on carbon coated grid by drop coating. B) Edge to edge distance of octadecylamine-capped gold nanoparticles measured from Figure A.

polydispersity of the gold nanoparticles conspires against extension of the hexagonal ordering to larger length scales.

Even though the gold nanoparticles in this study are not monodisperse, it is observed from the TEM micrographs that the particles are well separated from each other with an apparently uniform inter-particle separation. Figure 5.12B and 5.13B are the plots of the histogram of the edge to edge distance measured from the image shown in Figure 5.12A and 5.13A for 150 gold nanoparticles respectively. The histograms are strongly peaked at 20 ± 2 Å (figure 5.12 B) and 25 ± 3 Å (figure 5.13 B) which gives average separation of 20 ± 2 Å and 25 ± 3 Å for LAM and ODA-capped gold nanoparticles respectively. The interparticle separation in both cases are smaller than twice the length of LAM and ODA molecules indicating that the hydrocarbon chains from contiguous gold nanoparticles are interdigitated.

5.3.5. TGA/DTA study

It is clear from the TEM studies that amine capped gold nanoparticles also form well closed packed assembly like thiol modified nanoparticles. However, the nature of interaction between nanoparticles and gold nanoparticles is still not known. The strength of interaction and different kind of binding mode of amine molecule with the gold nanoparticles can be studied conveniently by TGA/DTA and FTIR spectroscopy. The TGA and DTA measurements were carried out with carefully weighed amount of the LAM and ODA-stabilized gold nanoparticles powder in the range from room temperature to 1000 ^{0}C.

Figure 5.14 shows a plot of the TGA data (left, curve 1: Au-LAM and curve 2: Au-ODA) and the DTA data (right, curve3: Au-LAM, curve 4: Au-ODA) as a function of sample temperature. Two prominent weight losses at 255^{0}C and 528 ^{0} C are ca. 7% and 1% for Au-LAM complex while for the Au-ODA complex, the weight losses are ca. 6% and 5% at 260 ^{0}C and 490 ^{0}C respectively. The total weight loss is ca. 8 and 11% of the overall weight of the Au-LAM and Au-ODA stabilized gold nanoparticle sample respectively and is attributed to desorption of surface-bound LAM and ODA molecules. The temperature agrees well with TGA data reported in the literature on the desorption of alkanethiols covalently bound to gold nanoparticles2.[15a,28] The percentage weight contribution of the surface bound LAM and ODA molecules agrees fairly well with the figure of ca. 8 and 12 % estimated theoretically by assuming that the area occupied by

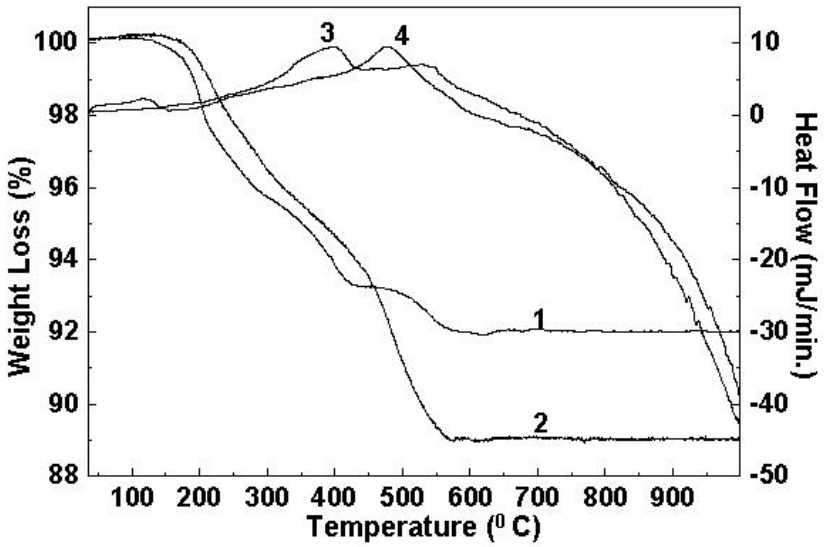

Figure 5.14. TGA/DTA curve of LAM and ODA capped gold nanoparticle. Left: TGA curve of LAM (curve 1) and ODA (curve 2) capped gold nanoparticles. Right : DTA of LAM (curve 3) and ODA (curve 4) capped gold nanoparticles.

LAM/ODA molecule is 25 Å^2 on the surface of gold nanoparticles (diameter 40 Å). The exothermic feature at 399^0 C corresponding to a weight loss of ca. 8% is attributed to sintering of the gold nanoparticles and desorption of the lauryl amine molecule from gold nanoparticles while this peak shifts to 477 ^{0}C for Au-ODA sample. The sintering of the gold nanoparticles leading to the exothermic feature observed is likely given that the stabilizing LAM and ODA monolayer desorbs at 392^0 C and 477 ^{0}C respectively. TGA and DTA study shows two prominent weight losses at 255 and 528 ^{0}C clearly indicates that amine molecules have two different kinds of interaction with gold nanoparticles.

5.3.6. FTIR studies

Figure 5.15 is the FTIR spectra as a function of temperature on drop coated film of LAM capped gold nanoparticles on a Si (111) substrate wherein the spectra were recorded after heating the film at 260^o C and 540^{o}C for 1 h. A comparison of the spectra in Figure 5.15 shows that three prominent features occur at ca. 2854, 2924, and 3414 cm^{-1} in the bare LAM film (curve 1) while the 3414 cm^{-1} feature is missing in the Au-LAM film (curve 2). The 3414 cm^{-1} feature in bare lauryl amine film corresponds to the N-H stretch vibrations from LAM molecules while this feature disappears on coordination of

LAM molecule with the surface of gold nanoparticles. The methylene antisymmetric and symmetric vibrations are observed at 2919 and 2850 cm^{-1} respectively in both the native amine film and the LAM-stabilized gold particle film (curves 1 and 2 respectively, Figure 5.15) and indicate that the hydrocarbon chains in the LAM monolayer surrounding the gold particles are in a close-packed, crystalline state[21]. The other most important observation is that the intensity of methylene symmetric and antisymmetric vibration mode decreases on heating the film at 260 ^{0}C (curve 3) and 540 ^{0}C (curve 4) which indicates that amine molecules desorbs from the surface of gold nanoparticles at these temperature which is fairly in good agreement with TGA study.

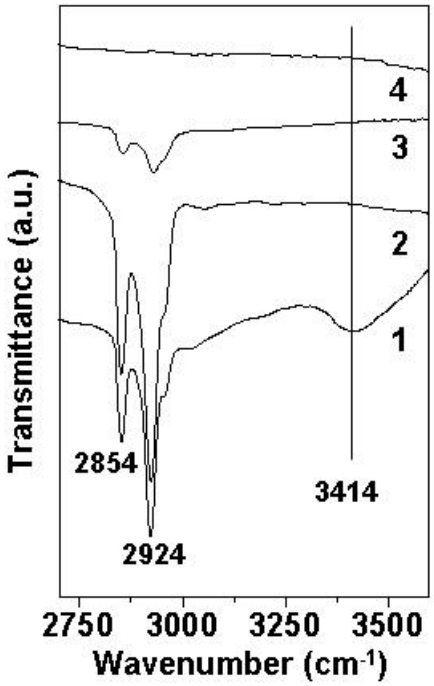

Figure 5.15. FTIR spectra of drop-coated films of pure laurylamine (curve 1) and Au-LAM capped gold nanoparticles on Si (111) wafer at room temperature (curve 2), after heating of Au-LAM film at 180 ^{0}C for one hour (curve 3) and after heating at 540 ^{0}C for one hour (curve 4) on Si (111) wafer.

The FTIR spectra of the ODA capped gold nanoparticles exhibit the same feature as those of the lauryl amine capped gold nanoparticles. It is clear from FTIR spectra that disappearance of NH stretch is due to the chemical interaction between amine groups with gold nanoparticles, which was further, studied with XPS.

5.3.7. XPS study

FTIR and TGA study clearly indicate that different kind of binding modes of amine molecules with gold nanoparticles exist but what kind of chemical bond it forms can only be clearly studied by X-ray photo emission spectroscopy. A solution-cast film of LAM-capped gold nanoparticles was formed on Si (111) substrates and analyzed by XPS as a function of temperature. The general scan spectrum of the film at room temperature showed the presence of C1s, N 1s, Cl 2p and Au 4f core levels with no evidence of impurities. The film was sufficiently thick and therefore, no signal was measured from the substrate (Si 2p core level). Figure 5.16A shows the Au 4f spectra recorded from the Au-LAM film deposited at room temperature (curve 1) and the spectra recorded after heating at 260 ^{o}C and 540 ^{o}C for 1 h (curves 2 and 3 respectively). The Au 4f spectrum in all cases could be resolved into a single spin-orbit pair (splitting ~ 3.7 eV) with a $4f_{7/2}$ binding energy (BE) of 83.8 eV (Figure 5.16, curve 1). There was no evidence for

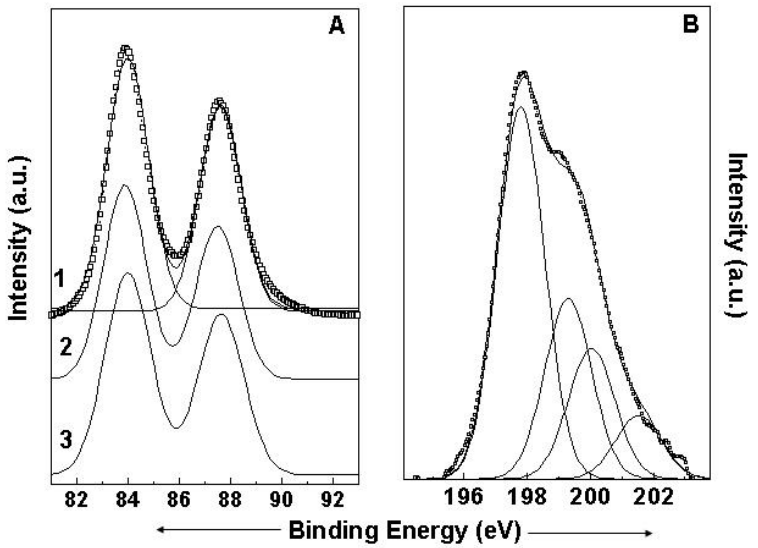

Figure 5.16: A) Au 4f core level spectra recorded from the LAM-stabilized gold nanoparticle film grown on a Si (111) substrate as a function of temperature. Curve 1: at room temperature; curve 2: after heating the film at 180 ^{0}C for one hour; curve 3: after heating at 540 ^{0}C for same time. The spin-orbit components are shown in the figure. B) Cl 2p core level spectrum recorded from the ODA-stabilized gold nanoparticle film grown on a Si (111) substrate as a function of temperature. The spectrum has been decomposed into two components by a non-linear least squares procedure.

additional components in the Au 4f spectrum and our result is in agreement with the XPS findings of Leff, Brandt and Heath for alkylamine-capped gold nanoparticles.[15a]

In addition to the Au 4f signal, a strong Cl 2p signal was also observed in the film suggesting the presence of $AuCl_4^-/AuCl_2^-$ ions on the surface of the gold nanoparticles. The Cl 2p core level could be satisfactorily fit to a two spin-orbit pair at 197.8 and 199.3 eV (2 $p_{3/2}$). These values are in good agreement with published values for chloride ion in $AuCl_4^-$ and $AuCl_2^-$ on the surface of gold nanoparticles. The lack of an additional Au 4f component arising from $AuCl_4^-/AuCl_2^-$ ions may be due to the very small surface concentration of the ions that is below the detection limits of the XPS instrument

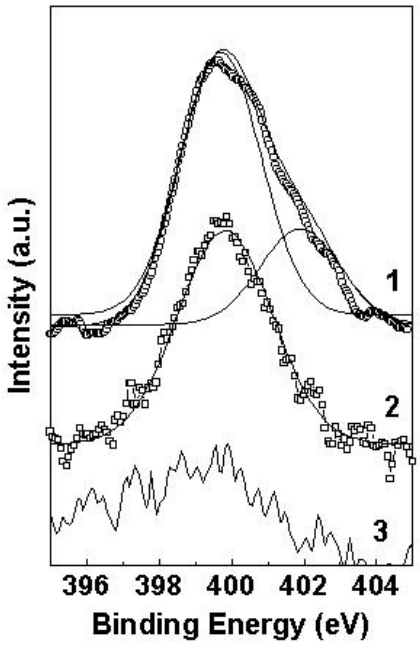

Figure 5.17: N 1s core level spectrum recorded from the LAM-stabilized gold nanoparticle film grown on a Si (111) substrate as a function of temperature. Curve 1: at room temperature; curve 2: after heating the film at 180 ^{0}C for one hour; curve 3: after heating at 540 ^{0}C for same time. The spectrum has been decomposed into two components by a non-linear least squares procedure

The binding of the laurylamine and octadecylamine molecules to the gold nanoparticles is through the amine functionality (proton NMR data, Figure 5.11) and therefore, it should be possible to resolve (if any) chemically distinct binding modes suggested by the TGA data (Figure 5.14) through the N 1s core level spectrum. The N 1s spectrum was recorded from the Au-LAM film after different heat treatment and is shown in Figure 5.17. Curve 1 represents the N 1s spectrum before heat treatment while curves 2 and 3 correspond to spectra recorded after 1 h heating of the films at 260 and 540 ^{o}C respectively. The N 1s spectrum from the as-deposited LAM-Au film could be

resolved into two chemically distinct species centered at 399.3 eV and 401.2 eV. The higher BE component is assigned to electron emission from nitrogens in the protonated amine groups electrostatically complexed with $AuCl_4^-$ ions present on the surface of the gold nanoparticles (Eq.1)

$$[Au^0{}_n(AuCl_4^-)_m](aq)+mRNH_3^+(org) \longrightarrow [Au^0{}_n(AuCl_4^-)_m](RNH_3^+)_m(org).....(1)$$

We believe that the phase transfer of the gold nanoparticles to the organic phase by complexation with the alkylamine molecules occurs through this electrostatic process. Control experiments on the phase transfer of gold nanoparticles with the aqueous phase held at pH 12 (under conditions where the amine groups would be unprotonated) did not lead to efficient phase transfer and the nanoparticles were found to form a film at the liquid-liquid interface. We would like to mention here that Schiffrin and co-workers have observed the presence of a complex of the form $R_4N^+Br^-$ on the surface of gold nanoparticles when this molecule ($R_4N^+Br^-$) was used as a phase transfer reagent.[30]

On heating the film at 260 ^oC for one hour, the form of the N 1s signal changes dramatically and the asymmetry arising from the presence of the high BE component at 401.3 eV is reduced significantly (compare curves 1 and 2, Figure 5.17). This indicates the almost complete loss of the electrostatically bound laurylamine component thus identifying the chemical nature of the species decomposing/desorbing at this temperature in the TGA data (Figure 5.14, curve 1). The lower BE component remains unchanged both in intensity and BE (399.3 eV, curve 2) after heating at 260^oC suggesting that it is the more strongly bound laurylamine component and does not undergo any chemical change under these conditions. The N 1s spectrum recorded from this film after further heating at 540 ^oC for 1 h is shown as curve 3 in Figure 5.17. It is seen that the intensity of this signal is considerably reduced indicating that the more strongly bound laurylamine component desorbs almost completely at this temperature. This result also agrees with the TGA data for Au-LAM (curve 1, Figure 5.14) where almost complete loss of the laurylamine layer was indicated at this temperature.

The strongly bound low BE component in the N 1s spectrum of LAM-Au films needs to be identified. The presence of the Cl 2p core level unequivocally establishes the presence of either $AuCl_4^-$ or $AuCl_2^-$ ions on the surface of the gold nanoparticles. It is well

known that during reduction of $AuCl_4^-$ ions, Au^{3+} (in the $AuCl_4^-$ ions) is rapidly reduced to Au^{+1} (in $AuCl_2^-$ ions) and finally to Au^0.[31] The $AuCl_2^-$ ions are fairly long-lived[32] and could be bound to the surface of the gold nanoparticles along with $AuCl_4^-$ ions resulting in their stability in the aqueous environment. It is known that gold in the +1 oxidation state has a propensity to form a complexes with different ligands such as RNC, piperidine, cyclohexylamine, 3-bromopyridine[33a-c] and also form interesting stable complexes of the form $AuCl(NH_2R)$ with alkylamines.[33] We believe that during complexation of the alkylamine molecules with the gold nanoparticles prior to phase transfer, such complexes are formed on the surface of gold nanoparticles (Eq.2).

$$[Au^0_n(AuCl_2^-)_m](aq) + mRNH_3^+(org) \longrightarrow Au^0_n[AuCl(RNH_2)]_m(org) + HCl \quad (2)$$

These complexes are considerably more stable than the electrostatically bound complexes (Eq.1, 260 ^oC TGA weight loss and high BE N 1s XPS feature) and may be identified with the 399.3 eV N 1s component in the LAM-Au film and the 540 ^oC weight loss in the TGA data (Figure 5.14, curve 1).

5.3.8. Place exchange study of ODA- gold nanoparticles

It is well known that alkanethiol molecules bound to the surface of gold nanoparticles may be place-exchanged with other thiol molecules.[34] It would be of interest to see whether alkylamine molecules on the surface of gold nanoparticles can also be place-exchanged. As a simple test, we studied the replacement of laurylamine molecules by another amine, ethylene diamine (EDA). The choice of a diamine was mediated by the fact that should place-exchange occur, this would lead to the possibility of cross-linking of the gold nanoparticles and a visible change in the optical properties.

Figure 5.18 shows UV-vis spectra of laurylamine-capped gold nanoparticles in toluene as a function of varying EDA concentration in the solution. Curves 1, 2, 3 and 4 correspond to UV-vis spectra recorded from the as-prepared LAM-capped gold nanoparticle solution in toluene and 0.1 M, 0.01 and 0.001 M of EDA in the gold nanoparticle solutions respectively. It is clear from the graph that there is considerable broadening of surface plasmon resonance and that the broadening increases as the concentration of diamine increases. The broadening of the surface plasmon band is a clear indication of

aggregation of the gold nanoparticles in solution which can happen only by an exchange of the laurylamine molecules with EDA. Thus, place exchange between molecules bearing amine functionality may be accomplished.

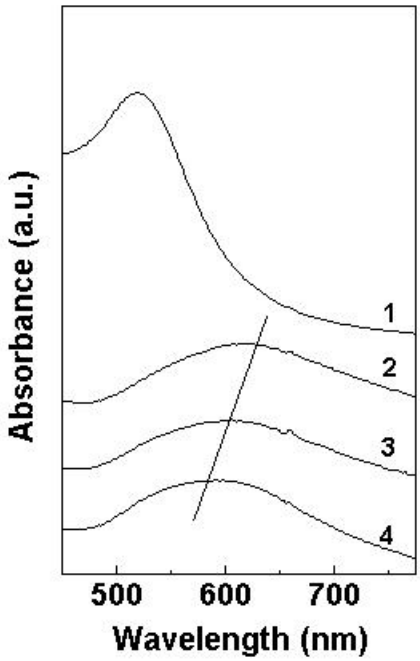

Figure 5.18: UV-vis spectra of LAM capped gold nanoparticles (curve 1) and after addition of 10^{-1} M (curve 2), 10^{-2} M (curve 3) and 10^{-3} M concentration (curve 4) of ethhylenediamine (EDA) to LAM capped gold nanoparticle solution in toluene.

5.4. Phase transfer of silver nanoparticles

5.4.1. Experimental section

The silver hydrosol was prepared by sodium borohydride reduction of silver sulfate as described in chapter 2. To 100 ml of the silver nanoparticle solution thus prepared, 100 ml of a 2 x 10^{-4} M solution of octadecylamine (ODA) in hexane was added to yield immiscible layers of the colorless organic solution on top of the yellow colored silver hydrosol (Figure 5.19, test tube on the left). Vigorous shaking of the test-tube resulted in transfer of the silver nanoparticles into the organic phase and this was observed by the yellow coloration of the organic phase and a corresponding loss of color from the aqueous phase (Figure 5.19, test tube on the right) when the two layers separated out.

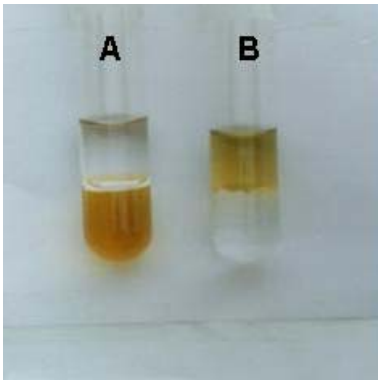

Figure 5.19: Immiscible layers of (A) the silver hydrosol (at the bottom) and the clean hexane solution containing ODA (on top) before shaking. (B) Alkylamine derivatized Ag nanoparticles in hexane (on top) and clean aqueous solution at the bottom after the phase transfer by shaking the biphasic mixture shown in A (see text for details).

The ODA-capped silver nanoparticles were separated out and dry powder of silver nanoparticles was obtained by rotavapping the organic phase thereafter purified by repeated washing with ethanol. The process of washing with ethanol removes uncoordinated ODA molecules from the silver nanoparticle powder and these were redispersed in chloroform. Thin films of the silver nanoparticles were formed on Si (111) substrates by immersion of the substrates in Ag-ODA solution in chloroform and evaporation of the solvent for different characterization techniques.

5.4.2. UV-vis. and Thermal study

Silver nanoparticles exhibit a strong and sharp surface plasmon of resonance which is extremely sensitive to medium and surface modification therefore the UV-vis. study was done before and after phase transfer as well as stability of silver sol in organic medium was investigated as a function of time. Figure 5.20A shows the UV-vis spectra recorded from the as-prepared aqueous silver nanoparticle solution (curve 1) and the hexane phase after transfer of the silver nanoparticles by complexation with ODA molecules at various times after the phase transfer : curve 2, immediately after the phase transfer; curves 3 and 4, 24 and 36 h after phase transfer. The resonance at ca. 380 nm in the UV-vis spectra arises due to excitation of surface plasmon vibrations in the silver nanoparticles and is responsible for the striking yellow color of silver nanoparticle solutions. It is observed that the surface plasmon resonance is broadened and shifted to

ca. 415 nm (curve 2) after phase transfer of the nanoparticles indicating surface binding of the ODA molecules to the silver surface. We would like to mention here that there is no time dependent change in absorption spectra (curves 3,4) clearly indicating that the silver nanoparticles in the organic phase are extremely stable in time with no precipitation observed even a month after the phase transfer had been effected. Curve 5 represents the UV-vis spectrum of the aqueous phase after phase transfer of silver nanoparticles into hexane. It can clearly be seen that the surface plasmon of resonance band at 380 nm has been reduced considerably in intensity thus indicating the almost complete phase transfer of silver nanoparticles into the organic phase. During vigorous shaking of the biphasic mixture, ODA molecules bind to the silver nanoparticles thus rendering them hydrophobic and amenable to transfer to the non-polar organic phase. The silver nanoparticle-hexane solution was rotavapped and this resulted in a blackish solid

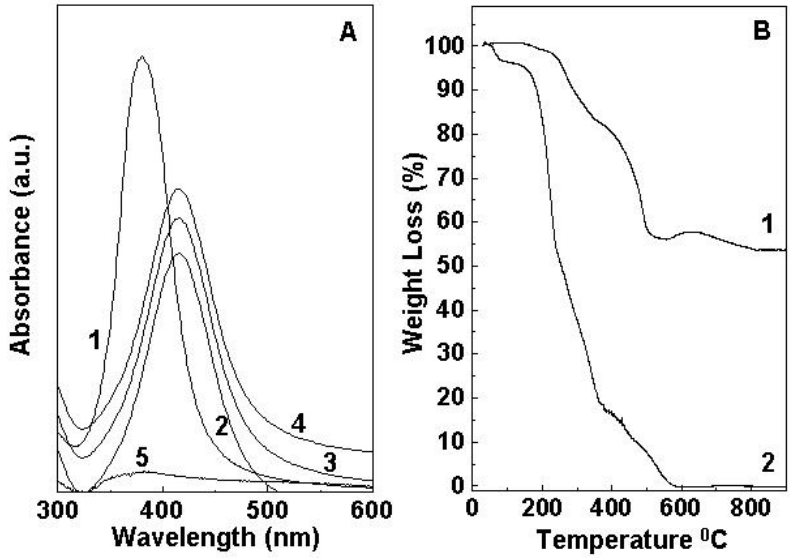

Figure 5.20: A) UV-vis spectra of silver sol before and after phase transfer:, curve 1: as-prepared silver sol in aqueous phase; curve 2: immediately after phase transfer of silver nanoparticles into hexane; curve 3: silver nanoparticles in hexane phase after 24 hours of transfer; curve 4: silver nanoparticles in hexane after 36 hours of transfer; curve 5: spectrum of the aqueous phase after phase transfer of silver nanoparticles into hexane. **B)** TGA curve of pure ODA (curve 1) and ODA-capped silver nanoparticles (curve 2, see text for details).

powder that could be readily redissolved in different solvents such as toluene, benzene, chloroform etc.

As mentioned above, the silver nanoparticles are capped with a monolayer of ODA molecules that provide sufficient hydrophobilcity to the particles to accomplish their phase transfer into hexane. In order to understand how the ODA molecules interact with the silver nanoparticles, TGA measurement of purified powder of ODA-stabilized silver nanoparticles was done. Figure 5.20B shows the data obtained from purified powder of ODA capped silver nanoparticles (curve 1) and pure ODA (curve 2). It is observed that, there is a ca. 40 % weight loss at 232 ^{o}C which is followed by almost complete loss of the powder in the heating crucible by 600 ^{o}C. The complete weight loss of pure ODA (curve 2) is due to evaporation of ODA from crucible. ODA-Ag complex shows an overall weight loss of ca. 43.3 % at 334 ^{0}C (curve 1) followed by negligible weight loss in the temperature range 434 – 800 ^{o}C. The weight loss at 334 ^{0}C is due to desorption of the ODA molecules bound to the silver nanoparticles. The increase in desorption temperature of ODA from Ag-ODA complex indicate that the interaction between amine with silver nanoparticles is quite strong. This temperature agrees well with TGA data reported in the literature on the desorption of alkyl amine covalently bound to gold nanoparticles.[8A] The percentage weight contribution of the surface bound ODA molecules is higher as compared to theoretical estimation of ca. 12% (by assuming the area occupied by ODA molecule as 25 Å^2 on the surface of silver nanoparticles with diameter 70 Å) which indicates that the higher weight loss may be due to the presence of uncoordinated ODA molecules in the powder or evaporation of silver nanoparticles.

5.4.3. FTIR and NMR study

It is clear from the TGA data that the increase in desorption temperature of ODA molecule from the surface of silver nanopaticles is due to the interaction of amine molecules with silver particles. In order to understand the nature of interaction, FTIR, NMR and XPS measurements of ODA capped silver particles were carried out. Figure 5.21A shows the FTIR spectra recorded from solution-cast films of pure ODA (curve 1) and ODA-capped silver nanoparticles (curve 2) on a Si (111) substrate. A comparison of the spectra in Figure 5.21A reveals the presence of three prominent features at ca. 2840, 2907, and 3317 cm^{-1} in the bare ODA film (curve 1) while the 3317 cm^{-1} feature shifts to 3126 cm^{-1} in the Ag-ODA film (curve 2). The 3317 cm^{-1} band in the bare ODA film

corresponds to N-H stretching vibrations from ODA molecules which become broad and appear at 3126 cm^{-1} in ODA-Ag complex due to the coordination of amine molecules with the surface of silver nanoparticles. Such a shift in the N-H stretch vibration mode on formation of salts with anions such as $PtCl_6^{-2}$ has been observed in Langmuir-Blodgett films of ODA.[35]

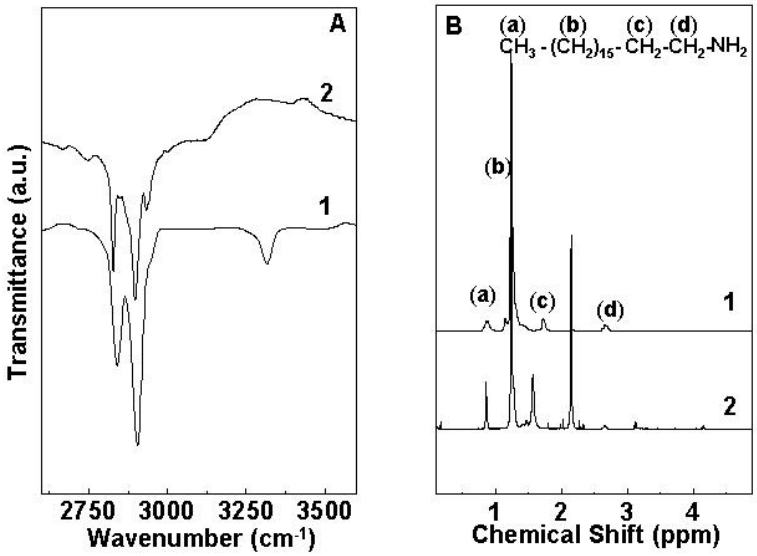

Figure 5.21: **A)** FTIR spectra of drop-coated films of pure octadecylamine (curve 1) and ODA capped silver nanoparticles on Si (111) substrate. **B)** ^1H NMR spectra of pure octadecylamine (curve 1), purified powders of Ag-ODA (curve 2) dispersed in $CDCl_3$.

There are very few reports on the stabilization of silver nanoparticles with alkyl amines and consequently, the nature of the co-ordination of ODA molecules with the silver nanoparticles remains an issue not fully understood, Manna *et al*. have reported on the stabilization of silver nanoparticles with amine derivatives such as *N*-hexadecylethylenediamine.[36] They have reported that reaction of $AgNO_3$ with *N*-hexadecylethylenediamine results in the formation of a complex of the form Ag(hexadecylethylenediamine)$_2NO_3$ and furthermore, that this complex can be used as a precursor for the synthesis of stable silver nanoparticles capped with the diamine molecules[36]. The most important feature distinguishing the free diamine and the diamine-protected silver particles was a shift in the N-H stretch vibrational mode from 3345 to 3340 cm^{-1}. In this study, we observe a broad band at 3126 cm^{-1}. This large shift and broadening of the peak indicate that the interaction of ODA molecule with silver

nanoparticles is stronger than the Ag-diamine complex. The methylene antisymmetric and symmetric vibrations from the hydrocarbon chains of ODA are observed at 2907 and 2840 cm^{-1} respectively in both the native amine film and the ODA-stabilized silver nanoparticle film (curves 1 and 2 respectively, Figure 5.21A) and indicate that the hydrocarbon chains in the ODA monolayer surrounding the silver particles are in a close-packed, crystalline state[21].

Purified powders of ODA-Ag nano were dispersed in $CDCl_3$ and characterized by ^1H NMR spectroscopy. Curves 1, and 2 in Figure 5.21 B correspond to the ^1H NMR spectra recorded from pure ODA and ODA-capped silver nanoparticles dispersed in $CDCl_3$ respectively. The NMR spectrum of pure amine (curve 1) shows prominent resonances at 2.7, 1.72, 1.26 and 0.85 ppm which correspond to the protons from hydrocarbon chain present in different chemical environments and are identified as α-CH_2, β-CH_2, methylene and methyl groups from the hydrocarbon chain respectively (see schematic given in the inset of Figure 5.21B). The NMR spectrum of ODA-Ag nano (curve 2) shows broad multiplets at 2.1, 1.55, 1.26 and 0.89 ppm which correspond to α-CH_2, β-CH_2, methylene and methyl groups from the hydrocarbon chains of the surface-bound amine molecules respectively. It is clear from a comparison of the spectra recorded from the pure amine and amine-modified silver nanoparticle that the resonance at 2.7 ppm of typical α-CH_2 protons in pure ODA (curve 1) shifts to 2.1 ppm in the amine-modified silver nanoparticle sample (curves 2). This shift in resonance clearly indicates that the ODA molecules bind to the silver nanoparticle surface through the amine functional group. Previous ^{13}C NMR studies of alkanethiol monolayers bound to the surface of gold nanoparticles showed a broadening and large shift in resonance arising from the carbons next to the sulfur atoms in the thiol groups indicating strong interaction of the thiol groups with gold nanoparticles.[15a,29] In another report on ^1H NMR investigation of alkylamine monolayers bound to gold nanoparticles, a similar broadening and large shift in resonance of α-CH_2 protons was observed[15a] and has been interpreted as arising due to the presence of metal core which can create large inhomogeneities in the magnetic field about local chemical environments. This shift and broadening strongly depends on the interaction of capping agent with metal core. The ODA-Ag nano complex shows a relatively small shift in the resonance of α-CH_2 protons relative to alkylamines

bound to gold nanoparticles[15a] suggesting that the interaction of amine groups with silver nanoparticles is weaker.

5.4.4. XPS study

A solution-cast film of ODA-capped silver nanoparticles was formed on Si (111) substrate and analyzed by XPS as a function of temperature. Figure 5.22A shows the Ag 3d core level spectrum recorded from the Ag-ODA film formed by the drop-coating technique.

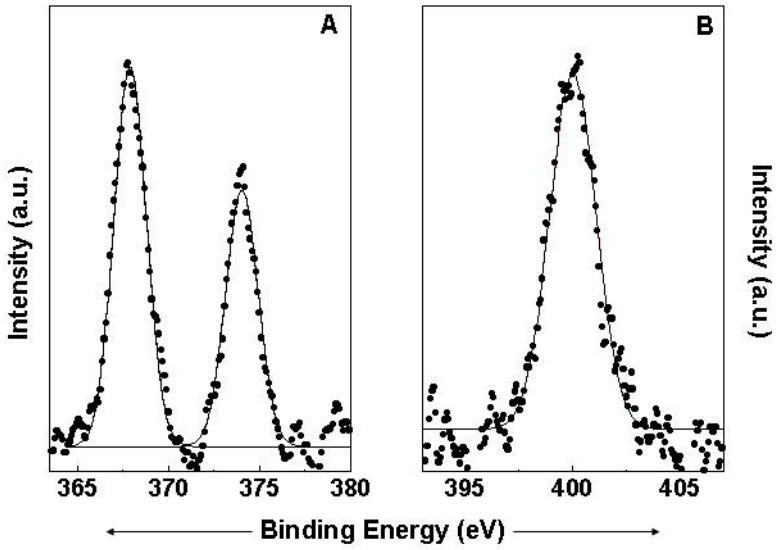

Figure 5.22: **A)** Ag 3d core level spectrum recorded from a ODA-stabilized silver nanoparticle film deposited on a Si (111) substrate. **B)** N 1s core level spectrum recorded from a ODA-stabilized silver nanoparticle film grown on a Si (111) substrate.

The Ag 3d spectrum could be resolved into a single spin-orbit pair (splitting ~ 7 eV) with a $3d_{5/2}$ binding energy (BE) of 368 eV (the core levels were aligned with respect to the adventitious C 1s BE of 285 eV). This BE corresponds to that of metallic silver[37]. There was no evidence for additional components in the Ag 3d spectrum due to coordination of amine molecules with silver atoms at the surface of the nanoparticles. The binding of the octadecylamine molecules to the silver nanoparticles is through the amine functionality (proton NMR data) and therefore, it should be possible to resolve (if any) chemically distinct binding modes. The N 1s spectrum was recorded from the Ag-ODA film and is shown in Figure 5.22B. The N 1s spectrum clearly is composed of a

single chemically distinct component centered at 400 eV, this result indicates that there is only one mode of binding of the amine molecules with the silver nanoparticles.

5.4.5. Transmission electron microscopy study

Drop-coated films of the ODA-Ag nano solution were formed on carbon-coated copper grids by solvent evaporation for transmission electron microscopy (TEM) measurements. Figure 5.23A shows a representative TEM image of ODA-capped silver nanoparticles while Figure 5.23B is a plot of the particle size distribution (PSD)

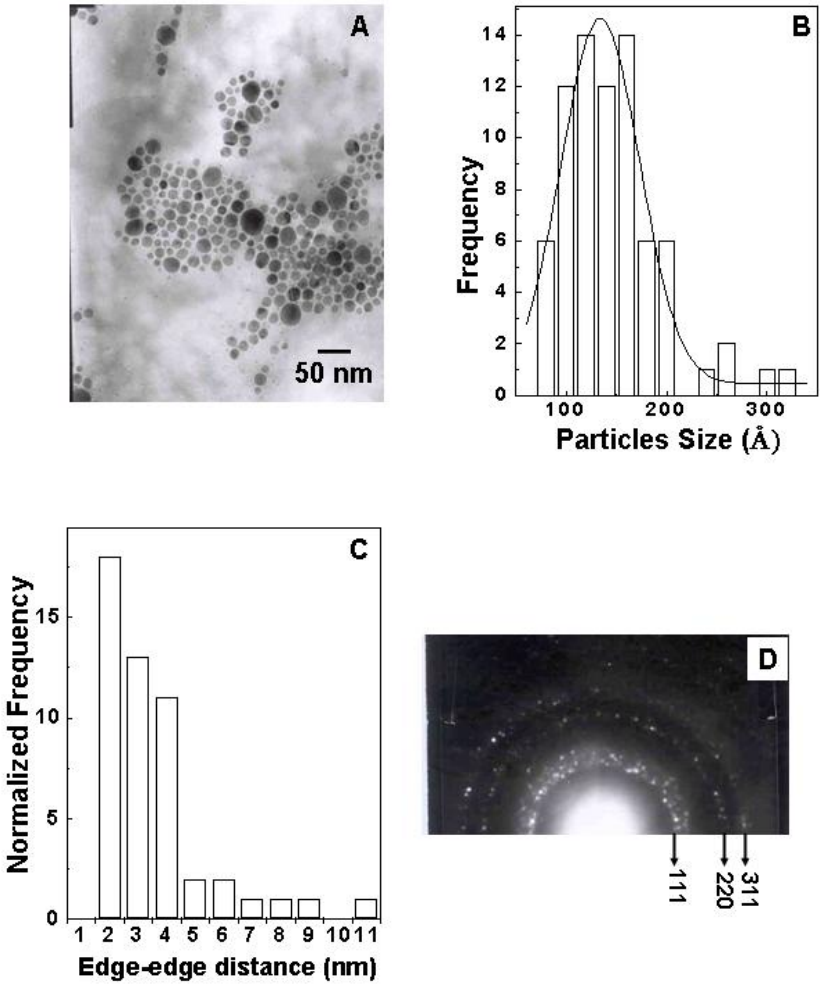

Figure 5.23: A) TEM image of ODA capped silver nanoparticle film formed on carbon coated grid by drop coating. **B)** Particle size distribution of ODA capped silver nanoparticles measured from figure A. **C)** Edge to edge distance of ODA capped silver nanoparticles measured from figure A. **D)** Selected area electron diffraction pattern of silver nanoparticles.

histogram measured from an analysis of 100 particles in Figure 5.23A and other micrographs. It is clear from the TEM picture that the particles are fairly polydisperse in size and they are organized into a two-dimensional hexagonal close packed structure. A Gaussian fit to the PSD histogram yielded a particle size of 130 ± 30 Å. The particles in the 2-D assembly are to a large extent well-separated from one another and appear to have a uniform inter-particle separation. The edge-edge distance is strongly peaked at ca. 25 Å (Figure 5. 23 C) which is less than twice the length of ODA molecules (~ 54 Å). This result indicates that the hydrocarbon chains from neighboring nanoparticles are interdigitated, the protective hydrocarbon sheath of the ODA molecules preventing aggregation of the particles. Figure 5.23D is the diffraction pattern obtained from the silver nanoparticles which shows the nanoparticles are crystalline.

5.5. Conclusions

- It has been shown that CdS nanoparticles synthesized in an aqueous medium may be transferred into non-polar organic solvents by co-ordination with ODT molecules present in the organic phase.
- The ODT molecules covalently bind to the CdS nanoparticle surface and render the surface sufficiently hydrophobic to facilitate the phase transfer. Films of the ODT-stabilized CdS nanoparticles could be formed on solid supports by evaporation of the organic component in the solution.
- The phase transfer of aqueous gold and silver nanoparticles into organic medium via direct coordination of octadecylamine molecules present in the organic phase with nanoparticles has been demonstrated.
- The phase transfer is accomplished without addition of acid, a feature common to phase transfer protocols involving alkanethiol molecules as the hydrophobizing agents.
- The fatty amine capped gold nanoparticles and silver are extremely stable, could be easily precipitated out of solution and redissolved in different organic solvents without significant variation in the particle size.

- It has been demonstrated that gold and silver nanoparticles may be modified by alkylamine molecules and can be organized into close-packed thin film on different substrate.
- It is also clear from this study that primary amine molecules anchor to the gold nanoparticle surface by two kinds of bonding, electrostatic and covalent while in case of silver, amine molecules have only one kind of binding mode. However the exact nature of bonding in the case of silver is still not known.
- This approach is promising for growing heterocolloidal particle assemblies of quantum dots by evaporation induced self-assembly with possible application in the electronics industry.
- This approach for the hydrophobization of nanoparticles may be extended to control the inter particle separation in the nanopaarticle films by altering the chain length of the surfactant.

5.6. References:

1. Zeiri, L.; Efrima, S. *J. Phys. Chem*. **1992**, *96*, 5908.
2. a) Hirai, H.; Aizawa, H.; Shiozaki, H. *Chem. Lett*. **1992**, 1527.b)Hirai, H.; Aizawa H.; Shiozaki, H. *J. Colloid Interface Sci*. **1993**, *161*, 471. (c) Meldrum, F. C.; Kotov, N. A.; Fendler, J. H.*Langmuir* **1994**, *10*, 2035. (d) Andres, R. P.; Averback, R. S.; Brown, W. L.; Brus, L. E.; Goddard, W. A., III; Kaldor, A.; Louie, S. G.; Moscovits, M.; Peercy, P. S.; Riley, S. J.; Siegel, R. W.; Spaepew, F.; Wang, Y. *J. Mater. Res*.**1989**, *4*, 704.
3. a) Turkevich, J.; Garton, G.; Stevenson, P. C. *J. Colloid Sci.* **1954**, *9*, 26. b) Handley, D. A. *Colloidal Gold : Principles, Methods and Applications*; Hayat, M. A., Ed.: Academic Press, San Diego, **1989**, Vol.1, Chapter 2. c) Duff, D. G., Baiker, A., Edwards, P.P. *Langmuir* **1993**, *9*, 2301.
4. Underwood, S.; Mulvaney, P. *Langmuir* **1994**, *10*, 3427.
5. a) Sarathy, K. V.; Kulkarni, G. U.; Rao, C. N. R. *Chem.Commun.***1997**, 537. b) Sarathy, K. V.; Raina, G.; Yadav, R. T.; Kulkarni, G. U.; Rao, C. N. R. *J. Phys. Chem. B*. **1997**, *101*, 9876.
6. Wang, W.; Efrima, S.; Regev, O. *Langmuir* **1998**, *14*, 602.

7. a) Sastry, M.; Patil, V.; Mayya, K. S.; Sainkar, S. R.; Singh, P. *Thin Solid Films* **1998**, *324*, 239.b) Damle, C.; Gole, A.; Sastry, M. *J. Mater. Chem.* **2000**, *10*, 1389 b) Sastry, M.; Gole, A.; Patil, V. *Thin Solid Films* **2001**, *384*,125. d) Mayya, K. S.; Caruso, F. *Langmuir* **2003,** *19,* 6987.

8. a) Yan, J.; Dong, S. *Langmuir* **1997**, *13*, 3251.b) Liu, J.; Alvarez, J.; Kaifer, A. E.; *Adv.Mater*. **2000**, *12*, 1381.

9. Lala, N.; Lalbegi, S.P.; Adyanthaya, S. D.; Sastry, M. *Langmuir* **2001**, *17*, 3766.

10. a) Colvin, V.L..; Goldstein, A.N.; Alivisatos, A.P. *J.Am.Chem.Soc.***1992**, *114*, 5221.b) Herron, N.; Calabrese, J.C.; Farneath, W.E.; Wang, Y. *Science* **1993**, *259*, 1426.

11. a)Brust, M.; Walker, M.; Bethell, D.; Schiffrin, D.J.; Whyman, R. *J. Chem. Soc. Chem. Commun.* **1994**, 801; b) Porter, L.A.; Ji, D.; Westcott, S.L.; Graupe, M.; Czernuszewicz, R.S.; Halas, N.J.; Lee, T.R. *Langmuir* **1998**, *14*, 7378.

12. a) Weisbecker, C.S.; Merritt, M.V.; Whitesides, G.M. *Langmuir* **1996**, *12*, 3763;b) Templeton, A. C.; Hostetler, M.J.; Kraft, C.T.; Murray, R.W. *J.Am.Chem.Soc.* **1998**, *120*, 1906.

13. a) Brust, M.; Fink, J.; Bethell, D.; Schiffrin, D. J.; Kiely, C. *J. Chem. Soc. Chem. Commun.* **1995**, 1655; b) Johnson, S. R.; Evans, S. D.; Mahon, S. W.; Ulman, A. *Langmuir* **1997**, *13*, 51; c) Mayya, K. S.; Patil, V.; Sastry, M. *Langmuir* **1997**, *13*, 3944.

14. a) Maye, M.M.; Chun, S.C.; Han, L.; Rabinovich, D.; Zhong, C-J. *J. Am. Chem. Soc.* **2002**, *124*, 4958; b) Tan, Y.; Li, Y.; Zhu, D. *Langmuir* **2002**, *18*, 3392; c) Liu, J., Mendoza, S., Roman, E., Lynn, M.J., Xu, R., Kaifer, A.E., *J.Am.Chem.Soc.*, 1999, **121**, 4304.

15. a) Leff, D. V.; Brandt, L.; Heath, J. R. *Langmuir* **1996**, *12*, 4723; b) Green. M O'Brien, P. *Chem.Commun.* **2000**, 183; c) Chen, X.Y.; Li, J.R.; Jiang, L. *Nanotechnology* **2000**, *11*, 108; d) Brown, L.O.; Hutchison, J. E. *J.Am.Chem.Soc.* **1999**, *121*, 882; e) Brown, L. O.; Hutchison, J. E. *J. Phys. Chem. B.* **2001**, *105*, 8911; f) Sastry, M.; Kumar, A.; Mukherjee, P. *Colloids Surf. A* **2001**, 181, 255; g) Selvakannan, PR.; Mandal, S.; Pasricha, R.; Adyantaya, S. D.; Sastry, M. *Chem. Commun.* **2002**, 1334.

16. Xu, C.; Sun, L.; Keplay, L. J.; and Crooks, R. M. *Anal. Chem.* **1993**, *65*, 2102.

17. Henglein, A. *Chem.Rev.* **1989**, *89*, 1861.
18. Chakraborty, P.K.; Ghatak, K.P. *J.Phys.D. (Appl.Phys.)* **1999**, *32*, 2438.
19. Zhao, X.K.; Fendler, J.H. *J.Phys.Chem.* **1991**, *95*, 3716.
20. Jeffrey, J.W. *Methods in Crystallography*; Academic Press : New York, 1971.
21. Terrill, R. H.; Postelwaithe, T. A.; Chen, C.; Poon, C.; Terzis, A.; Chen, A.; Hutchinson, J. E.; Clark, M. R.; Wignall, G.; Londono, J. D.; Superfine, R.; Falvo, M.; Johnson, Jr., C. S.; Samulski, E. T.; Murray, R. W. *J. Am .Chem. Soc.* **1995**, *117*, 12537.
22. Patil, V.; Mayya, K.S.; Pradhan, S.D.; Sastry, M. *J.Am.Chem.Soc.* **1997**, *119*, 9281.
23. Shirley, D.A. *Phys.Rev.B.* **1972**, *5*, 4709.
24. Kundu, M.; Khosravi, A.A.; Kulkarni, S.K.; Singh, P. *J. Mater. Sci.* **1997**, *32*, 245.
25. Laibinis, P.E.; Whitesides, G.M.; Allara, D.L.; Tao, Y-.T.; Parikh, A.N.; Nuzzo, R.G. *J. Am. Chem. Soc.* **1991**, *113*, 7152.
26. Bandyopadhyay, K.; Mayya, K.S.; Vijayamohanan, K.; Sastry, M. *J.Electron Spectrosc.* **1997**, *87*, 101.
27. Tanuma, S.; Powell, C.J.; Penn, D.R. *Surf.Interface Anal.* **1993**, *20*, 77.
28. Hostetler, M. J.; Stokes, J. J.; Murray, R.W. *Langmuir* **1996**,*12*, 3604.
29. Badia, A.; Gao, W.; Singh, S.; Demers, L.; Cuccia, and Reven, L. *Langmuir* **1996,** 12, 1262.
30. Fink, J.; Kiely, C. J.; Bethell, D.; and Schiffrin, D. J. *Chem, Mater* **1998**, *10*, 922.
31. Jones, P. G.; Freytag, M. *Chem. Commun*. **2000**, 277.
32. Henglein, A. *Langmuir* **1999**, 15, 6738.
33. a) Bachman, R. E; Fioritto, M. S.; Fetics, S. K. and Cocker, T. M. *J. Am. Chem. Soc.* **2001**, 123, 5376. b) Ahrens, B.; Jones, P. G. Fischer, A. K. *Eur. J. Inorg. Chem.* **1999**, 1103. c) Jones, P. G.; Freytag, M. *Chem. Commun*. **2000**, 277. d) Guy, J. J.; Jones P. G.; Mays, M. J. Sheldrick, G. M. *J. Chem. Soc. Dalton Trans.* **1977**, 8.
34. Song, Y.; Murray, R.W. *J.Am.Chem.Soc.* **2002**, *124*, 7096.
35. Bardosova, M.; Tregold, R.H.; Ali-Adib, Z. *Langmuir* **1995**, *11*, 1273.
36. Manna, A. ; Imae, T.; Iida, M. ; Hisamatsu, N. *Langmuir* **2001**, *17*, 6000.
37. Fadley, C. S., Shirley, D. A., *J. Res. Nat. Bur. Stands.* **1970**, *74A* , 543.

CHAPTER VI

Reverse Phase Transfer of nanoparticles: From organic to aqueous phase

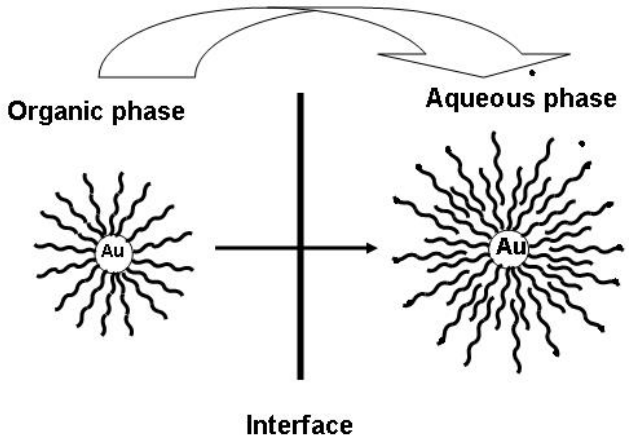

The phase transfer of hydrophobized nanoparticles dispersed in an organic solvent into water is described. Vigorous shaking of the biphasic mixture of a surfactant in water and the hydrophobic nanoparticles in the organic solvent results in a pink, foam-like appearance. Drying of the colored aqueous phase leads to the formation of a highly stable reddish powder of gold nanoparticles that may be readily redispersed in water. These were then characterized by UV-vis spectroscopy, differential scanning calorimetry (DSC), thermogravimetric analysis (TGA) and Fourier transform infrared spectroscopy (FTIR). The surfactant molecules form interdigitated bilayer with the primary monolayer of ligand directly coordinated to the gold nanoparticle surface. This bilayer formation renders the nanoparticles surface highly hydrophilic facilitating the phase transfer. These particles may be dispersed in water at very high concentrations with good stability even in presence of high amounts of electrolyte and over a wide range of solution pH.

The work described in this chapter has been published: 1) Swami, A.; Kumar, A.; Sastry, M. Langmuir 2003, 19, 1168. 2) Swami, A.; Jadhav, A.; Kumar, A.; Adyanthaya, S. D.; Sastry, M. Proc. Indian Acad. Sci. (Chem. Sci.) in press.

6.1 Introduction

As described in the first chapter the reverse phase transfer (from organic phase to aqueous phase) protocols are very important to obtain high concentrations of nanoparticles in aqueous medium which is not possible by aqueous based synthesis protocols. Number of procedures is available for the phase transfer of nanoparticles from aqueous phase to organic phase while those in the reverse direction i. e. from organic phase to aqueous phase are very few.

The first report for the reverse phase transfer was reported by Rotello and coworkers which was based on the place exchange mechanism. In this report they prepared carboxylic acid functionalized nanoparticles (Au-COOH) by exchanging the alkanethiol molecules on the gold surface with 11-thioundecanoic acid leading to a gold nanoparticle surface covered with carboxylic acid groups.[1a] This process makes the nanoparticles sufficiently hydrophilic for the dispersion in water. Similar strategy was followed by Gittins and Caruso[1b] in which they showed facile and rapid one-step method for the direct and complete transfer of gold and palladium nanoparticles synthesized in toluene and stabilized by tetraalkylammonium salts across the phase boundary (organic to aqueous).[1b] This was accomplished by addition of an aqueous 0.1 M 4-dimethlyaminopyridine (DMAP) solution to aliquots of the gold/ palladium nanoparticles in toluene. The DMAP molecules replace the tetraalkylammonium salts and form a labile donor-acceptor complex with the gold atoms on the surface of the nanoparticles through the endocyclic nitrogen atoms.[1b] These authors have shown that the aqueous gold and palladium solutions are extremely stable with no sign of degradation even after storage for several months. In other work Gittins and Caruso[1c] have also demonstrated the phase transfer of silver, gold, platinum and palladium nanoparticles using a number of exchanging ligands such as mercaptoundecanoic acid [MUA: HS-$(CH)_{10}$COOH], mecaptosuccinic acid etc. However, these methods change the surface chemistry of nanoparticles permanently and generally result in inefficient phase transfer.

It is well known from the literature that the silver,[2] magnetite nanoparticles,[3] and gold nanorods[4] can be stabilized by using interdigitated bilayer of lipid or surfactant molecules. We envisaged that nanoparticles stabilized by hydrophobic groups can be

made hydrophilic utilizing a bilayer strategy and can be transferred to aqueous medium. This chapter deals with our studies on the reverse phase transfer of nanoparticles from organic phase to aqueous phase. Here, we demonstrate that the hydrophobized nanoparticles dispersed in organic solvent can be phase transferred into water containing a surfactants such as cetyltrimethylammonium bromide (CTAB) or sodium dodecylsulfate (SDS). Vigorous shaking of the biphasic mixture (hydrophobized Au-in - chloroform/surfactant -in-water) results in the swift transfer of the hydrophobized nanoparticles into the aqueous phase. These nanoparticles are exceptionally stable in the aqueous phase at high concentration and can be stored as a powder, which can be readily redispersed in water. Analysis of the phase transferred gold nanoparticle solution and the purified powder of nanoparticles by UV-vis spectroscopy, Differential scanning calorimetry (DSC), Thermogravimetric analysis (TGA) and Fourier transform infrared (FTIR) spectroscopy indicated that the nanoparticles are capped with an interdigitated bilayer of capping agent such as alkylamine and water soluble surfactant such as CTAB, SDS.

6.2. The phase transfer of hydrophobized gold nanoparticles into water containing CTAB and SDS molecules

The hydrophobized gold nanoparticles were prepared by direct coordination of gold nanoparticles in aqueous phase with long chain fatty amine molecules present in organic phase as described in chapter five. Two separate batches of 25 mL of hydrophobized gold nanoparticles in chloroform were added to 25 mL of 10^{-3} M CTAB or 25 mL of 10^{-3} M SDS solution in water. The concentration of gold nanoparticles in chloroform was estimated to be 2×10^{-4} M by UV-vis. spectroscopy. Vigorous shaking of the biphasic mixture resulted in phase transfer of the gold nanoparticles from chloroform to water, as shown in the schematic, giving a pink-foam like appearance to the aqueous layer. This layer was then separated from the organic phase, dried and the resulting dry powder was redispersed in 25 mL of double-distilled water. This solution was centrifuged three times at 10 000 rpm and 25 ^{o}C for 20 min to remove uncoordinated CTAB/SDS molecules from solution. Further removal of water from the solution by rotavapping and drying under vacuum in N_2 atmosphere gave a reddish, dry powder of surface modified

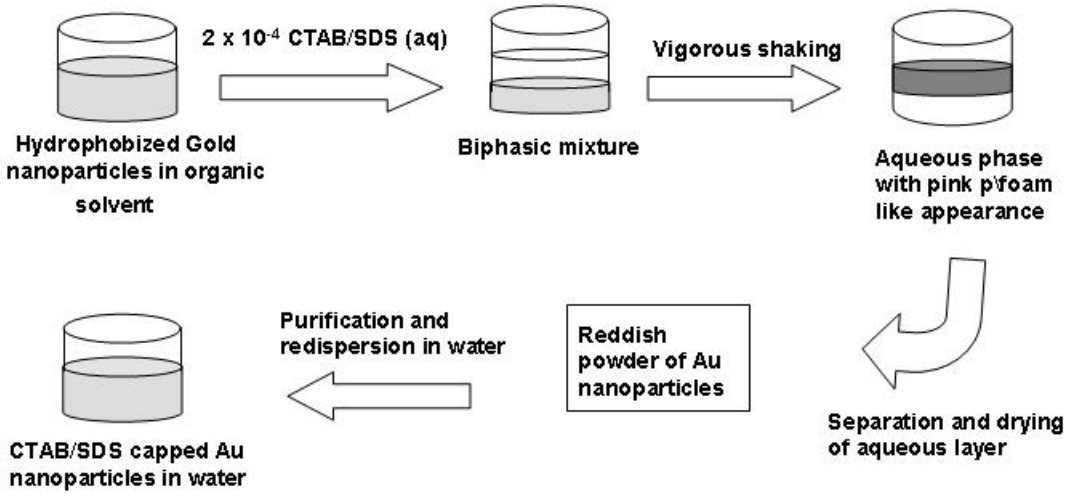

Scheme 1: Process for the phase transfer of hydrophobized nanoparticles from organic phase to aqueous phase.

gold nanoparticles. These were again redispersible in water and are stable against many harsh conditions such as varying pH as well as in presence of high concentrations of electrolyte without any aggregation.

6.3. UV-visible spectroscopy studies

Figure 6.1A and 6.2A show pictures of the gold nanoparticle solution at different stages of surface modification with CTAB and SDS molecules. Tube 2 in Figure 6.1A and 6.2A contain hydrophobized nanoparticles in chloroform whose preparation details are described in chapter 5. As mentioned before, vigorous shaking of the biphasic mixture (hydrophobized-Au-in -chloroform/CTAB or SDS-in-water) resulted in the swift transfer of the hydrophobized nanoparticles (tube 2) into the aqueous phase.

Tube 3 in Figure 6.1A and 6.2A contains gold nanoparticles in water phase-transferred from chloroform by CTAB and SDS respectively. For comparison, the gold hydrosol prepared by borohydride reduction of chloroauric acid (10^{-4} M) is also shown (tube 1). The presence of gold nanoparticles in the aqueous phase is clearly shown by the ruby red color of the solution and the occurrence of surface plasmon vibrations in the nanoparticles at ca. 520 nm (Figure 6.1B and 6.2B).[5,6] Curve 4 in both the figures corresponds to the spectrum of the chloroform layer after phase transfer of hydrophobized gold nanoparticles into water. The disappearance of the absorption at 520

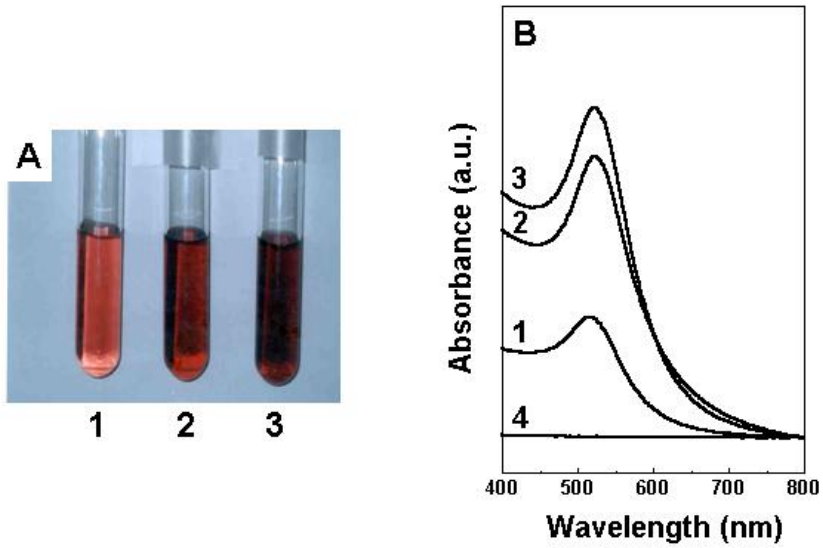

Figure 6.1: A) Picture showing various stages of modification of gold nanoparticles – as-prepared borohydride reduced gold hydrosol (tube 1), dodecylamine (DDA)-modified gold nanoparticle solution in chloroform (tube 2), and DDA modified nanoparticles after phase transfer into an aqueous solution of CTAB (tube 3). B) UV-vis spectra corresponding to the three gold nanoparticle solutions shown in A.; curves 1, 2, 3 correspond to solutions from tubes 1, 2, 3 respectively. Curve 4 corresponds to the spectrum recorded from the organic layer after phase transfer.

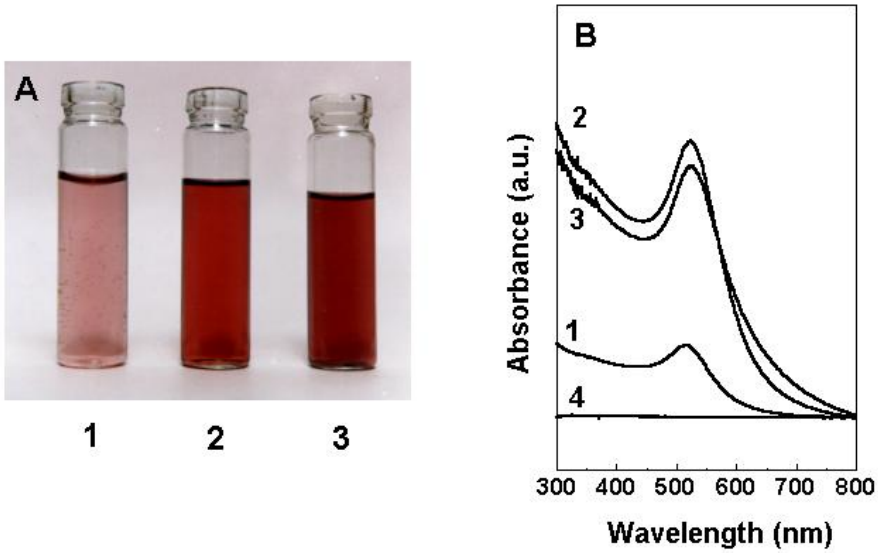

Figure 6.2: A) Picture showing the as-prepared borohydride reduced gold hydrosol (tube 1), ODA-modified gold nanoparticle solution in chloroform (tube 2), and octadecylamine (ODA) modified nanoparticles after phase transfer into an aqueous solution of SDS (tube 3). B) UV-vis spectra corresponding to the three gold nanoparticle solutions shown in A.; curves 1, 2, 3 correspond to solutions from tubes 1, 2, 3 respectively. Curve 4 corresponds to the spectrum recorded from the organic layer after phase transfer of the ODA-capped gold nanoparticles into water.

nm in curve 4 clearly indicates that almost complete transfer of gold nanoparticles (hydrophobized Au) from chloroform to water has been achieved. The surface plasmon wavelength of gold nanoparticles phase-transferred into water was 521 nm and no time-dependent change in the UV-vis spectra of this solution was observed. This clearly shows that the gold nanoparticles in water are quite stable with little evidence of aggregation.

6.4. Thermal analysis

In order to understand how CTAB or SDS molecules interact with hydrophobized gold nanoparticles and facilitate nanoparticle phase transfer, TGA and DSC measurements of the purified powder of the phase-transferred Au nanoparticles were done. Figure 6.3 and 6.4 are the DSC and TGA measurements of gold nanoparticles modified by CTAB and SDS respectively. In figures 6.3A and B, curve 1 corresponds to data recorded from the phase-transferred powder and curve 2 is that recorded from pure CTAB. Purified CTAB-DDA-Au nanoparticles display three endothermic peaks at 65, 100 and 255 ^{0}C (curve 1).

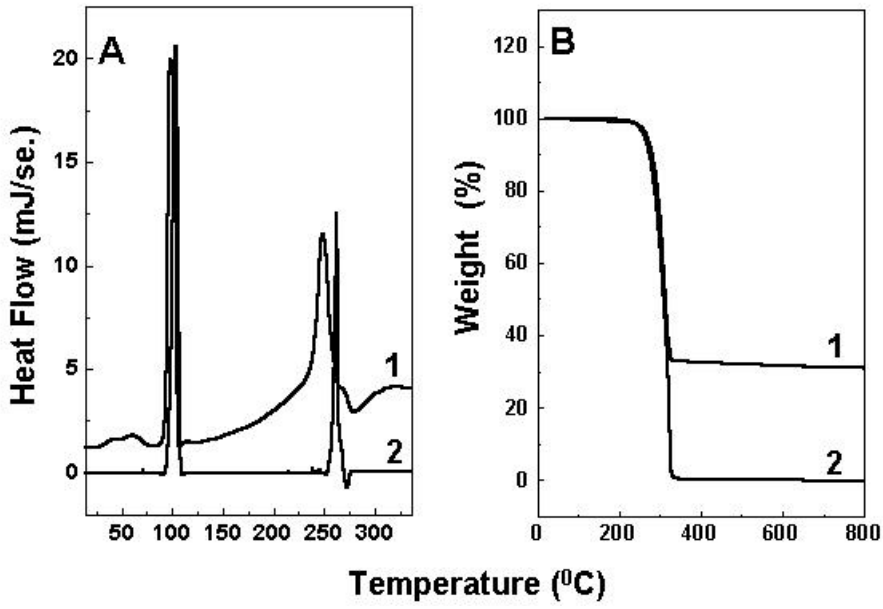

Figure 6.3: A) DSC data recorded from pure CTAB (curve 2) and surface modified gold nanoparticles with interdigitated bilayer of DDA and CTAB (curve 1). B) TGA data recorded for pure CTAB (curve 2) and surface modified gold nanoparticles with interdigitated bilayer of DDA and CTAB (curve 1).

Weight losses of ca. 68 % and 100 % at 253 ^{0}C for CTAB-DDA-Au nanoparticles (Figure 6.3 B, curve1) and pure CTAB powder (curve 2) respectively. From a comparison of Figures 6.3A and B, it is observed that the broad endothermic peak at 65 ^{o}C (Figure 6.3A, curve 1) is not accompanied by a weight loss and that pure CTAB does not have any DSC signature in this region (Figure 6.3A, curve 2).

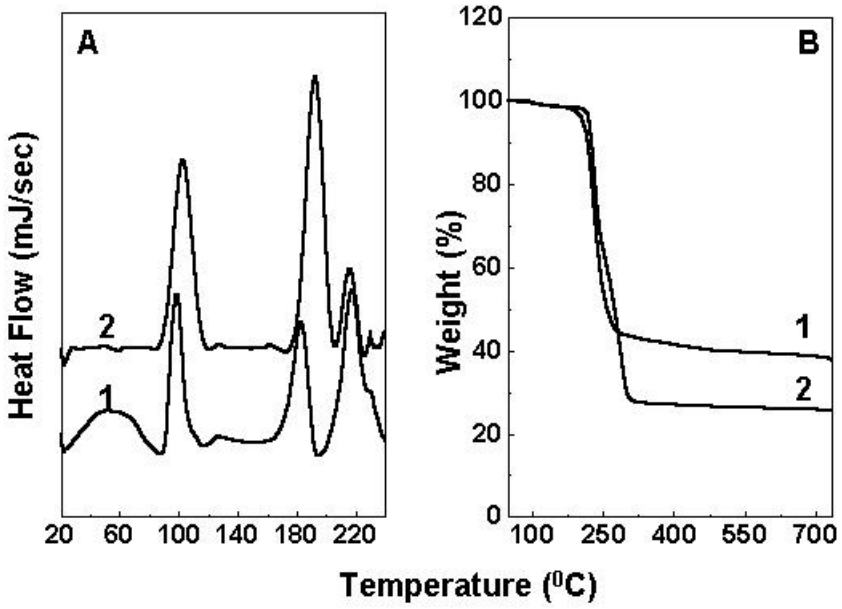

Figure 6.4: A) DSC data recorded from powders of pure SDS (curve 2) and ODA-capped gold nanoparticles after phase transfer into water (curve 1). The curves have been shifted vertically for clarity. B) TGA data recorded for powders of pure SDS (curve 2) and ODA-capped gold nanoparticles after phase transfer into water (curve 1).

In Figures 6.4A and B, curve 1 corresponds to data recorded from the phase-transferred powder (modified with SDS) and curve 2 is that recorded from pure SDS. Figure 6.4 A shows four endothermic peaks at 55 ^{0}C, 100 ^{0}C, 183 ^{0}C and 218 ^{0}C for the phase transferred of Au nanoparticles (curve 1) and barring the feature at 55^o C, are similar to those observed for the pure SDS sample (curve 2). The corresponding TGA data (Figure 6.4B) shows that close to 75% weight loss occurs at 215 ^{0}C for pure SDS (curve 2) while the weight loss for the phase transferred ODA-capped Au nanoparticle powder is ca. 60% and occurs at roughly the same temperature (curve 1). Negligible weight loss in the range 325 ^{0}C - 700 ^{0}C is observed in both samples. From the DSC and

TGA data, it is seen that the one significant difference between pure SDS sample and SDS/ODA-capped gold nanoparticle powder is the presence of broad endothermic peak at 55 ^{0}C in the latter (curve 1, Figure 6.4A) that is not accompanied by a weight loss (curve 1, Figure 6.4B). Similar observation was observed in case of CTAB and CTAB modified gold nanoparticles at 65 ^{0}C (curve 1, Figure 6.3A).

We believe that the endothermic peak in the region of 55-65 ^{o}C is due to the melting of ordered regions of the hydrocarbon chains arising from interdigitated segments of the primary DDA/ODA and CTAB/SDS secondary monolayers (boxed regions, Scheme 2). In a previous study, some of us have shown that silver nanoparticles capped with interdigitated bilayer of lauric acid show similar no weight loss endothermic features at ca. 50 ^{o}C.[2] An interdigitated structure is expected to be energetically favorable in an aqueous environment due to the maximization of hydrophobic interactions between the interdigitated hydrocarbon chains.[7] Based on this result, we propose that the phase transfer of the hydrophobized gold nanoparticles and their redispersibility in water arise due to formation of an interdigitated structure as shown in Scheme 2.

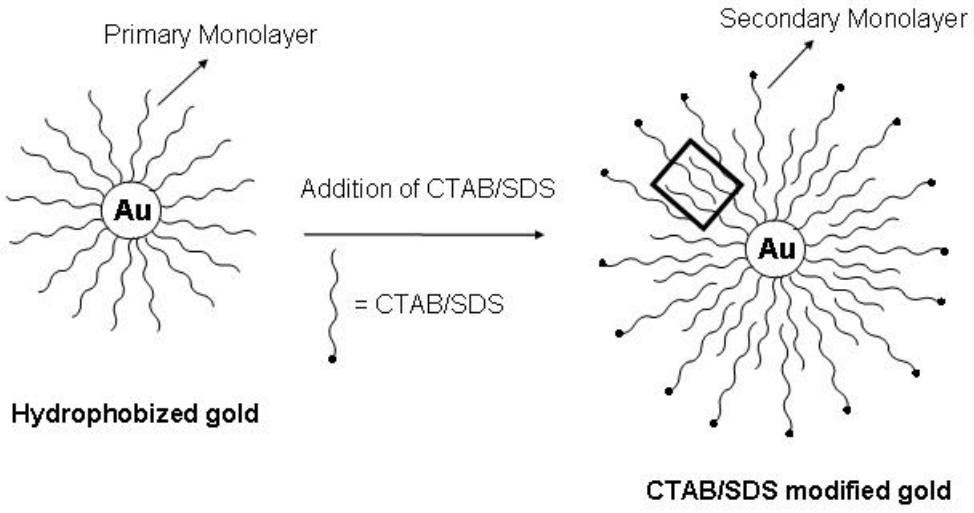

Schematic 2: Diagram showing the formation of an interdigitated secondary monolayer of CTAB/SDS molecules on the surface of hydrophobized gold nanoparticles. The box encloses ordered, interdigitated regions of the bilayers.

Further analysis of the DSC and TGA data from pure CTAB and CTAB-DDA-Au nanoparticle powder yields another endothermic process at 253 ^{o}C accompanied by weight losses in both cases (Figures 6.3A and B). The melting point and boiling point of

pure CTAB are 218 and 235 ^{0}C. At the boiling point, the CTAB molecule decomposes so the 100% weight loss could be due to evaporation/decomposition of CTAB molecules. This feature may be attributed to desorption of free CTAB molecules as well as a fraction of the surface-bound CTAB-DDA bilayers. The DSC and TGA data of pure SDS and SDS-ODA-Au nanoparticle powder show endothermic process at 215 ^{o}C accompanied by a weight loss in both cases (Figures 6.4A and B). These features correspond to desorption of free SDS molecules as well as a fraction of the surface-bound SDS-ODA bilayers. In both cases this desorption temperature is in good agreement with the reported temperature by Leff *et. al*.[8] for DDA modified gold nanoparticles. The TGA data shows complete weight loss at 253 ^{o}C in the case of pure CTAB (Figure 6.3B, curve 2) while a 68 % weight loss at same temperature is observed from the CTAB-DDA-Au powder (Figure 6.3B, curve 1). The weight loss at 253 ^{o}C (curve 1) is attributed to desorption of free, uncomplexed CTAB molecules as well as a fraction of the bilayers of CTAB and DDA on the gold nanoparticles.

The percentage weight contribution of the surface bound DDA and CTAB molecules is higher than a theoretical estimation of ca. 25% (by assuming the area occupied by DDA molecule as 25 Å^2 on the surface of gold nanoparticles with diameter 35 Å and ratio of DDA and CTAB as 1:1). It is clear from the TGA data that the higher weight loss observed in this study is due to the presence of uncoordinated CTAB molecules in the powder.

The origin of the features at 183 ^{0}C (curve 1, Figure 6.3A) and 192 ^{0}C (curve 1) of Figure 6.4A is not clear at this moment. That they occur in the broad weight loss region attributed to desorption of gold nanoparticle-surface bound SDS and ODA molecules (Figure 6.4B) indicates that they are associated with breaking of bonds between the interdigitated bilayers and the gold surface. The TGA data reveals that the percentage weight contribution of the surface bound ODA and SDS molecules is higher than a theoretical estimation of ca. 24 % (by assuming the area occupied by ODA molecule as 25 Å^2 on the surface of gold nanoparticles with diameter 35 Å and the ratio of ODA : SDS to be 1:1). The higher weight loss observed in this study is most likely due to the presence of uncoordinated SDS molecules in the powder, which in spite of repeated washing and centrifugation remains in the sample as in the case of CTAB

modified case. Another important observation is the residual weight in the case of SDS even after heating to 700 ^{0}C. We believe this is due to the formation of stable sodium-sulfur compounds after burning away of the hydrocarbon component in SDS. The difference in the residual weights of the two samples at 700 ^{o}C is attributed to the presence of gold nanoparticles along with sodium and sulfur residue in the phase-transferred gold nanoparticle powder (Figure 6.4B).

6.5. FTIR spectroscopy studies

Drop-coated films of aqueous solution of purified powder of CTAB-DDA-Au/SDS-ODA-Au was prepared on a Si (111) substrate and analyzed by FTIR spectroscopy. The spectra obtained from a CTAB-DDA-Au nanoparticle film (curve 1) as well as a solution - cast pure CTAB film (curve 2) in the spectral range 1200 – 1800 cm^{-1} and 2700 – 3600 cm^{-1} are shown in Figures 6.5A and B respectively. Since CTAB molecules form an interdigitated bilayer structure with primary monolayer of DDA and is not directly bound to the gold nanoparticle surface, the FTIR spectrum of surface

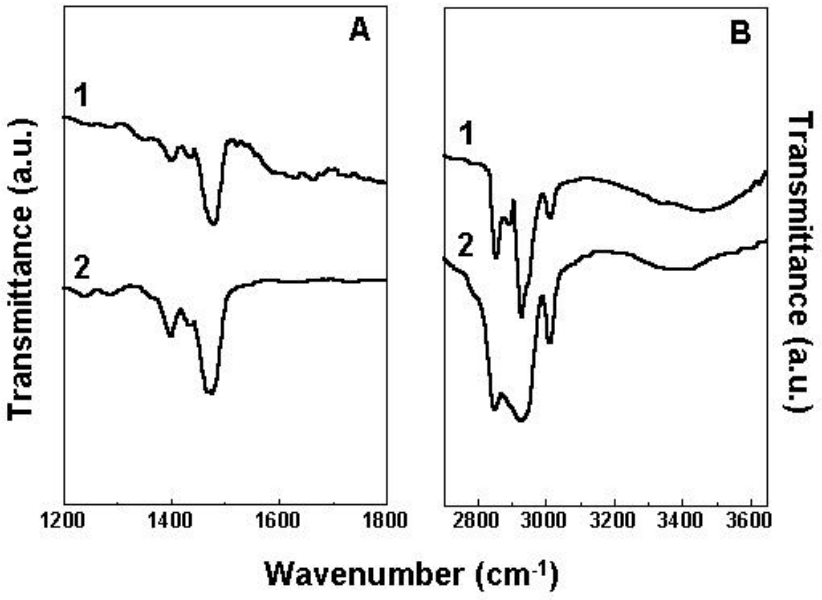

Figure 6.5A and B: FTIR spectra of surface modified gold nanoparticles with interdigitated bilayer of DDA and CTAB (curve 1) and pure CTAB (curve 2) in different spectral windows.

modified gold nanoparticles (CTAB-DDA-Au) looks similar to that of pure CTAB. Both curves show a resonance at 1480 cm^{-1}, which can be assigned to methylene scissoring vibrations.[9] The methylene antisymmetric and symmetric vibrations are observed at 2920 an 2850 cm^{-1} respectively in both the cases.[9]

Figure 6.6 is FTIR spectra recorded from the drop coated film of the aqueous solution of purified powder of SDS-ODA-Au nanoparticles. The spectra obtained from an SDS-ODA-Au nanoparticle film (curve 3), ODA-Au nanoparticles (curve 2) as well as a solution-cast pure SDS film (curve 1) in the spectral range 3500 – 2500 cm^{-1} and 1500 – 600 cm^{-1} are shown in Figures 6.6A and 6.6B respectively. The spectrum of pure SDS (curve 1) shows peaks at 1252 cm^{-1} (feature a) and 1083 cm^{-1} (feature b), which are assigned to S=O stretching vibrational modes of sulphonic acid groups present in SDS (Figure 6.6B). These two features are not observed in the ODA-Au (curve 2, before phase transfer of the gold nanoparticles with SDS) while they are clearly seen in SDS-ODA-Au (curve 3, after phase transfer of the ODA-capped gold nanoparticles with SDS) indicating

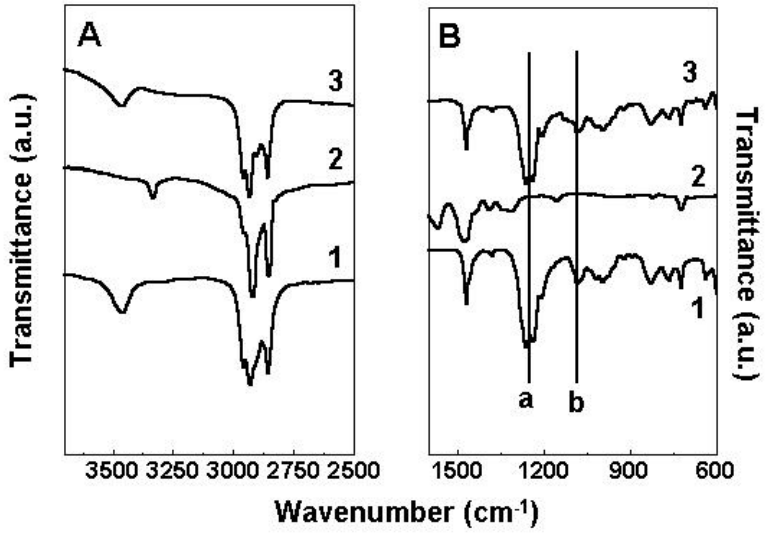

Figure 6.6A and B: FTIR spectra of pure SDS (curve 1), ODA-capped gold nanoparticles (curve 2) and surface modified gold nanoparticles with interdigitated bilayers of ODA and SDS (curve 3) in different spectral windows.

that SDS molecules are present around the surface of the gold nanoparticles after phase transfer. The fact that the S=O stretch vibrational frequencies do not change in the phase-transferred gold nanoparticle sample clearly indicates that SDS is not directly coordinated

to the gold nanoparticles. This rules out the possibility of an exchange of surface-bound ODA molecules by SDS molecules during phase transfer as a possible mechanism for hydrophobization of the gold surface. Curves 2 and 3 (Figure 6.6B) corresponding to FTIR spectra of ODA-Au and SDS-ODA-Au show a resonance at 1470 cm^{-1}, which can be assigned to methylene scissoring vibrations in the hydrocarbon segment of the molecule[9]. The methylene antisymmetric and symmetric vibrations are observed at 2920 cm^{-1} and 2850 cm^{-1} respectively in both the cases and are clearly seen in Figure 6.6A[9]. Another prominent resonance at 3456 cm^{-1} is observed in the case of SDS and SDS-ODA-Au samples and corresponds to O-H stretching vibration mode from water entrapped in both powders.

6.6. TEM studies

A drop-coated film of aqueous solution of purified powder of CTAB-DDA-Au and SDS-ODA-Au was formed on carbon-coated copper grid by solvent evaporation and analyzed by transmission electron microscopy (TEM). Figures 6.7A and 6.8A show representative TEM images of CTAB and SDS capped gold nanoparticles and Figures 6.7B and 6.8B are the particle size distribution (PSD) measured from Figure 6.7A and 6.8A respectively. It is clear from the picture that the particles are fairly polydisperse. An analysis of the PSD histogram yielded gold nanoparticles of size 16 ± 2 nm for CTAB capped gold and 9 ± 2 for SDS capped gold nanoparticles. The average size of the nanoparticles is more than that of the as- prepared gold nanoparticles formed by borohydride reduction of chloroauric acid.[10] Murray and co-workers have shown that the particle size of N, N-trimethyl(undecylmercapto)ammonium chloride protected nanoparticles is higher than the actual individual nanoparticles due to ionic association between terminal trimethylammonium groups and counter anions during solvent evaporation.[11] This association leads to clumping of nanoparticles which hinders imaging of the core sizes of individual monolayer protected nanoparticles in the TEM. We believe that the larger particle size of the phase transferred gold nanoparticles relative to the hydrophobized nanoparticles in the organic solvent observed in the present study may be due to a similar process of screening of electrostatic interactions by sodium or bromide counter ions.

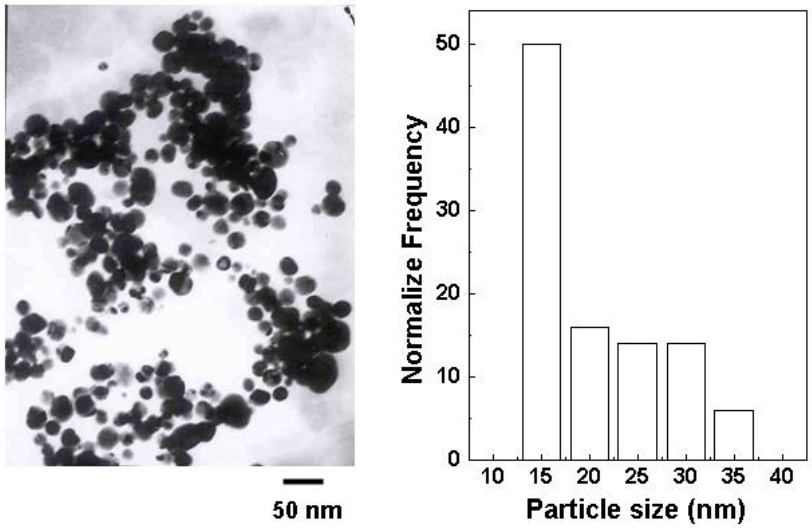

Figure 6.7: A) Transmission electron micrograph (TEM) of a film of gold nanoparticles phase transferred into water (CTAB-DDA-Au). B) Histogram showing the particles size distribution measured from Figure A.

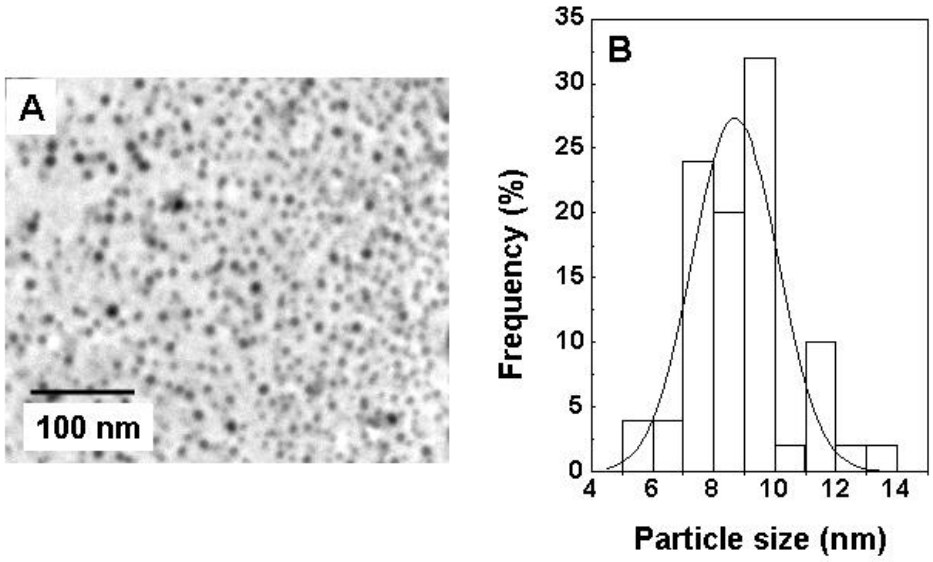

Figure 6.8: A) Representative TEM micrograph of a film of gold nanoparticles phase transferred into water (SDS-ODA-Au). B) Histogram showing the particle size distribution measured from Figure A. The solid line represents a Gaussian fit to the data.

6.7. Stability study of nanoparticles

The electrolyte-induced precipitation of colloidal gold nanoparticles in aqueous phase is well known in literature. Strouse *et al*. have shown that the gold nanoparticles

can be precipitated by addition of electrolyte and furthermore, that under certain conditions, they can be redispersed in water.[12] The stability of CTAB-DDA-Au/SDS-ODA-Au nanoparticle solution of this study was checked as a function of electrolyte (NaCl) concentration. Curve 1 in Figure 6.9A is the UV-vis spectrum of the CTAB-DDA-Au nanoparticles in water and curves 2, 3, 4, 5 and 6 correspond to spectra of the CTAB-DDA-Au gold nanoparticles solution after addition of 0.1 M, 0.5 M, 1 M, 2 M and 3 M NaCl respectively. The UV-vis spectra after addition of different amounts of NaCl are almost identical indicating that the even large concentration of salt does not destabilize the nanoparticle solution.

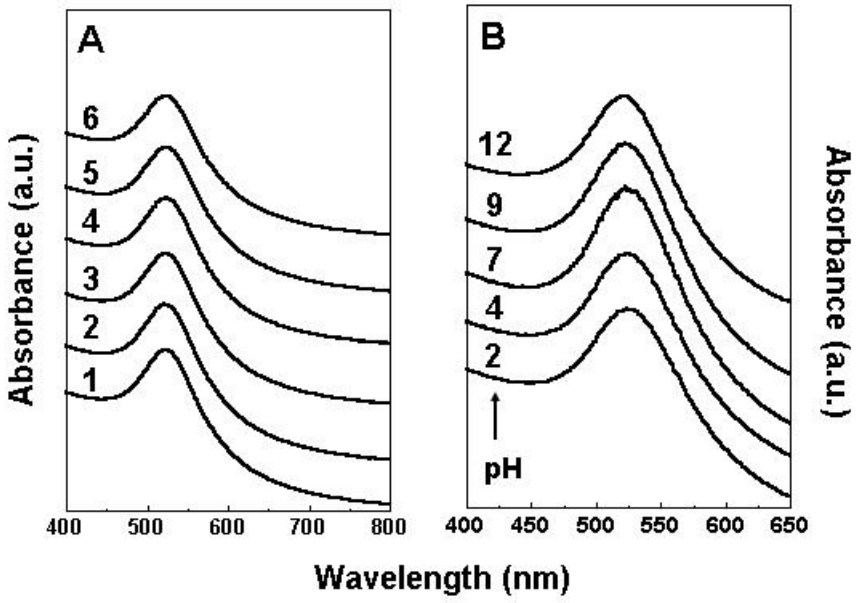

Figure 6.9: A) UV-vis spectra of phase transferred gold nanoparticles from organic to aqueous phase (CTAB -DDA- Au) as a function of NaCl concentration. Curve 1, before addition of NaCl; curve 2, after addition of 0.1M NaCl; curve 3, at 0.5 M NaCl; curve 4, at 1 M NaCl; curve 5, at 2 M NaCl and curve 6, at 3 M NaCl. B) UV-Vis spectra of gold nanoparticles transferred to aqueous phase via interdigitated bilayers (CTAB-DDA-Au) as a function of solution pH (pH of the gold nanoparticle solution is indicated next to the respective curves).

Figure 6.10A shows the UV-vis spectra of SDS-ODA-Au gold solution as a function of NaCl concentration. Curve 1 is SDS-ODA-gold nanoparticles before the addition of NaCl and curve 2, 3, 4 and 5 correspond to the nanoparticles solution after addition of 0.1 M, 0.5M, 1M and 2M NaCl. Again, it is clear from the UV-vis. spectra that the position of surface plasmon resonance does not change on addition of salt

concentration which indicates that the particles are highly stable even in large concentration of NaCl. Since gold nanoparticle solution of CTAB-DDA-Au/SDS-ODA-Au were very stable at high

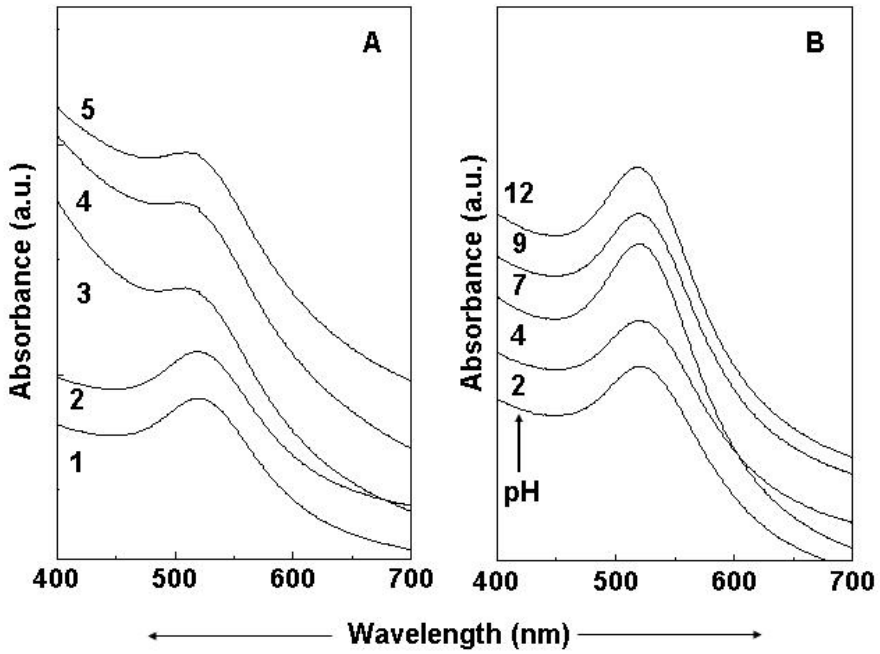

Figure 6.10: A) UV-vis spectra of phase transferred gold nanoparticles from organic to aqueous phase (SDS -ODA- Au) as a function of NaCl concentration. Curve 1, before addition of NaCl; curve 2, after addition of 0.1M NaCl; curve 3, at 0.5 M NaCl; curve 4, at 1 M NaCl and curve 5, at 2 M NaCl B) UV-Vis spectra of gold nanoparticles transferred to aqueous phase via interdigitated bilayers (SDS-ODA-Au) as a function of solution pH (pH of the gold nanoparticle solution is indicated next to the respective curves).

ionic concentrations, it would be interesting to test the stability of gold solution as a function of solution pH. Figures 6.9B and 6.10B show the UV-vis spectra recorded from CTAB-DDA-Au and SDS-ODA-Au nanoparticle solutions respectively under different solution pH conditions (pH listed next to the corresponding spectra). As in the case of the spectra recorded from the gold nanoparticle solution at different ionic strengths, the spectra recorded as a function of solution pH are almost identical with little evidence for aggregation of the particles. The exceptional stability of the bilayer-capped gold nanoparticle solutions as a function of ionic strength and pH is a salient feature of this work.

6.8. Conclusions

- The formation of water-dispersible gold nanoparticles by phase transfer of DDA-capped gold nanoparticles from chloroform to water using CTAB and SDS molecules has been demonstrated.
- The phase transfer is achieved by interdigitation of hydrocarbon tails of CTAB/SDS molecules with that of hydrocarbon sheath formed by primary monolayer of DDA/ODA on gold nanoparticle surface.
- CTAB/SDS modified gold nanoparticles are stable in presence of high concentration of salt and in wide range of pH.

6.9. References:

1. a) Simard, J.; Briggs, C.; Boal, A. K.; Rotello, V. M. *Chem. Commun.* **2000**, 1943. (b) Gittins, D. J.; Caruso, F. *Angew. Chem. Int. Ed.* **2001**, *40*, 3001; (c) Gittins, D. J.; Caruso, F. *ChemPhysChem* **2002**, *3*, 110.
2. Patil, V.; Mayya, S.; Pradhan, S. D.; Sastry, M. *J. Am. Chem. Soc*. **1997**, *119*, 9281.
3. Shen, L.; Laibinis, P.; Hatton, T. A. *Langmuir* **1999**, *15*, 447.
4. Nikoobakht, B.; El-Sayed, M. A. *Langmuir* **2001**, *17*, 6368.
5. Sastry, M.; Kumar, A.; Mukherjee, P. *Coll .Surf. A*. **2001**, *181*, 255.
6. Underwood, S.; Mulvaney, P. *Langmuir* **1994**, *10*, 3427.
7. Israelachvili, J. N.; *Intermolecular and Surface Forces; Academic Press: New York* **1985**, 102.
8. Leff, D. V.; Brandt, L.; Heath, J. R. *Langmuir* **1996**, *12*, 4723.
9. Hostetler, M. J.; Stokes, J. J.; Murray, R. W. *Langmuir* **1996**, *12*, 3604.
10. Patil, V.; Malvankar, R. B.; Sastry, M. *Langmuir* **1999**, *15*, 8197.
11. Cliffel D E, Zamborini F P, Gross S M and Murray R W 2000 *Langmuir* **16** 9699.
12. Cumberiand, S. L.; Strouse, G. F. *Langmuir* **2002**, *18*, 269.

CHAPTER VII

Conclusions

A concluding remark on the salient features of the work described in the thesis is mentioned in this chapter. Possible avenues for future work are briefly delineated.

7.1 Summary of the work

There is great excitement in the organization of nanoparticle using the "bottom-up" approach, which is inspired by biological concepts wherein nanoparticles synthesized in colloidal form and thereafter self-assembled into the form of thin film or in different geometry. The kind of organization of nanoparticles illustrated in this thesis is essentially based on non covalent interactions. The surface modified nanoparticles have been assembled in a layer-by-layer fashion on glass substrate by using electrostatic interactions. In order to form multilayer films of gold and silver, the nanoparticles of gold and silver have been derivatized with bifunctional molecules, 4-aminothiophenol and 4-carboxythiophenol respectively. The layer-by-layer assembly was effected by a simple beaker-based immersion procedure and fairly good quality multilayer structures are realized. These assemblies are stable up to 100 ^{0}C above which the particles sinter. Surface derivatization of nanoparticles with amino acid, valine leads to the amphoterization of nanoparticles i.e. negatively charged above the isoelectric point (pI) and positively charged below pI. The surface charge reversibility of gold nanoparticle at two pH values on either side of the isoelectric point has been used to sequentially assemble the gold particles on negatively charged glass substrate by using electrostatic interactions.

Electrostatic interactions have also been used to assemble the nanoparticles on DNA molecules which act as a template. The electrostatic complexation between positively charged amino acid, lysine modified gold nanoparticles on the negatively charged phosphate backbone of DNA molecules leads to the linear superstructure of nanoparticles in a lamellar fashion. This procedure was simplified by using the drop-coated film of DNA as a template to organize the lysine modified gold nanoparticles into linear superstructure. The DNA-lipid composite film has also been used as a template for synthesis and assembly of silver nanoparticles. This composite film was obtained by incorporation of DNA molecule in thermally evaporated fatty amine film and thereafter silver ions were incorporated by simple immersion in silver salt solution at physiological pH. The synthesis of nanoparticles was done by reducing silver ions present in DNA-lipid composite film by keeping it in hydrazine atmosphere. This approach shows promise for

extension to topologically more intricate structures based on rational DNA design as well as in the generation of nano-wires.

Nanoparticles dispersed in organic solvents are known to form large 2-D and 3-D ordered structures on many substrates by simple evaporation of the solvent. We hypothesized that the key step for the dispersion of nanoparticles in organic solvents is the hydrophobization of the nanoparticle surface. The thesis also describes the detailed investigation for new approaches for the hydrophobization of nanoparticles using amine/thiol chemistry and two-dimensional assembly of nanoparticles in thin film form. It is also clear from this study that primary amine molecules anchored on the gold nanopartcles surface by two kind of bonding, electrostatic and covalent. This approach for the hydrophobization of nanoparticles may be extended to control the inter nanoparticle separation in the nanoparticle films by altering the chain length of the surfactant.

Certain application requires the phase transfer of nanoparticles in aqueous phase. Therefore we also studied phase transfer of nanoparticles form organic phase into aqueous phase which is based on interdigitation of hydrocarbon tails of water soluble surfactant molecules with that of hydrocarbon sheath formed by primary monolayer of capping agent (DDA/ODA) on gold nanoparticle surface. These bilayer capped nanoparticles, dispersible in water are stable in harsh condition like at high salt concentration and at high pH.

Future scope

One of the most important prospects of our strategies is electrostatic complexation so that any kind of nanoparticles which can be charged using suitable surfactants can be organized by using oppositely charged templates in a pre-defined geometry. Hence technologically important, oxide and magnetic nanoparticles like TiO_2, Fe_3O_4 can be organized using this technique. In addition to the above, well defined superlattice structure may be obtained through alternate immersion of charged substrate in different surface modified nanoparticles solution. This shows promise for obtaining alternate metal-semiconductor nanoparticles layer. Furthermore, the nanoparticles can also be assembled in different geometries such as junctions (forks), polygons and polyhedra by

varying in the sequence of bases in synthetic DNA. The phosphorithiolate DNA interconnects the nanoparticles and forms an open, quasi-linear gold nanoparticles network. This opens up the exciting possibility of obtaining covalently linked gold nanoparticle structures in more complex geometries with a view to tailor the electron transport properties of the superstructures.

The catalytic activity of hydrogenation or carbonylation of nanoparticles also depends on the shape of nanoparticles. The shape of nanoparticles can be tailored by synthesizing them in aqueous based protocol. So future work need to be focused on phase transfer of various shapes of nanoparticles from aqueous phase to organic phase and investigation of liquid crystalline behavior. These nanoparticles of different shape can be used for catalytic purpose.

Our methods also show promise for obtaining high concentrations of gold nanoparticles in water which may possess important application in nanoparticle bioconjugation methodologies.

Finally, we would like to conclude that this thesis illustrates many simple and elegant strategies for the layer-by-layer, as well as linear assembly of nanoparticles. Many useful strategies for the phase transfer of nanoparticles from aqueous to organic phase and vice-versa have been presented.